UNIVERSITY OF CALIFORNIA
RIVERSIDE

Kinetic, Mechanistic, and Spectroscopic Studies of the Mo/Cu Containing CO dehydrogenase of *Oligotropha carboxidovorans*

A Dissertation submitted in partial satisfaction
of the requirements for the degree of

Doctor of Philosophy

in

Biochemistry and Molecular Biology

by

Jarett Michael Wilcoxen

December 2013

Dissertation Committee:
Dr. Russ Hille, Chairperson
Dr. Richard Debus
Dr. Leonard Mueller

The Dissertation of Jarett Michael Wilcoxen is approved:

_____

_____

_____

Committee Chairperson

University of California, Riverside

ACKNOWLEDGEMENT

I would like to thank Dr. Russ Hille for his mentorship, advice and support during my time at UC Riverside. I have learned a great deal about how to be an effective and professional researcher and appreciate the encouraging and helpful atmosphere developed in the lab between colleagues. Especially appreciated is the independence given to all of his students to create their own path in the lab, as well as the opportunities to meet and visit other professionals in the field.

I would like to thank Dr. Brian Hoffman and Dr. Martin Kirk for the productive collaborations and insight. I would also like to thank Dr. Silke Leimkühler for the time and training spent in her lab, as well as all of her students for being helpful and welcoming.

Finally, I would like to thank Dr. Leonard Mueller and Dr. Richard Debus for being on my thesis committee and all your advice along the way.

Dedication

To Casey, my parents, and all those who have supported me along the way.

"The Answer to the Great Question…"
"Of Life, the Universe and Everything…"
"Is…"
"Forty-two," said Deep Thought, with infinite majesty and calm.

Douglas Adams
The Hitchhiker's Guide to the Galaxy

ABSTRACT OF THE DISSERTATION

Kinetic, Mechanistic, and Spectroscopic Studies of the Mo/Cu Containing CO dehydrogenase of *Oligotropha carboxidovorans*

by

Jarett Michael Wilcoxen

Doctor of Philosophy, Graduate Program in Biochemistry and Molecular Biology
University of California, Riverside, December 2013
Dr. Russ Hille, Chairperson

Carbon monoxide dehydrogenase from *Oligotropha carboxidovorans* catalyzes the oxidation of carbon monoxide to carbon dioxide, providing the organism both a carbon source and energy for growth. In the oxidative half of the catalytic cycle, electrons gained from CO are passed intramolecularly through two [2Fe-2S] clusters and finally to a FAD cofactor. From FAD the electrons are ultimately passed to the electron transport chain of the Gram-negative organism.

In the current study we have examined a variety of aspects of this enzyme in the oxidative- and reductive-half reactions and propose mechanisms for the oxidation of carbon monoxide and the proximal electron acceptor of the enzyme.

First, we have identified the proximal acceptor of reducing equivalents. We have found CO dehydrogenase passes electrons directly to the quinone pool without using a cytochrome as an intermediary as had previously been proposed. This establishes a new category of redox-partner for the xanthine oxidase family of enzymes.

Next, we examined the active site and find silver can be replaced for copper in the active site. Cyanide effectively removes the copper and a Ag(I)-thiourea solution can reactive the enzyme, albeit at a lower turnover rate. The silver reconstitution can be verified by EPR, evident by the lack of coupling to the copper I=3/2 nucleus and in its place the sliver I=1/2 nucleus. This altered but active form of the protein is used to compare and contrast with the native copper- containing enzyme to develop a mechanism for CO oxidation.

We then examined the EPR of CO dehydrogenase reduced by CO by electron nuclear double resonance spectroscopy (ENDOR). The ENDOR spectra of this state confirm that the ^{63,65}Cu exhibits strong and almost entirely isotropic coupling with a_{iso} of +148 MHz. When the intermediate is generated using ^{13}CO, coupling to the ^{13}C is observed, with a_{iso} = +17.3 MHz. A

comparison with the couplings seen in related, structurally assigned Mo(V) species from xanthine oxidase leads us to conclude that the intermediate contains a partially reduced, Mo(V)/Cu(I), center with CO bound at the copper.

We next further characterized the kinetics and mechanism of hydrogenase activity previously reported and find CO dehydrogenase effectively catalyzes H_2 oxidation to protons. This activity is found to be independent of pH and does not appear to be reversible. A new EPR signal was found and is attributed to the H_2 bound state with the molybdenum in an oxidation state, Mo(V), that prevents further catalysis.

Finally, we have examined the inhibition of the enzyme by *n*-butylisonitrile and bicarbonate. We find that *n*-butylisonitrile reduces the and irreversibly inhibits the enzyme as is suggested by the crystal structure and computational studies previously reported. Bicarbonate acts as an uncompetitive inhibitor, reducing v_{max} and K_m, while also producing a new EPR signal of the bicarbonate complex.

TABLE OF CONTENTS

LIST OF FIGURES

LIST OF TABLES

Chapter 1

Introduction

1.1. General Background

1.1.1. Molybdenum and Tungsten in Biology

Molybdenum is the most abundant metal in the oceans taking the form of molybdate ($Mo^{VI}O_4^{2-}$) with a concentration of about 10 µg/L, which is higher in concentration than even cooper and zinc,[1] and is roughly 100 times more than tungsten which lies just below molybdenum on the periodic table. This is not the case however, in the much more reducing and high temperature hydrothermal vents where tungsten is soluble $W^{VI}S_4^{2-}$ while molybdenum in the form $Mo^{IV}S_2$ is insoluble. While molybdenum is widely distributed across all three kingdoms of life, tungsten is only found in prokaryotes (particularly archaea), i.e. those organisms that reside near hydrothermal vents and include some of the most ancient organisms known. This difference in solubility (and hence bioavailability) is in line with the hypothesis that early life began in a hot, anaerobic, and reducing environment. Organisms in such an environment would have been able to incorporate tungsten in order to carry out oxidation-reduction chemistry with the oxidation states of W(VI), W(V) and W(IV) available. It is important to note that the biologically relevant oxidation states of molybdenum and tungsten enzymes (IV, V and VI) allow these metals to be intermediaries in one- and two-

electron transfer processes, adding to the versatility in biology of these metals.[2] The tungsten-sulfur bonds that are found in tungsten containing enzymes are more stable at high temperatures than molybdenum-sulfur bonds, and the reduction potentials of the tungsten compounds are lower than the corresponding molybdenum compounds, a more useful attribute given the presumed low-potential environment in which life arose. Following the accumulation of O_2 in the atmosphere and lower temperatures, molybdenum replaced tungsten as it became more biologically available in the oxidizing conditions allowing organisms to carry similar oxidation-reduction chemistry established in early earth. In some cases these metals are exchangeable in the biological cofactors they are found. Typically, tungsten-containing enzymes grown in a molybdenum rich nutrient broth will incorporate molybdenum instead of tungsten in the active sites of proteins while maintaining activity, examples of this are aldehyde oxidoreductase (AO) from *Pyrococcus furiosus* and formate dehydrogenase from *Desulfovibrio alaskensis*.[3,4]

1.1.2. Molybdenum and Tungsten in Chemistry

Molybdenum, with an atomic number of 42, belongs to the 6th group and 5th row in the periodic table with tungsten, atomic number 74, just below in the 6th row.[5] The electronic configuration of molybdenum and tungsten are $[Kr]5s^1 4d^5$ and $[Xe]4f^{14} 6s^2 5d^4$ respectively each with allowed oxidation states from -2 to +6. Molybdenum and tungsten are similar in many ways, with similar atomic

radii, 140 pm and 141pm respectively, similar valence electron configurations, as well as the same oxidation state range and the same maximum coordination number of eight.[5] Also similar is the type of catalysis performed, both being able to perform the very difficult task of breaking the N_2 triple bond to form 2 NH_3 molecules, mimicking the biological enzyme nitrogenase that carries out the same reaction.[6] The differences between molybdenum and tungsten come in the stabilities of various complexes, as well as solubility and reduction potential as mentioned before. These key differences lead to different substrate and reaction specificities, giving versatility to the industrial and biological catalysis in which these metals play a role.

1.1.3. Molybdenum and Tungsten Enzymes

Molybdenum or tungsten enzymes are present in nearly all forms of life, from the ancient archea to humans, and catalyze environmentally and biologically important reactions in sulfur, nitrogen, and carbon metabolism.[2] They are able to detoxify sulfite, nitrite and arsenite, harness energy from purine degradation, and convert the biologically toxic carbon monoxide to the fixable carbon dioxide.[7] The molybdenum necessary for molybdenum containing enzymes is first taken up by the cell in the form molybdate ($Mo^{VI}O_4^{2-}$) through ATP dependent ABC-type transporter.[1] Once in the cell there are two main types of metal centers in which the metal is found. The first is the most unique of the molybdenum containing enzymes is the molybdenum-containing cofactor of

nitrogenase which incorporates molybdenum into a [CFe_7S_9Mo-homocitrate] cluster termed the Fe-Mo cofactor and is the location of nitrogen reduction to ammonia, Figure 1.1. The cofactor is produced from small Fe-S fragments made by NifS and NifU to form a precursor K-cluster that is the pair of [4Fe-4S] clusters.[8] The K-cluster is then transferred to NifB where a series of radical s-adenosylmethionine (SAM) dependent reactions to combine the Fe/S clusters and insert the center carbon to form the L-cluster (CFe_8S_9), which is transferred to NifEN for insertion of the molybdenum and homocitrate and formation of the mature M-cluster, which is then inserted into the apo-nitrogenase.[8]

The mononuclear enzymes which contain molybdenum or tungsten are divided into five families of enzymes separated by sequence homology and overall structure, although all contain at least one equivalent pyranopterin cofactor. The tungsten containing enzymes are thought to be the more ancient, and can be divided into two families: the aldehyde:ferredoxin oxidoreductase family and the formate dehydrogenase family, both families contain a single tungsten coordinated by two equivalents of the pyranopterin cofactor.[2] The mononuclear molybdenum containing enzymes are divided into three families; the Xanthine oxidase (XO) family, sulfite oxidase (SO) family and dimethyl-sulfoxide reductase (DMSOR) family and the nitrogenase family mentioned above. [2]

The cofactor utilized by the mononuclear molybdenum or tungsten enzymes is the pyranopterin cofactor (L), often referred to as the molybdopterin

(MPT) when molybdenum is coordinated. This cofactor coordinates one molybdenum or tungsten via an enedithiolate side chain with one or two equivalents of the cofactor and maintains a five or six coordinate metal with the additional ligands coming from a variety of combinations of cysteine, seleno-cysteine, aspartate, water, hydroxide, molecular oxygen or sulfur, Figure 1.1.[9] The pyranopterin cofactor is synthesized in cells using a GTP as a starting material, Figure 1.2. Through a radical SAM-dependent reaction, GTP is converted to an intermediate termed cyclic pyranopterin monophosphate (cPMP) by the MoaA and MoaC gene products in bacteria (or MOCS1A and MOCS1B respectively in humans).[10] The cPMP is then converted to the mature cofactor by the action of MoaD, MoaE and MoaB gene products (MOCS2 and MOCS3 in humans).[10,11]

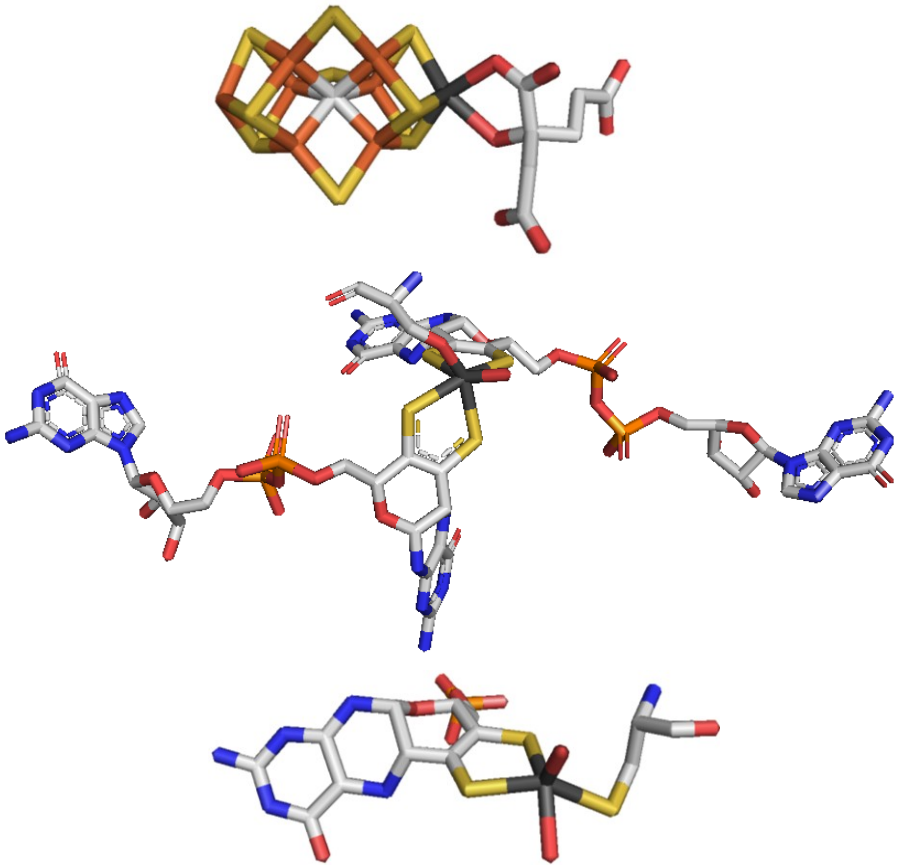

Figure 1.1. Molybdenum coordination in biology

The Fe-Mo cofactor of Nitrogenase (PDB: 3U7Q) (*top*) and bis-molybdopterin-guanine dinucleotide cofactor of DMSO reductase (PDB: 1EU1) (*middle*) and the molybdopterin cofactor of sulfite oxidase (PDB: 1SOX) (*bottom*) with molybdenum in dark grey and carbon in light grey. All other atoms are CPK rendered using Pymol.

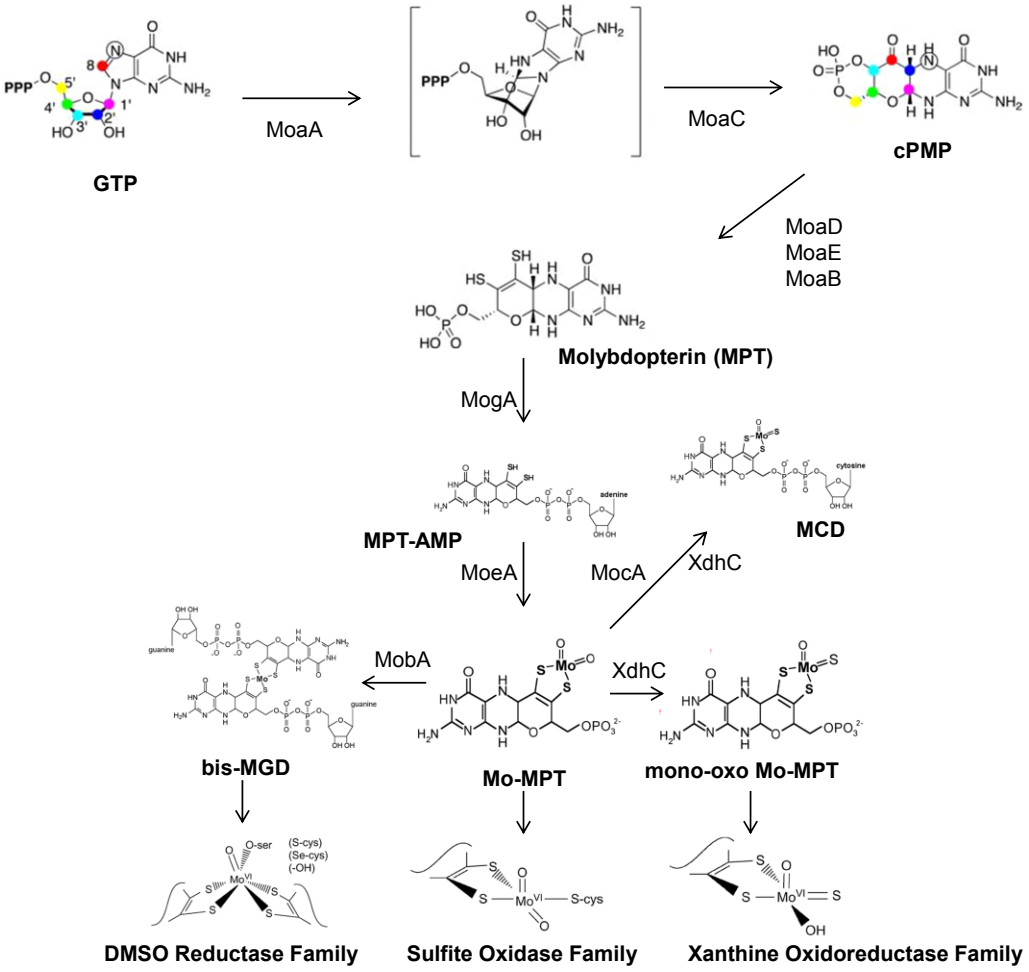

Figure 1.2. The biosynthetic pathway of the molybdenum cofactor for the mononuclear molybdenum enzymes.

The pterin cofactor is synthesized thought numerous steps starting with a radical SAM enzyme that converts GTP into the basic structure of the cofactor cPMP.

The pyranopterin cofactor is then modified by addition of ATP to the phosphate, a necessary intermediate catalyzed by MogA, before MoeA coordinates molybdenum to the dithioline portion of the pyranopterin cofactor creating the basic form of the molybdenum cofactor.[11] This step is catalyzed by a single bifunctional enzyme, gephyrin, in humans.[10] The cofactor can now be inserted directly into enzymes of the sulfite oxidase family where a cysteine is ligated to the molybdenum.[11] In the case of the xanthine oxidoreductase family the XdhC gene product must first sulfurate an equatorial position of the molybdenum, with the help of NifS, and subsequently insert the cofactor in the already-folded apo-xanthine dehydrogenase (XDH) in bacteria, this step is usually preceded by addition of a cytodine to form the molybdopterin-cytodine dinucleotide (MCD) cofactor by the MocA gene product.[11] Finally the last variety of the cofactor that is used in molybdenum and tungsten enzymes is the bis-molybdopterin-guanine dinucleotide cofactor (bis-MGD). This form of the cofactor, formed by the MobA gene product, is found in enzymes of the dimethyl-sufoxide reductase (DMSOR) family (and is the only form found in tungsten enzymes).[7] It is comprised of a guanine nucleotide addition to pyranopterin cofactor and as indicated in Figure 1.1 is present in the enzyme in a ratio of 2:1 compared to the metal.[11] Additional variations of the dinucleotide form of the cofactor have also been reported where guanine or cytodine are replaced by adenine (MAD) or inodine (MID).[2]

Of the three mononuclear molybdenum families the longest studied is the xanthine oxidase family. Members of this family typically catalyze the hydroxylation of a carbon center and act on a variety of relatively activated substrates from aldehydes to aromatic heterocycles.[9] The active site of the oxidized enzyme in this family is typically found in a distorted square pyramidal coordination geometry around the molybdenum, Figure 1.3. The molybdenum is coordinated by the reduced (tetrahydro) pterin cofactor, in the mononucleotide or cytodine dinucleotide form, by the enedithiolate moiety in the equatorial plane along with a catalytically labile equatorial hydroxide, an equatorial sulfido ligand and apical oxo ligand.[7] All members of this family also possess two [2Fe-2S] ferredoxin type clusters and a flavin adenine dinucleotide (FAD) cofactor, Figure 1.4. In this family there is also a conserved glutamate adjacent to the equatorial Mo-OH of the molybdenum. Enzymes, such as XDH, generate, rather than consume reducing equivalents with NAD^+ or oxygen as the typical electron acceptor.[7] Notable exceptions to the general structure of the active site are found in nicotinate dehydrogenase where selenium replaces the equatorial sulfido group, carbon monoxide dehydrogenase where a copper is present coordinated between the equatorial sulfur and a cystiene residue (and reducing equivalents are passed directly to the quinone pool rather than to NAD^+), and 4-Hydroxybenzoyl-CoA reductase from *Thauera aromatic* which catalyzes a dehydroxylation with reducing equivalents from ferredoxin. This enzyme also

contains an additional [4Fe-4S] cluster in addition to the standard set of redox-active centers.[9,12]

Like the xanthine oxidase family, members of the sulfite oxidase family contain a single equivalent of the oxidized pterin cofactor in their active sites (present as the mononucleotide form) in a square-pyramidal geometry, although in this case the equatorial sulfido ligand is replaced by a cyteine ligand of the protein, Figure 1.3. The members of this family are involved in oxygen transfer in order to detoxify substrates such as sulfite to sulfate and assimilate nitrate. Recently there have been a surge of new members of this family discovered with roles in drug metabolism such as the mARC (mitochondrial amidoxime-reducing component) enzymes in eukaryotes as well as members with unknown function that possess the catalytic core such as YedY gene product and the molybdenum cofactor sulferase C-terminal (MOSC) domain proteins.[9]

Possibly the most diverse of the three families of the mono-nuclear molybdenum enzymes is the DMSO reductase family of enzymes. Members of this family have two equivalents of the MGD form of the cofactor coordinating the molybdenum (Figure 1.3), with one pterin in the oxidized (di-hydro) and one in the reduced form. The overall geometry at the molybdenum is distorted trigonal prismatic, with a terminal (and catalytically labile) Mo=O and serine in the case of DMSO reductase, Figure 1.3. Other members of the family may have a sulfur or selenium instead of oxygen, and cysteine, seleno-cysteine, or aspartate instead of serine. The diversity in metal coordination gives the enzymes a great variety in

substrate specificity and type of reaction carried out. The overall structure of this family varies the most of any family, with the presence of a variety of combination of redox active centers including [2Fe-2S] clusters, [3Fe-4S] clusters, [4Fe-4S] clusters, flavin mononucleotide and heme, along with some members possessing a molybdenum center as the sole redox-active group. There is moderate structural homology between the DMSO reductase family of enzymes with the aldehyde:ferredoxin oxidoreductase family of tungsten containing enzymes, but only minimal sequence homology. Members of the DMSO reductase family catalyze oxygen atom transfer, oxidation/reduction (de)hydroxylation/hydration reactions.

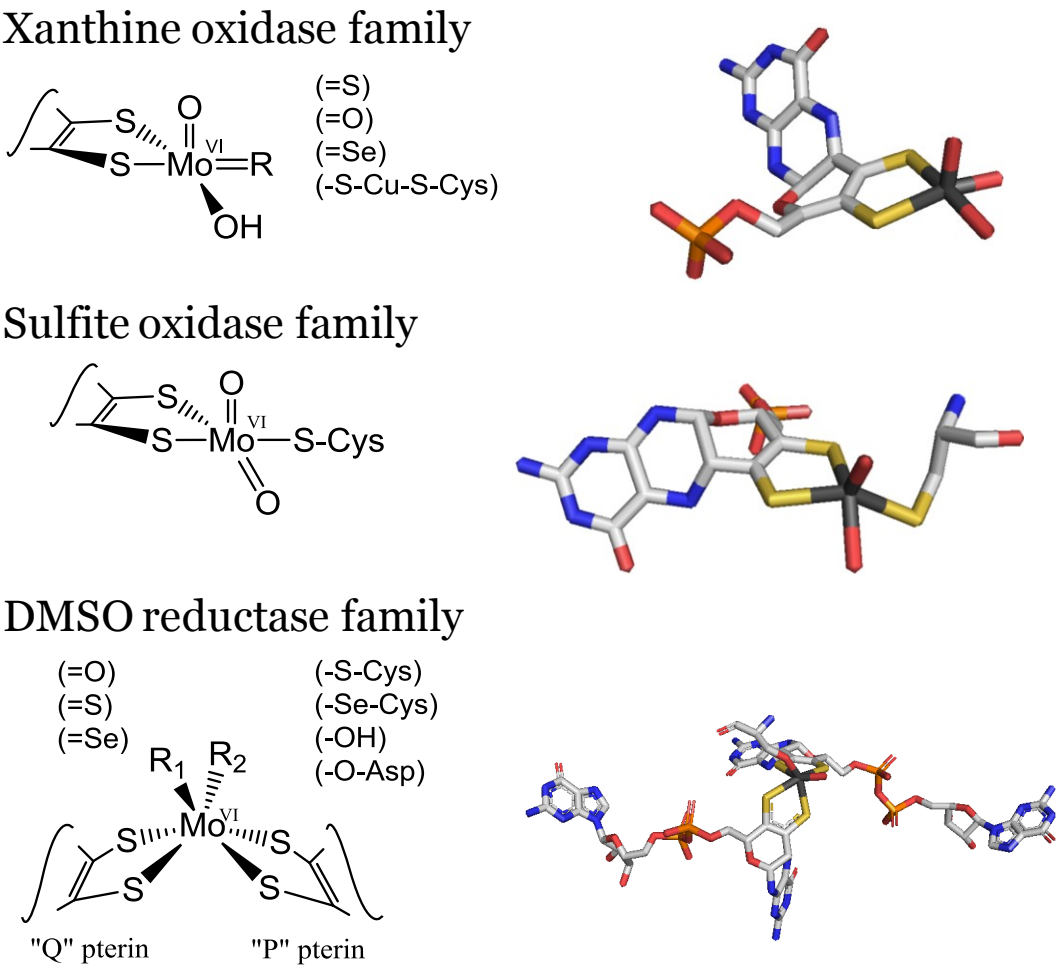

Figure 1.3. Molybdenum family members- active site structures.

The three families of mononuclear pternin contaioning molybdenum enzymes with the active sites of the xanthine oxidase family (PDB: 1AOR) (top), sulfite oxidase family (PDB: 1SOX) (middle) and DMSO reductase family (PDB: 1EU1) (bottom) for representative members shown. Molybdenum is in dark grey, carbon in light grey, and all other atoms in CPK rendered using Pymol.

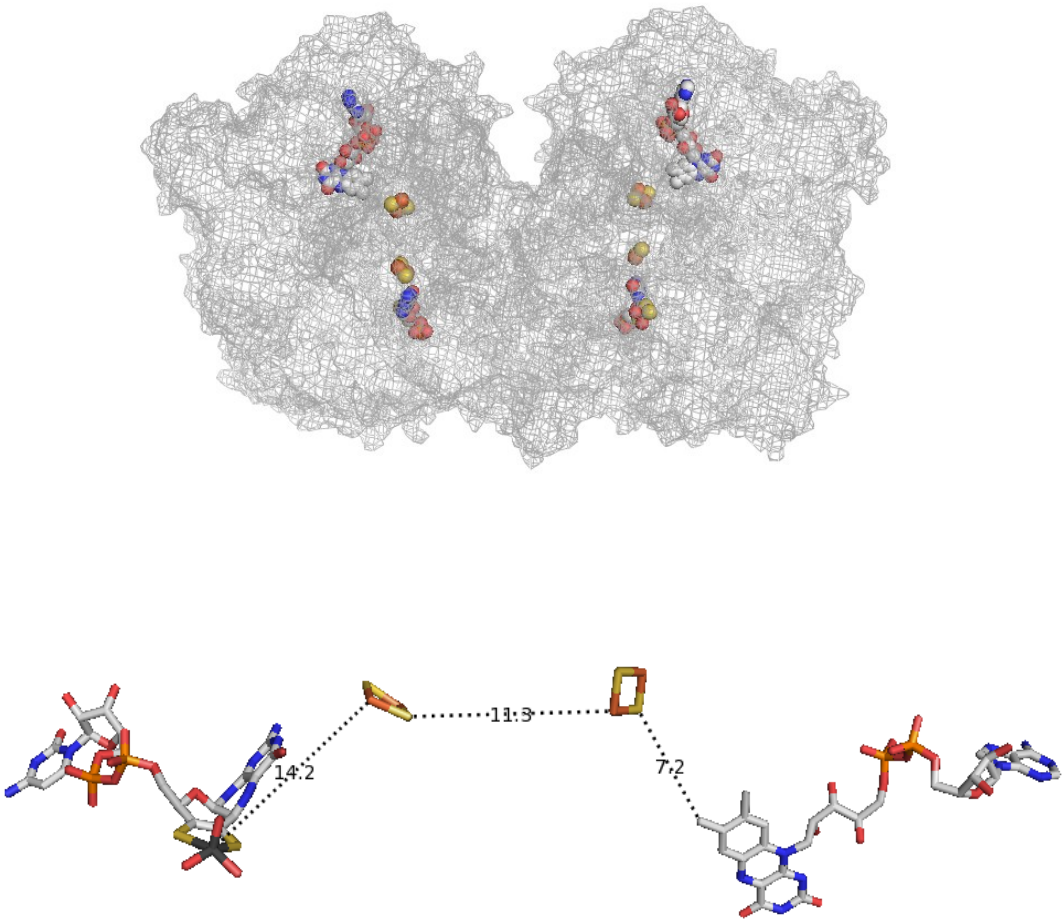

Figure 1.4 General Structure and cofactors for the xanthine oxidase family members

Xanthine oxidase family cofactors shown in a mesh protein structure (*top*) with distances between each cofactor (*bottom*). Molybdenum in dark grey and all other atoms in CPK rendered using Pymol (PDB: 1AOR).

1.2 Carbon Monoxide Dehydrogenase

1.2.1 Carboxidotrophic bacteria

The ability for organisms to oxidize carbon monoxide (CO) to carbon dioxide, using the reducing equivalents thus obtained for energy and the carbon dioxide thus generated as a carbon source is likely an ancient reaction, present in archaea living near hydrothermal vents in an environment that mimics the hot anaerobic conditions of early Earth. Carbon monoxide-oxidizing enzymes can be found in a variety of bacteria from the strictly anaerobic acetogen *Morella thermoacetica* or the methanogen *Methanosarcina barkerii* to aerobic chemolithotrophic organisms such as *Oligotropha carboxidovorans* and *Hydrogenophaga pseudoflava.*[13-16] Although the ability to oxidize CO is widespread in bacteria, especially archaea, the enzymes responsible for this reaction fall into two distinct groups. The first is the nickel- and iron- containing CO dehydrogenase found in obligate anaerobes that is oxygen-sensitive (this form of the enzyme also catalyzes the final step in acetyl-CoA synthesis in some bacteria).[17] The second consists of molybdenum- and copper- containing enzymes found in the aerobic bacteria *Oligotropha carboxidovorans* and *Hydrogenophaga pseudoflava,* and are not oxygen-sensitive. Of the molybdenum containing CO dehydrogenases there are two forms reported; The first, Form I, is that of the well described molybdenum- and copper- containing CO dehydrogenase of *O. carboxydovorans.* The second, Form II, has been identified through genomic sequencing and whole cell extract assays.[18] The difference

between Form I and Form II is an active site loop that contains the cysteine ligated to copper, this cysteine appears to be missing in the Form II enzymes resulting in a much lower activity level for CO.[18] With over 300 organisms found to have the capacity to oxidize CO aerobically, not all can grow on CO as a source of energy and carbon,[18] this activity is likely retained to detoxify from carbon monoxide.

1.2.2 CO dehydrogenase from aerobic carboxidotrophs

The molybdenum- and copper- containing CO dehydrogenase from aerobic, chemolithotrophic organisms such as *Oligotropha carboxidovorans* and *Hydrogenophaga pseudoflava* is a member of the xanthine oxidase family based on its overall amino acid sequence and overall structure.[14,15,19-23] In the reaction carried out by CO dehydrogenase, CO is oxidized to CO_2, yielding two reducing equivalents according to the following stoichiometry:

$$CO + H_2O \longrightarrow CO_2 + 2H^+ + 2e^- \ (E^0 = -558mV \text{ at pH } 7)$$

The reducing equivalents thus obtained by the enzyme are passed to the intramembrane quinone pool and on to a CO insensitive cytochrome C oxidase to provide energy for cell growth.[12] A portion (~16%) of the CO_2 generated as a product of the reaction is fixed non-photosynthetically by the pentose phosphate cycle [24,25] with an overall stoichiometry of:

$$2.19\ CO + O_2 \longrightarrow 1.83\ CO_2 + 0.36 \text{ cell carbon} + \text{energy}$$

The reaction is of profound environmental importance, since aerobic bacteria such as *O. carboxidovorans* clear an estimated $4x10^8$ metric tons of CO from the atmosphere annually.[26]

1.2.3 Structure of the molybdenum- and copper- containing CO dehydrogenase

The crystal structure of CO dehydrogenase has been solved from two organisms, *Oligotropha carboxidovorans* and *Hydrogenophaga pseudoflava*; the structure from *O. carboxydovorans*, the focus of the present thesis, will be used for further discussion. The functional enzyme is a $(\alpha\beta\gamma)_2$ hexamer, with an overall butterfly shape, and each αβγ type protomer consisting of a small 17.8 kDa subunit (*coxS*) containing two [2Fe-2S] clusters, a medium 30.2 kDa subunit (*coxM*) containing an FAD cofactor, and a large 88.7 kDa subunit (*coxL*) that possesses the molybdenum center, Figure 1.5. [27,28] The CO dehydrogenase from *O. carboxidovorans* is encoded by the mega plasmid pHCG3 in the *cox* gene cluster, Figure 1.6. This complex gene cluster consists of accessory genes involved in the maturation of the protein and possible membrane anchoring proteins used to dock CO dehydrogenase located downstream of the structural genes.[29,30] The overall protein fold notwithstanding, two aspects make CO dehydrogenase unique in the XOR family: first, the reaction itself is not strictly speaking a hydroxylation and does not involve the cleavage of a C-H bond; and second, the active site consists of a unique binuclear molybdenum and copper center rather than a mononuclear molybdenum center such as is seen in all other

family members. As shown in Figure 1.7, the active site is an $LMo^{VI}O_2$-(μS)-$Cu^{I}(OH/H_2O)$-$SCys_{388}$ structure, where L represents the pyranopterin cytodine dinucleotide cofactor. [20,23,31] The copper is essential for catalysis and maintains the Cu^{I} (closed shell d^{10}) oxidation state throughout the catalytic cycle.

Amino acid residues in the active site are more similar to the aldehyde oxidase type members of the family with a conserved glutamate and a glutamine hydrogen bonding to the apical oxygen. There are, however, key differences between CO dehydrogenase and the aldehyde oxidases. The first is a much narrower substrate access channel than seen in the other family members, with Phe_{390} sterically blocking much of the access to the active site. Also unique is the FAD-containing subunit, where a tyrosine (Tyr_{193}) blocks much of the solvent access to the flavin, Figure 1.8. This loop is not present in the same location in bovine xanthine oxidase and in xanthine dehydrogenase loop is present with an Ile residue in place of Tyr. Also unique are Ile_{101} and Ser_{272} where xanthine dehydrogenase has Phe and Asp respectively. Changes like these have been shown to affect redox potential of the flavin and activity towards oxygen or NAD^+ in xanthine oxidase and xanthine dehydrogenase.[32]

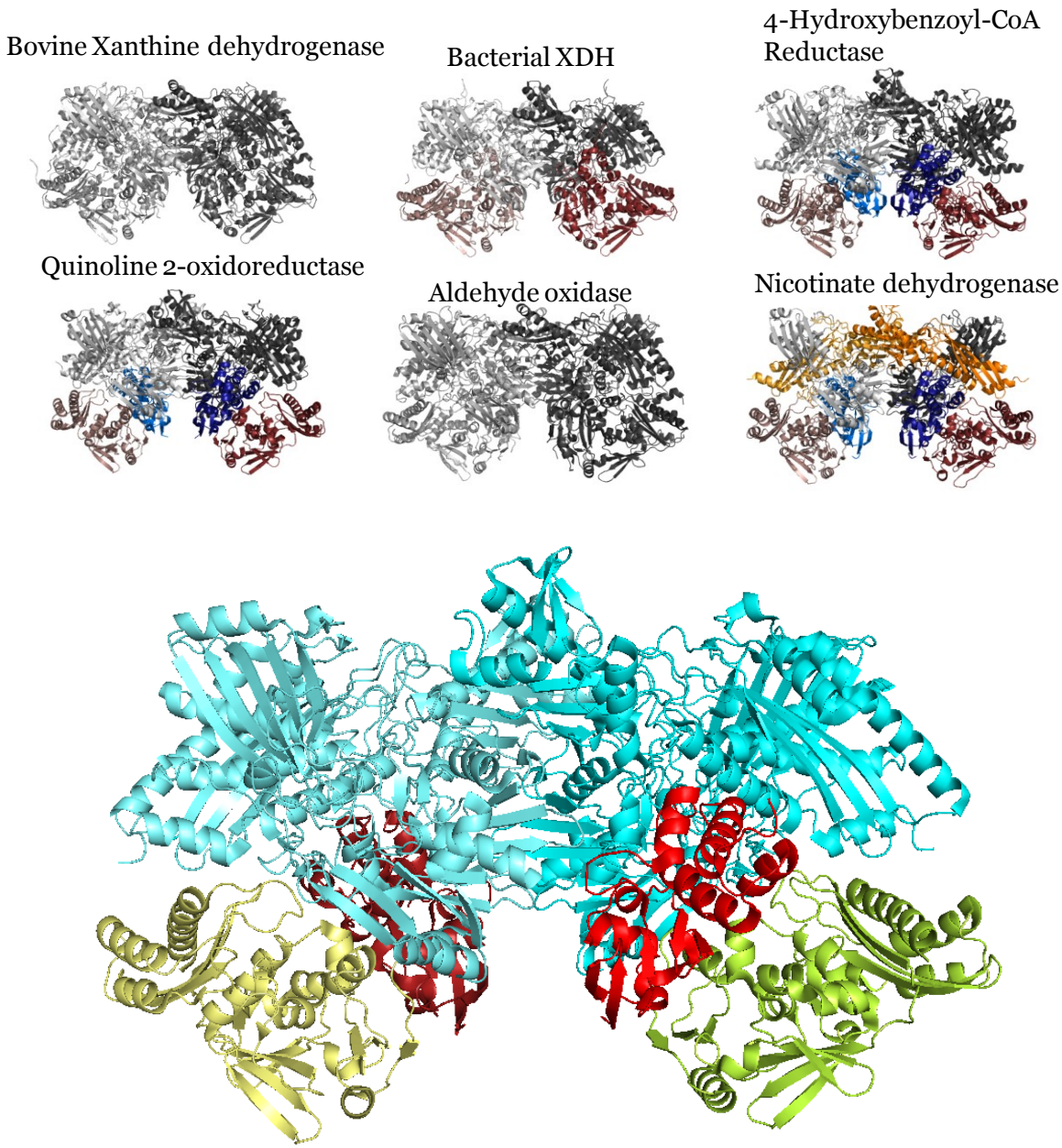

Figure 1.5 Structures of xanthine oxidase family members

Structures showing secondary structure of xanthine oxidase family members (top and middle) and CO dehydrogenase (bottom). In CO dehydrogenase the large subunits containing the molybdenum cofactor is in teal, the small subunits containing two [2Fe-2S] clusters in each are in red and themedium subunit containing the FAD cofactor in yellow. Images were rendered using Pymol (PDB: 1N5W).

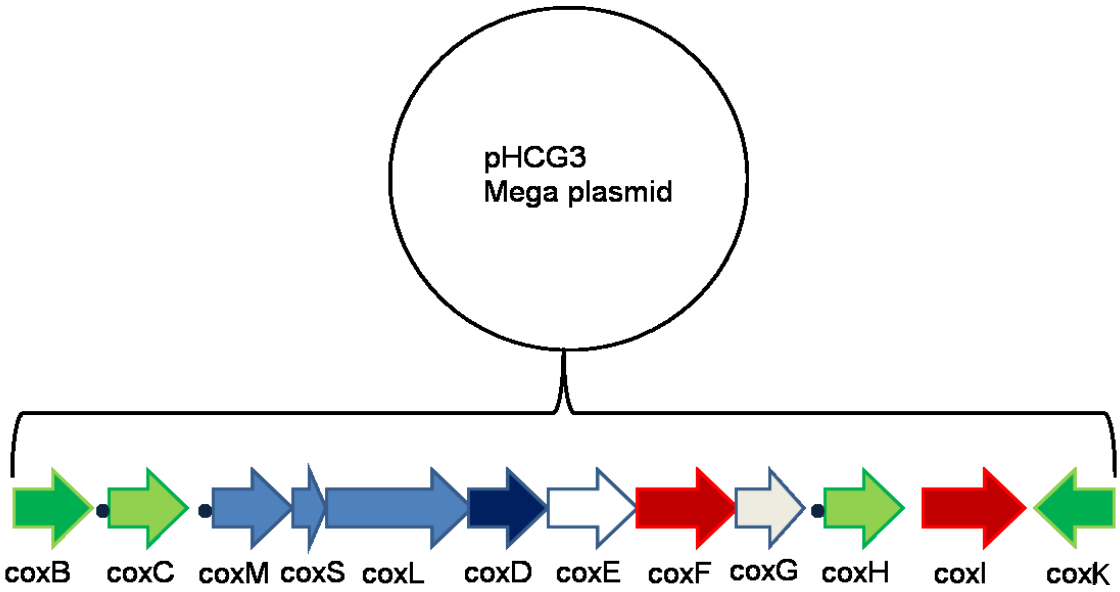

Figure 1.6 Cox gene cluster of the pHCG3 mega plasmid

Schematic overview of the pHCG3 mega plasmid of O. carboxidovorans. Structural genes are in light blue, a putitive AAA+ ATPase in dark blue, putitive xdhC like genes in red and putitive membrane proteins in light green. With the exception of the structural genes, sequences with high similarity are colored in identical color schemes.

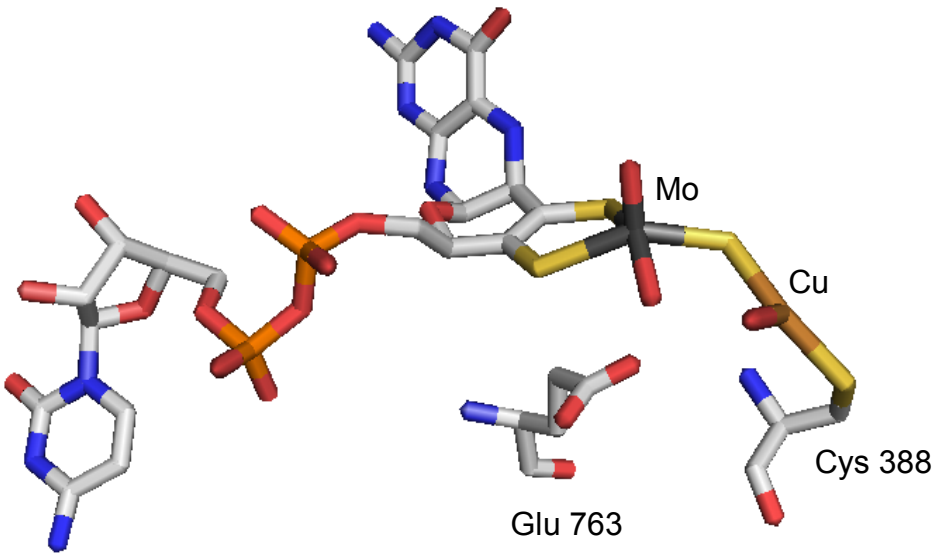

Figure 1.7. The active site of CO dehydrogenase

The active site of CO dehydrogenase was rendered using Protein Data Bank entry 1N5W. Atom colors are CPK with molybdenum in dark grey and copper in brown coordinated by Cys_{388}.

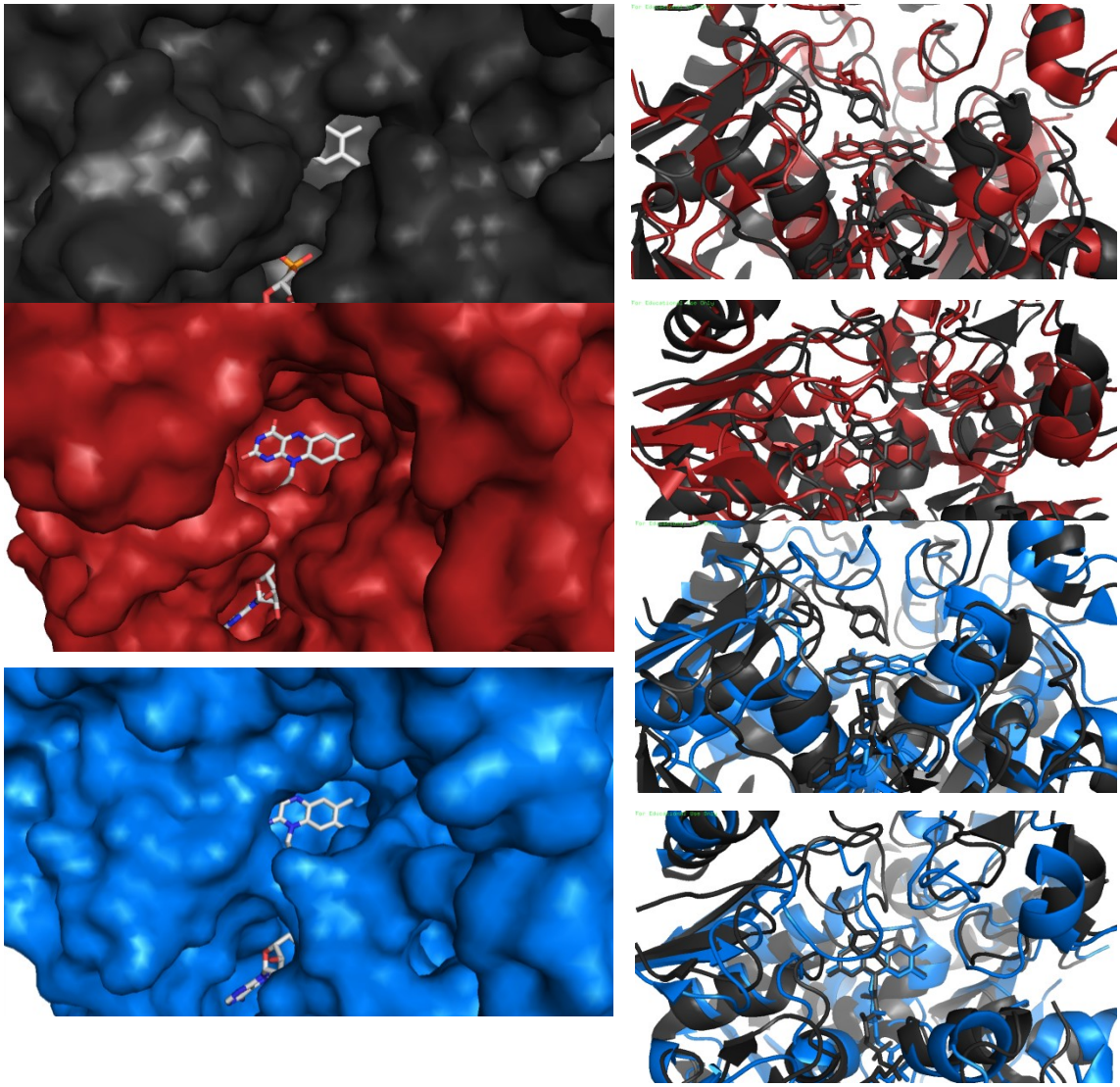

Figure 1.8. The flavin binding site on the medium subunit of CO dehydrogenase

FAD site of CO dehydrogenase (black) (PDB: 1N5W), xanthine dehydrogenase (red), and xanthine oxidase (blue) (PDB: 2W3S) in surface representation (left side) and ribbon structure (right side) (PDB: 3ETR) indicating solvent accessibility and the role of Tyr 193 in blocking access to the FAD cofactor in CO dehydrogenase.

1.3 Mechanism of Carbon Monoxide Dehydrogenase

1.3.1 Carbon monoxide chemistry

Carbon monoxide (CO) is a colorless, odorless gas that is isoelectronic and isosteric to cyanide (CN^-) and dinitrogen (N_2). The molecule consists of a triple bond between carbon and oxygen resulting in (despite the greater electronegativity of oxygen relative to carbon) a partial negative charge on the carbon. The highest occupied molecular orbital (HOMO) has σ molecular orbital character with a lobe projecting away from the carbon towards the oxygen, allowing CO to bond to metal by a weak Lewis σ base through the carbon, Figure 1.9. The lowest unoccupied molecular orbital (LUMO) of CO is a π* orbital, that can overlap with metal t_{2g} *d* orbitals that have local π symmetry allowing CO to act as a Lewis π acid, Figure 1.9.[33] When CO coordinates to a metal there is σ donation to the metal and π back-donation from the metal *d* orbitals into the π* orbital that results in weakening of the CO triple bond. The extent of donation and back-donation affect the C-O bond length: greater π back donation into the π* orbital of CO this creates a stronger metal carbon bond but gives the CO triple bond more double bond character, metals with an occupied *d*-orbital typically follow this case. The degree of triple bond or double bond character can easily be detected by Fourier-transform infrared spectroscopy methods in the C-O stretching frequency. Metal carbonyls can undergo a variety of reactions due to the polarization of the CO molecule. Specifically the CO can be activated towards nucleophillic attack at the carbon atom or electrophillic attack at the oxygen atom.

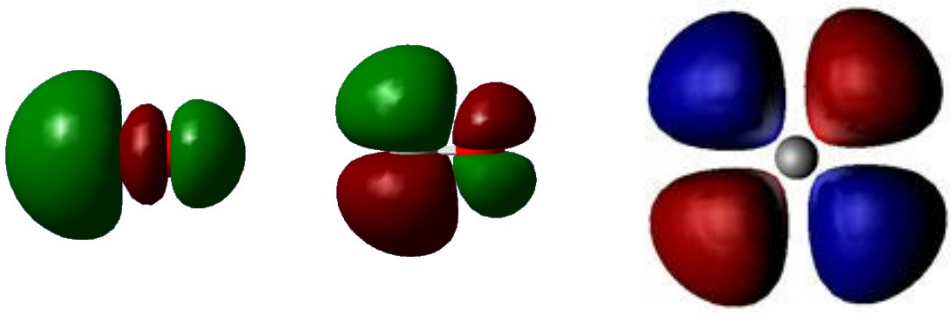

Figure 1.9. Molecular orbitals of CO

The carbon monoxide highest occupied molecular orbital (HOMO) (*left*), lowest unoccupied molecular orbital (LUMO) (*middle*) and generic metal d_{xy} orbital (*right*). Orbitals were rendered using Gaussian 03W.

1.3.2 Catalysis and Proposed Mechanisms of CO dehydrogenase

Recently the kinetics of CO oxidation by CO dehydrogenase have been characterized by Zhang. et. al.[34] CO oxidation is found to be rate-limiting in catalysis, taking place at roughly $51s^{-1}$.[34] This rate is independent of pH and CO concentration (due to experimental limitations concentrations were limited to greater than 5 μM).[34] Once oxidation of CO has taken place the two reducing equivalents gained in the reaction are passed sequentially to the proximal then distal Fe/S cluster and finally to the FAD, Figure 1.4. Once at the FAD the electrons can be passed to the electron transport chain for ATP production via the quinone pool.[12]

From work done on xanthine oxidase and given the general structural similarity between the two proteins it can be inferred that the electron transport between the redox-active cofactors occurs through a tunneling mechanism with electron transfer between the redox-centers much faster than that of the oxidative- or reductive- half reaction rates.[35,36] Mo-to-Fe/SI electron transfer and the reverse are calculated to be 8,300 and 1,800 s^{-1}, respectively.[37] Given the distance from the molybdenum to Fe/SI the observed rate constants suggests that the pterin cofactor does not function as a “wire” providing exceptionally effective electron transfer.[37] The rate constants for electron transfer from the Fe/SII center to the flavin (generating the semiquinone) and the reverse are 25 s^{-1} and 145 s^{-1}, respectively. Given the short distance between the centers it is likely a the simultaneous uptake of protons with the reduction of the FAD slows

the observed rate.[37] In mammalian xanthine oxidase [2Fe-2S] II, the cluster distal to the molybdenum center, has the highest reduction potential with a value of -303 mV, the other redox- active clusters of xanthine oxidase had values of: Mo^{VI}/Mo^{V}, -405 mV; Mo^{V}/Mo^{IV}, -397 mV; [2Fe-2S] I (the proximal cluster), -336 mV; FAD/FADH, -378 mV; $FADH/FADH_2$, -223 mV.[38]

With all four cofactors of CO dehydrogenase with an accessible paramagnetic state, electron paramagnetic resonance (EPR) spectroscopy becomes a valuable tool for investigating reaction intermediates and active site structure. CO dehydrogenase has five known EPR spectra that originate from the molybdenum active site, the FAD cofactor (FADH• semiquinone), and one from each of the [2Fe-2S] clusters, Figure 1.10. Two of the molybdenum based signals represent an inactive species and two originate from the active protein. In all cases the enzyme is partially reduced to give the Mo(V) oxidation state with either CO or a general reductant such as dithionite. The EPR signal of the active site is determined to be a molybdenum based signal and not copper by a $\mathbf{g}_{avg}$ of less than that of the free electron (**g=** [2.0023]), where copper based signals are typically greater than that of the free electron. There is, however, substantial super hyperfine coupling to the Cu^{I} nucleus in the active site ($|\mathbf{A}_{1,2,3}(^{63,65}Cu)|$= [117, 164, 132] MHz).[34] The Fe-S clusters of the enzyme are also EPR active, but only observable at very low temperatures (<20K, where the molybdenum based signal is easily observable at 50-150K) due to the rapid spin relaxation of the clusters. These clusters have approximate g- values of **g**(Fe/S I) = [2.000,

1.938, 1.919] and **g**(Fe/S II) = [2.08, 1.998, 1.900]. There spectra while very similar to xanthine oxidase have a g_1 feature from Fe-SII that is shifted to higher g-value, Figure 1.10, possibly indicating a slightly perturbed reduction potential compared to that of xanthine oxidase.

The large coupling from copper in the EPR spectra is examined further by Gourlay et. al. where active site models [Tp^{iPr}MoO(OAr)(μ-S)Cu(1,4,7-trimethyl-1,4,7-triazacyclononane) (Tp^{iPr}) = hydrotris(3-isopropylpyrazol-1-yl)borate; OAr) = $OC_6H_3{}^tBu_2$-3,5 (**1**) and OC_6H_4Ph-4 (**2**)] are investigated, Figure 1.11.[39] The structure of the model closely resembles the Mo^{VI}-μS-Cu^{I} core of the active site present in the enzyme. EPR and computational methods are used to analyze the model compounds of the active site with the goal of describing the molecular orbitals to provide an explanation behind the strong copper coupling observed. The result of this work indicate the model compound have similar coupling to the copper as seen in CO dehydrogenase, with coupling constants of about 130 MHz indicating a similar electronic structure in the model compound as seen in the enzyme.[39] The computational work with the model indicates that the singly occupied molecular orbital (SOMO) which formally represents the Mo^{V} state is extensively delocalized over the μS and Cu of the active site, Figure 1.11, with the following contributions Mo (Mo d_{xy}, 44%), μS (S *p*, 25%) and Cu (Cu d_{xz}, d_z^2 with some *s* character, 21%).[39] With these findings it was proposed that oxidation of CO need not involve the molybdenum directly, with CO coordinating to copper, nucleophillic attack of the carbon by hydroxide and the utilization of the large

redox- active orbital to pass electrons to the molybdenum maintaining the Cu^{I} state in the course of catalysis.[39]

In addition to this proposed mechanism of catalysis there are several other mechanisms proposed for the reaction carried out by CO dehydrogenase using x-ray crystallography and computational methods. The first mechanism proposed is based off a crystal structure using *n*-butylisonitrile as a substrate. The crystal structure, at 1.1 Å resolution, shows *n*-butylisonitrile bound with the carbon bonded to the equatorial sulfur and oxygen on the molybdenum making a four-member ring and the nitrogen coordinated to the Cu(I).[23] The equivalent complex with CO (isonitriles are isoelectric with CO) is proposed to be the key intermediate in a mechanism where CO inserts between the Cu and μS, is subsequently oxidized and the μS-Cu bond reforms, Figure 1.12.[23]

Two additional mechanisms have been proposed based on computational studies to assess the likelihood the proposed inhibitor-bound complex is indeed a legitimate catalytic intermediate.[23,40,41] In the first study, it is found that the inhibitor-based intermediate leads to a stable state from which the enzyme could progress though a water inserted between the molybdenum and oxygen of the formed CO_2, and the authors conclude that this pathway is a plausible reaction scheme.[41] The second computational work suggests that the inhibitor bound structure is likely formed only in the reaction with isonitrile oxidation, and suggests, like the previous computational study, that there is a minimum for this structure, but that the intermediate represented a dead-end intermediate with CO

and the enzyme is unlikely to recover, Figure 1.13.[40] Both studies concluded that while there is evidence in the crystal structure, it need not represent a true catalytic intermediate.[40,41] There is, however, agreement on the starting state of the active site where the two oxygens coordinated to molybdenum are present in the oxo- form and CO binds to the Cu(I) of the binuclear cluster.[40,41]

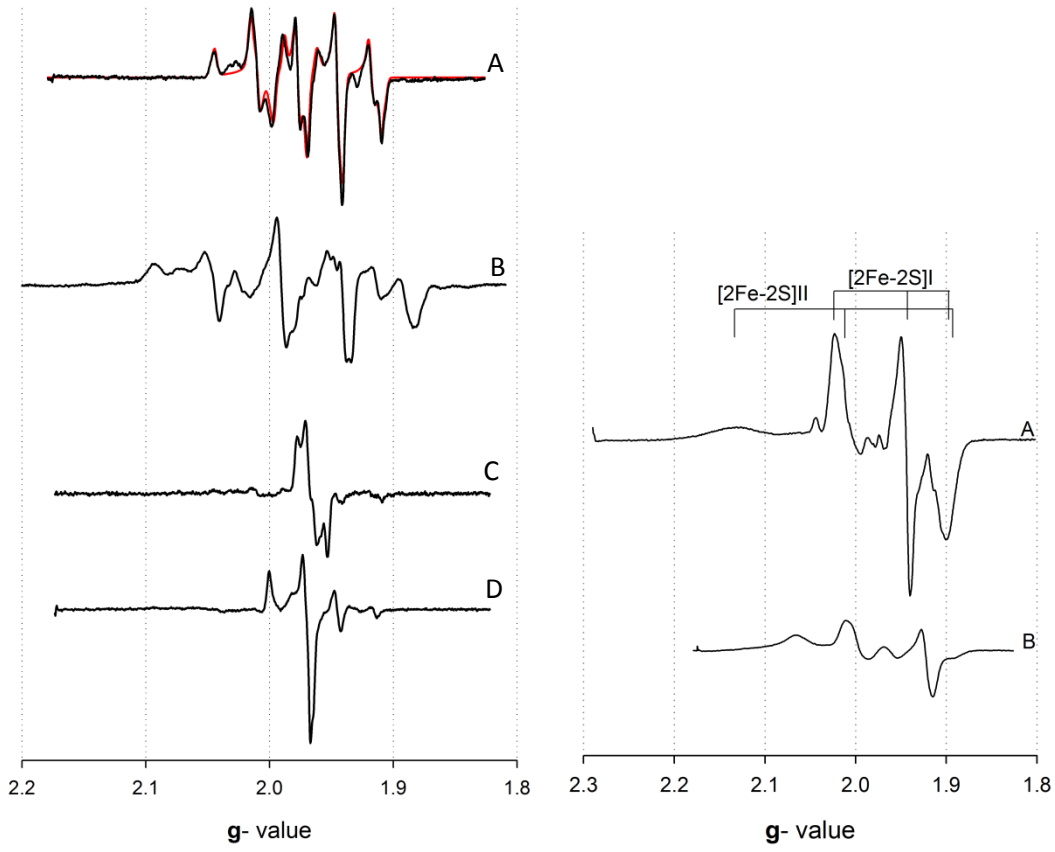

Figure 1.10. Electron paramagnetic resonance (EPR) spectra of CO dehydrogenase.

Left: A. CO dehydrogenase partially reduced by CO, simulation in red with parameters $\mathbf{g}_{1,2,3}$ = 2.0010, 1.9604, 1.9549 and $\mathbf{A}_{1,2,3}$ = 117, 164, 132; *B*. CO dehydrogenase partially reduced by dithionite; *C*. CO dehydrogenase inactive species as isolated or reduced by dithionite; D. CO dehydrogenase inactive species, tri-oxo form, reduced by dithionite.

Right: *A*. Low temperature (18K) spectrum of CO dehydrogenase with two overlapping Fe-S clusters. *B*. Low temperature (18K) spectrum of xanthine dehydrogenase with two overlapping Fe-S clusters.

The EPR instrument settings were: 9.45 GHz microwave frequency; 4 milliwatt microwave power; 5 Gauss modulation amplitude; 150 K.

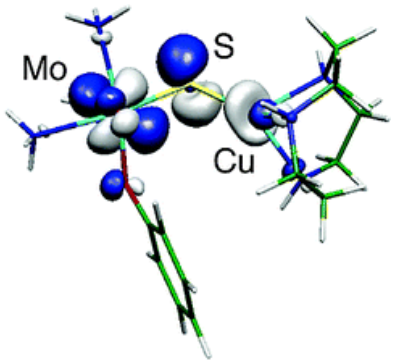

Figure 1.11. Singly occupied molecular orbital of the CO dehydrogenase active site

Active site model of CO dehydrogenase with the singly occupied molecular orbital (SOMO) shown in blue and white

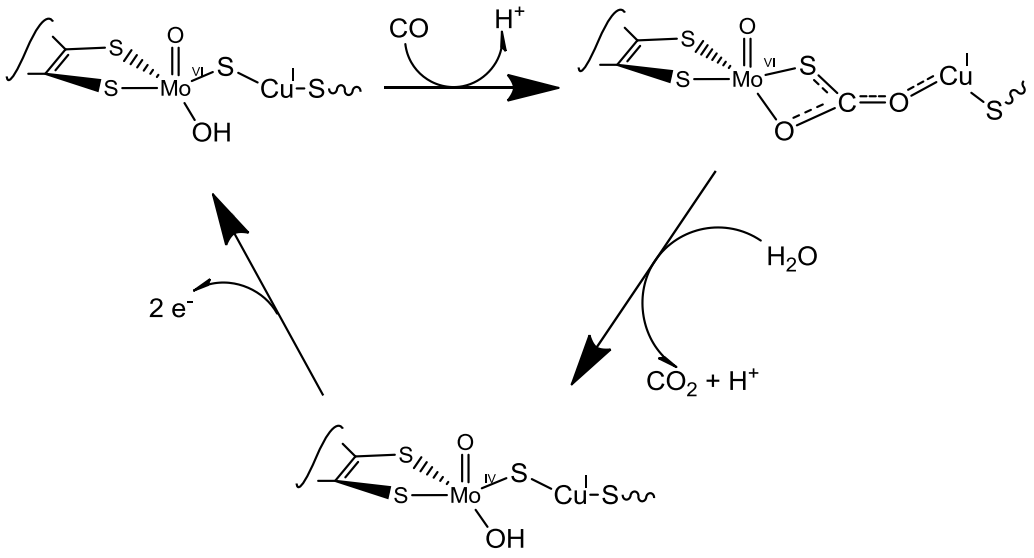

Figure 1.12. Mechanism of CO oxidation by CO dehydrogenase

Mechanism of CO dehydrogenase proposed by Dobbek et. al. by substituting CO for *n*-butylisonitrile in the observed crystal structure (PDB: 1N62).[23]

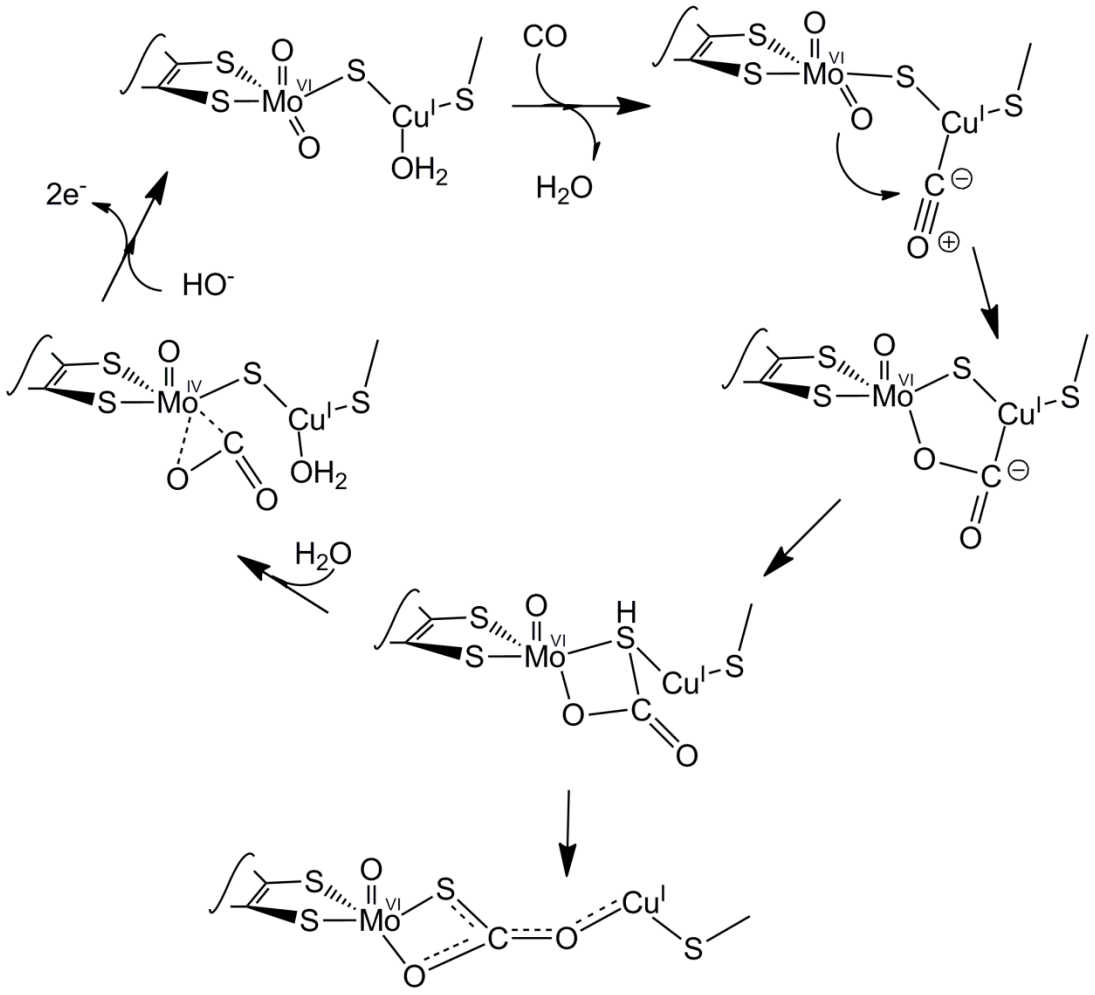

Figure 1.13. Mechanism of CO oxidation by CO dehydrogenase

Mechanism proposed by Hofman et. al. where CO initially coordinates to the Cu in the active site and proceeds to be oxidized. The structure seen crystalographically is described as a dead end intermediate.[40]

1.4. Introduction to present work

Although this enzyme has been described since the late 70's little information is known about the mechanism and roles of the active site metals or their assembly in the organism. In the present work, I have used a variety of experimental techniques to gain insight into the reaction mechanism of the molybdenum- and copper- containing CO dehydrogenase. The first and most widely used method is rapid reaction kinetics (using UV/visible absorption spectroscopy to follow the reaction of the enzyme with substrate) to obtain rate constants and equilibrium binding constants for the reaction. This technique has been applied to identify the physiological electron acceptor of the enzyme, characterize a metal-substituted form of the enzyme, describe the enzyme's reduction by a non-physiological substrate and evaluate inhibition by the product of the enzyme. The second technique utilized is electron paramagnetic resonance (EPR) spectroscopy. This method provides insight into the environment of the active site when molybdenum is in the Mo(V) state and has been used to further characterize the metal-substituted enzyme and, in conjunction with electron nuclear double resonance spectroscopy, establish the structure for a paramagnetic Mo^{V}/Cu^{I} species seen in the course of the reaction with CO, as well as provide an understanding for the unique redox-active molecular orbital of the enzyme's binuclear center. The third technique which is stated above is active site manipulation in order to perturb the reaction in order to gain better understanding of mechanism. In this study we removed the native

copper and replaced it with silver in order to perturb the mechanism and gain understanding of the role of the copper in this unique active site.

From the described studies we find carbon monoxide initially binds to the Cu(I) site of the binuclear center, displacing water, to be activated for nucleophillic attack by hydroxide or the equatorial oxo group on the molybdenum. The extent of back-bonding from metal to carbon determines degree of activation, evident in the metal substitution studies. The reducing equivalents generated by the oxidation of CO are then passed to the electron transport chain via the quinone pool.

Chapter 2

Materials and Methods

2.1. Materials

Carbon monoxide, carbon dioxide and hydrogen gas were obtained from Airgas, Inc. at a purity of at least 99.5%. 1,4-benzoquinone, 1,2-naphthoquinone-4-sufonic acid, 1,4-naphthoquinone, and ubiquinone-1 were purchased from Sigma-Aldrich. Isotopically enriched D_2O (99.9%) and D_2 (99.8%) were obtained from Cambridge Isotope Lab, Inc. All other chemicals and reagents were obtained at the highest quality and purity commercially available and used without additional purification.

2.2. Bacterial Cultivation and Enzyme Purification

O. carboxidovorans (ATCC 49405) cells were grown at 30° C, pH 7 in a 19 L fermentor (BioFlo 415, New Brunswick) containing minimal media comprised of 3.57 g/L Na_2HPO_4, 1.5 g/L KH_2PO_4, 1.5g/L NH_4Cl, 0.098 g/L $MgSO_4$ (anhydrous), 0.02 g/L $CaCl_2$•2 H_2O, 0.0012 g/L $Fe^{3+}(NH_4)$-citrate, 1ml silicone emulsion (anti-foam) and CO as the carbon source (introduced as a mixture of 20% CO and 80% air, or 11% CO, 86% Air and 3% CO_2). Fermentor batches were inoculated with 1L cell growth from the previous fermentation batch, or a 1L inoculation of the minimal medium described above with the addition of 0.3% acetate and grown at

30° C in a shaker at 270 RPM. Cells were harvested in late log phase (OD_{436} >5), washed in 50 mM HEPES (pH 7.2) and stored at -80° C until needed.[16]

CO dehydrogenase was purified according to the procedure described by Zhang *et al*.[34] All chromatography steps were carried out on an ÄKTA purifier (GE Healthcare) at 4° C. About 100 g of thawed cells were suspended in 200 mL of 50 mM HEPES buffer containing 1 mM EDTA, 0.2 mM PMSF, and 5 mg of DNase I, pH 7.2, and disrupted with French press (FA-078A, Thermo Electron Co.). Cell debris was removed by ultracentrifugation at 100 k × g for 2 h. The supernatant was loaded onto a Q-sepharose column (40 cm × 2.6 cm) pre-equilibrated with 50 mM HEPES pH 7.2 and 1mM EDTA (Buffer A), and eluted by six column volumes of a linear gradient of 0 to 0.5 M NaCl in Buffer A. Fractions containing significant CO dehydrogenase activity were pooled, concentrated in an Amicon concentrator with 100 kDa MW cut-off, and passed through a Sephacryl S-300 column (40 cm × 2.6 cm) in buffer containing 50 mM HEPES, pH 7.2, 150 mM NaCl and 1 mM EDTA . Fractions were analyzed for both CO dehydrogenase activity and optical absorption; only those of high activity and free of contaminants were pooled and concentrated in the presence of additional 500 µM FAD then stored in liquid nitrogen until use. The purified enzyme showed an absorbance ratio of A_{280}/A_{450} ~5.5 and A_{450}/A_{550} ~3.1, Figure 2.1.

Side fractions from the chromatography steps that did not meet the above purity criteria were subjected to Butyl-Sepharose FF chromatography. Enzyme

(typically 1 mL of 200 μM CO dehydrogenase) was loaded onto the column in Buffer A (50 mM HEPES, 0.85 M ammonium sulfate, pH 7.2) and eluted with a linear gradient with Buffer B (50 mM HEPES, 20% 2-propanol, pH 7.2) over six column volumes. Fractions containing significant CO dehydrogenase activity were pooled and stored as above.

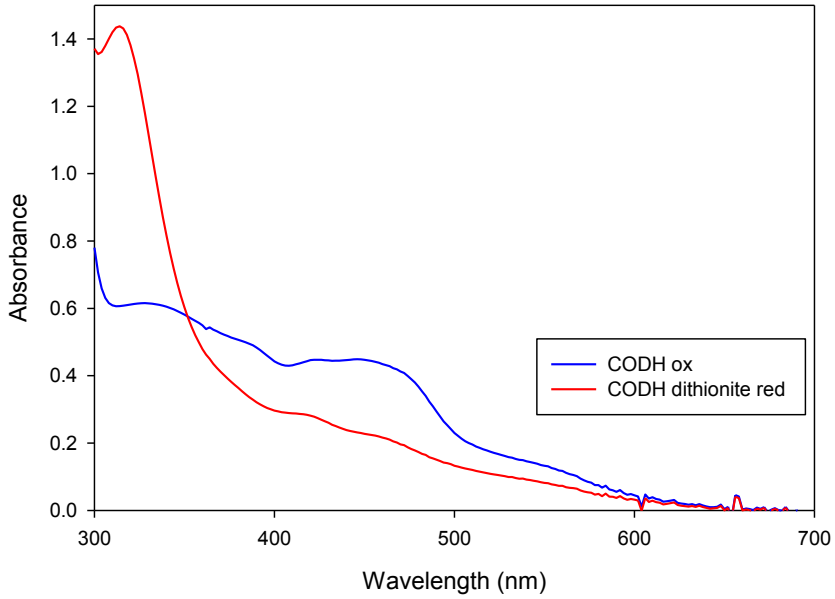

Figure 2.1. UV-visible spectra of CO dehydrogenase

UV-visible spectra of 15 µM CO dehydrogenase in 50 mM HEPES, pH 7.2, oxidized (blue) or dithionite reduced (red).

2.3. Purification of Cytochrome b_{561}

Cytochrome b_{561} was purified from *O. carboxidovorans* grown as described above. 100 g of thawed cells were resuspended in 50 mM HEPES (pH 7.2) containing 1 mM EDTA, 5 mg DNase, 0.2 mM PMSF and broken open by French press (FA-078A, Thermo Electron Co.). Cell debris were separated by ultracentrifugation at 100k x g for 2 h. Cell membranes were solubilized in 50 mM HEPES, pH 7.2, containing 1 mM EDTA, 0.2 mM PMSF and 10% v/v Triton X-100. The non-solubilized membranes were separated by ultra centrifugation at 100k x g for 2 h. The soluble fraction was loaded onto a CM anion exchange column (11cm x 1.5cm) using an ÄKTA FPLC apparatus (GE Healthcare) at 4°C; the column was pre-equilibrated with 50 mM HEPES, pH 7.2, containing 0.1 mM EDTA and 0.2% Triton X-100. Elution was carried out over 10 column volumes in a linear gradient from 0 mM to 500 mM NaCl. Fractions containing cytochrome b_{561} were pooled and concentrated using an Amicon concentrator equipped with a 10 kDa cutoff filter. The identity of cytochrome b_{561} was verified by UV-vis spectroscopy, Figure 2.2, with an absorbance peak at 415 nm in the oxidized cytochrome and 425 nm, 530 nm, and 561 nm in the reduced cytochrome. Approximately 20-50 µg of cytochrome b_{561} was obtained from 100 g of wet cell mass. Fractions containing other cytochromes were also saved and examined for activity with CO dehydrogenase.

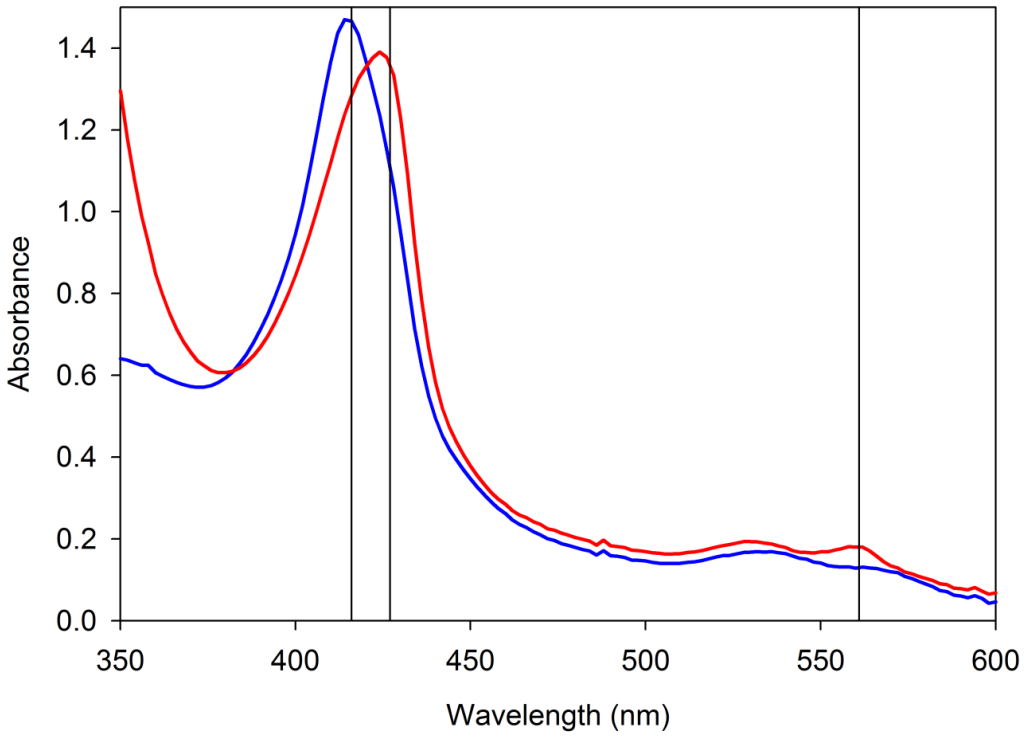

Figure 2.2. Spectra of the oxidized and reduced cytochrome b_{561}
Spectra of cyt b_{561} in 50mM Hepes (pH 7.2) 0.2% Triton X-100 : cyt b_{561} Reduced- Soret band at 427, α band at 561, β band at 530, cyt b_{561} oxdized- Soret band at 416, α band at 564, β band at 535. Oxidized cyt b_{561} was reduced by addition of dithionite.

2.4. Protein determination and activity assay

CO dehydrogenase concentrations were quantified by the absorbance at 450 nm (ε_{450}=36 $mM^{-1}cm^{-1}$ per monomer) and 550 nm and purity assessed by the ratios of absorbance at 280 nm, 420, nm, 450 nm and 550 nm: the purified enzyme had absorbance ratios of A_{280}/A_{450} ~5.5, A_{450}/A_{550} ~2.9 and A_{450}/A_{420} > 1.[34] Routine activity was determined by the CO-dependent reduction of methylene blue (ε_{615}=37.11 $mM^{-1}cm^{-1}$) at 30° C.[19,34] In this assay, a side-arm cuvette (Starna Cells, inc) was filled with 2 mL of 50 μM methylene blue in 50 μM KH_2PO_4, sealed with a rubber septum and made anaerobic by bubbling with argon. This anaerobic solution was then bubbled with CO for 15 minutes to a 1 mM CO concentration. The assay, monitoring the bleaching of methylene blue at 615 nm, was initiated by adding 10 μL of 5μM CO dehydrogenase with a Hamilton syringe and the time course recorded over 300s, taking the slope for rate determination using an HP 8452A UV-visible spectrophotometer. A second assay utilized 1,4-benzoquinone as oxidizing substrate, following reduction of, *e.g.*, 50 μM 1,4-benzoquinone at 246 nm. A serum-stoppered cuvette containing 50 μM 1,4-benzoquinone in 2mL of 50 μM HEPES, pH 7.2, was bubbled with 100% CO for 15 min in the dark, after which 10μL of 5 μM CO dehydrogenase solution was added by Hamilton syringe. The activity was determined using an extinction change for 1,4-benzoquinone reduction, $\Delta\varepsilon_{247}$=20.2 $mM^{-1}cm^{-1}$, obtained from the extinction coefficient ε_{247}=20.6 $mM^{-1}cm^{-1}$ and ε_{247}=0.42 $mM^{-1}cm^{-1}$ for the oxidized 1,4-benzoquinone.[42]

2.5. Copper reconstitution of CO dehydrogenase

Prior to use, all enzyme preparations were reconstituted with sulfur and copper using a modification of the procedure of Resch *et al.*[43] 50 µM CO dehydrogenase in 1.0 mL of 50 mM Tris-HCl, pH 8.2 was made anaerobic by alternately evacuating and flushing with O_2-scrubbed Ar gas over the course of an hour. Appropriate volumes of stock solutions of 10 mM methyl viologen and 100 mM Na_2S were added to give final concentrations of 0.1 mM and 2.0 mM, respectively, followed by the addition of a volume of a ~0.1 M dithionite stock solution sufficient to sustain the blue color of the reduced viologen. This was incubated at 20° C for 12-18 hr (or 8hrs at 37° C) under an atmosphere of argon gas. The enzyme was then passed through a G-25 chromatography column equilibrated with aerobic 50 mM Tris-HCl, pH 8.2 to remove excess Na_2S, dithionite and methyl viologen. The enzyme was then made anaerobic again following the above procedure. A stock solution of 10 mM Cu^{I}-thiourea was prepared by dissolving $Cu^{II}Cl_2$, thiourea, and sodium ascorbate as a reductant in a 1:3:1 (w/w) ratio in anaerobic water, and a sufficient volume of this stock solution was then added by Hamilton syringe to the enzyme solution at a final concentration of 0.2 mM. The Cu^{I}-enzyme solution was incubated 5-10 hr at 20° C. A final G-25 column, again equilibrated with aerobic 50 mM Tris-HCl, pH 8.2, was used to remove excess Cu^{I}. The enzyme was assayed for activity as described above with fully active enzyme giving a k_{cat} of ~50 s^{-1}. The degree of

functionality was independently determined by comparing the extent of enzyme bleaching by CO (which reduces only the fully functional enzyme) as observed at 450 nm with that seen using dithionite (which reduces both functional and non-functional enzyme) enzyme.[23] Our enzyme preparations were typically 40-50% active, comparable to the levels seen by others.[43] Unless otherwise stated, enzyme concentrations are given as functional enzyme, corrected for the fraction of non-functional enzyme present.

2.6. Copper removal and silver incorporation

In order to incorporate silver into the active site, the enzyme was first inactivated by incubation of 100 µM CO dehydrogenase with 5 mM KCN for 10 h under an atmosphere of Ar gas at 20 °C to remove the copper and bridging sulfur.[43] Activity was determined using the reduction of methylene blue (ε_{615}= 37.11 mM^{-1} cm^{-1}) in 50mM potassium phosphate, pH 7.2, at 30 °C as described in chapter 2.2.[19] Fully inactive enzyme displayed no reduction of methylene blue over a ten minute period.

Incorporation of silver into CO dehydrogenase was accomplished by a modification of the above copper reconstitution protocol developed by Resch *et. al.*[43] Approximately 50 µM CO dehydrogenase and 100 µM methyl viologen in 1.0 mL of 50 mM Tris-HCl (pH 8.2) was made anaerobic by alternately evacuating and flushing with O_2-scrubbed argon gas over the course of 1 h. An appropriate volume of an anaerobically prepared stock solution of 100 mM Na_2S

was added to give a final concentration of 2.0 mM, followed by the addition of a sufficient volume of an 0.1 M dithionite stock solution to sustain the blue color of the reduced viologen, followed by incubation at 20 °C for 12-18 h under an atmosphere of argon gas. The enzyme was then passed through a G-25 chromatography column equilibrated with aerobic 50 mM Tris-HCl (pH 8.2) to remove excess Na_2S, dithionite, and methyl viologen. Following elution from the column the enzyme was concentrate to 50 μM and made anaerobic. A stock solution of 10 mM Ag(I)-thiourea was prepared by dissolving $AgNO_3$ and thiourea in a 1:3 molar ratio in anaerobic water. An appropriate volume of this stock solution was then added to the anaerobic enzyme to give a final concentration of 0.2 mM Ag(I), followed by a 5-10 h incubation at 20 °C. A final G-25 column, equilibrated with aerobic 50mM HEPES (pH7.2), was used to remove excess Ag(I). Enzyme was assayed for activity,[19] and the degree of functionality was independently determined by comparing the extent of enzyme bleaching, as observed at 450 nm, by CO (which reduces only the fully functional enzyme) with that seen using dithionite (which reduces both functional and nonfunctional enzyme).[23] Our preparations of Ag substituted enzyme typically yielded 30% functional enzyme, compared to ~50% active protein in the native Cu reconstituted enzyme.[43] The catalytic velocities reported here have been corrected for the amount of nonfunctional protein by adjusting the enzyme concentration used for the concentration of functional enzyme. Substitution attempts were also made using $MnCl_2$, $CoCl_2$, $ZnCl_2$, AuCl, or $HgCl_2$ but no

evidence of successful substitution was observed by EPR of the partially reduced enzyme by CO or enzyme assay.

In order to confirm the presence of silver in the protein inductively coupled plasma atomic emission spectroscopy (ICP-AES) analysis was done. ICP-AES showed some trace amounts of copper still present in the enzyme preparations (<10% of the enzyme molybdenum) but likely not catalytically relevant as will be discussed in Chapter 4. EPR measurements were prepared and recorded as described below.

2.7. Steady-state kinetics

Steady-state studies monitoring the reduction of methylene blue and quinones were monitored by stopped-flow spectroscopy (using an Applied Photophysics, Inc. SX-18MV). Assays were prepared by bubbling anaerobic solutions of each in 50 mM HEPES (pH 7.2) with CO for 15 min to give 1 mM CO (previous studies having shown that concentrations of CO above 100 μM were saturating in steady-state assays[34]). The concentration ranges used were 11 μM to 97 μM for ubiquinone-1 and 8.4 μM to 191 μM for 1,4-benzoquinone or 50 μM methylene blue in 50 mM phosphate, pH 7.2, in the presence of 10-200 mM bicorbonate. The reaction was initiated by the addition of 10 μL of 2 μM CO dehydrogenase, and the reaction monitored by the spectral change at 275 nm or 246, respectively, over 300 s at 25°C. Activities were obtained from the initial

slopes of each assay, calculated using ε_{278}=14.7 $mM^{-1}cm^{-1}$ for ubiquinone-1[44] and $\Delta\varepsilon_{247}$=20.2 $mM^{-1}cm^{-1}$ for 1,4-benzoquinone.

For steady state kinetics using H_2 as reducing substrate, a syringe with substrate was prepared by bubbling Ar gas through a rubber septum into the solution for 15 min to make the solution anaerobic followed by bubbling with H_2 for 1 hr. Dilutions of H_2-saturated buffer (780 μM) were made with anaerobic 50 mM HEPES, pH 7.2 to give solutions ranging from 20 μM to 780 μM [H_2]. Saturated H_2 concentrations were calculated from a Henry's law constant of 0.00078 mol/kg•bar in water.[5] Initial rates were measured in triplicate at each concentration of H_2 (12-780 μM), averaged and plotted against H_2 concentration. Hyperbolic fits were obtained in SigmaPlot (Systat Software inc.) using the Michaelis–Menten equation to obtain k_{cat}^{H2} and K_m^{H2} values.

A solvent kinetic isotope study was performed under the same conditions as described above using 50 mM HEPES in D_2O, pD 7.2, with the addition of varying concentrations of ubiquinone-1 in D_2O. CO dehydrogenase in D_2O prepared by anaerobic buffer exchange G-25 column into 50 mM HEPES in D_2O, pD 7.2.

2.8. Rapid reaction kinetics

The oxidative half-reaction of CO dehydrogenase was monitored by stopped-flow spectroscopy (using an Applied Photophysics, Inc. SX-18MV). Standard reaction conditions were 50 mM HEPES, pH 7.2, 25°C. Enzyme at a

concentration of ~5 μM before mixing was placed in a glass tonometer equipped with a sidearm cuvette and made anaerobic by repeated evacuation and flushing with O_2-scrubbed Ar gas over the course of an hour. The anaerobic enzyme was then titrated to full reduction with an anaerobic solution of ~0.1M sodium dithionite in 50 mM HEPES, pH 7.2, monitoring enzyme reduction spectrophotometrically. The tonometer was then mounted on the stopped-flow apparatus and mixed with varying concentrations of anaerobic, oxidized quinone substrate in 50 mM HEPES, pH 7.2, the reaction being monitored by the absorbance increase observed at 450 nm or 550 nm due to the reoxidation of the enzyme. Kinetic transients thus obtained were fit to single exponents using the ProData Viewer software package to obtain rate constants, which were averaged and plotted as a function substrate concentration. When saturating kinetic behavior of k_{obs} as a function of [quinone] was observed, values for k_{ox}, the limiting rate constant at high [S], and dissociation constant, K_d, were obtained from hyperbolic fits to these plots using SigmaPlot (Systat Software, Inc.). When linear behavior was observed, the ratio k_{ox}/K_d was determined directly from the slope.

The reductive half-reaction of CO dehydrogenase was monitored by stopped-flow spectroscopy using the standard reaction conditions were 50 mM KH_2PO_4, pH 7.2, at 25 °C. Enzyme at a concentration of ~5 μM before mixing was placed in a glass tonometer and made anaerobic by repeated evacuation and flushing with O_2-scrubbed Ar over the course of an hour. The anaerobic

oxidized enzyme was then mounted on the stopped-flow apparatus and mixed with varying concentrations of CO (from 5-500μM after mixing) or H_2 solutions (12-390μM after mixing) in the presence or absence of 10-200 mM bicarbonate. The reaction was monitored by the absorbance decrease of the enzyme observed at 450 nm or 550 nm. Kinetic transients thus obtained were fit to single exponentials using the ProData Viewer software package to obtain the rate constants, which were averaged for each concentration of CO (or H_2) and plotted as a function substrate concentration. When saturating kinetic behavior for k_{obs} as a function of [S] was observed, values for k_{red}, the limiting rate constant at high [S], and dissociation constant, K_d, were obtained from hyperbolic fits to these plots using SigmaPlot.

The pH dependence of the reductive half-reaction over the pH range 6 to 10 was determined using 50 mM phosphate buffer for pH 6.0, 50 mM HEPES for pH 7.2, 50 mM TRIS-HCl for pH 8.0 and pH 9.0, and 50 mM CAPS for pH 10.0. The activation energy of the reaction with H_2 was determined in 50 mM HEPES, pH 7.2 over the temperature range 5 to 30 °C and analyzed using an Arrhenius or Eyring plot of the data to obtain the activation parameters of the enzyme.

Primary and solvent kinetic isotope effects were determined by performing the experiment using D_2 as substrate or in D_2O as solvent, respectively. In preparing solutions in D_2O, the differing ionization constant of D_2O relative to H_2O was taken into account using the formula pD = (pH meter reading) + 0.4.

Enzyme-monitored turnover experiments, following the reaction of enzyme with CO or H_2 and electron acceptor by the absorbance change of the enzyme, were performed using the stopped flow apparatus by mixing 5 μM (after mixing) anaerobic CO dehydrogenase (prepared as above) with a solution containing 500 μM CO (or 390 μM H_2) and 20-50 μM 1-4 benzoquinone and monitoring wavelengths from 300 nm to 700 nm. Substrate solutions were prepared by making an appropriate buffer anaerobic using Ar for 15 min followed by bubbling of an CO or H_2 until a saturated solution was obtained. To this solution 10 μL of an appropriate anaerobic stock solution of the electron acceptor was added.

2.9. Titrations of CO dehydrogenase with quinones

Titrations were performed using 4 μM to 8 μM CO dehydrogenase in 50 mM HEPES, pH 7.2 at 20°C. Titrations of oxidized enzyme with oxidized quinone were carried out aerobically, following the spectral change observed in the vicinity of 450 nm. Titration of oxidized enzyme with reduced quinone (prepared by directly bubbling Ar in a cuvette for 15 min to make anaerobic and titrated to reduction with 0.1 M sodium dithionite using a Hamilton syringe, following quinone reduction at 247 nm) was carried out anaerobically. Enzyme solutions being made anaerobic so by alternately evacuating and flushing the enzyme solution in an anaerobic cuvette with O_2-scrubbed Ar gas for 1 hour. Aliquots of anaerobic, reduced 1,4-benzoquinone were then added via Hamilton syringe and the absorption change in the visible region monitored

spectrophotometrically. For 1,4-benzoquinone, plots of absorbance change *vs.* [quinone] were used to obtain K_d, which was determined by fitting the data to the hyperbolic equation:

$$A_{obs} = (\Delta A_{max} \cdot x)/(K_d + x)$$

2.10. Inhibition of CO dehydrogenase by diphenyliodonium chloride

Inactivation of the FAD cofactor of CO dehydrogenase was accomplished by covalent modification of the FAD with diphenyliodonium chloride using a modification of the procedure of Chakraborty and Massey.[45] 10 µM CO dehydrogenase in 50 mM HEPES, pH 7.2 was flushed with Ar for 1 hr and reduced with ~2 fold excess sodium dithionite. Diphenyliodonium chloride was added to a final concentration of 1 mM and incubated at 20° C for 2 hr. Excess diphenyliodonium chloride was removed by G-25 column and the enzyme assayed for activity. Spectral changes and specific activity of the enzyme with ubiquinone-1 and methylene blue were used to assess the degree of inhibition, as described above.

2.11. Electron paramagnetic resonance (EPR) spectroscopy

EPR spectra were recorded using a Brüker Instruments ER 300 spectrometer equipped with an ER 035M gaussmeter and HP 5352B microwave frequency counter. Temperature was controlled at 150 K using a Brüker ER 4111VT liquid N_2 cryostat. Samples were prepared with anaerobic 40-100 µM

CO dehydrogenase (native Cu or Ag substituted, see above) in 50 mM HEPES, pH 7.2 (or in 50 mM HEPES, pD 7.2), and added to a sealed Ar flushed EPR tube and titrated to reduction with a stock solution of 0.1 M dithionite, or by incubation with a suitable substrate (CO, H_2 or D_2). The EPR spectrum of the enzyme in D_2O was obtained by passing CO dehydrogenase (native or Ag substituted) through a Sephedex G-25 column equilibrated with HEPES-D_2O buffer, pD 7.2. Once in D_2O buffer, samples were made anaerobic and reacted with substrate or reduced with dithionite as described above. Samples were immediately frozen in an ethanol-dry ice bath and stored in liquid N_2. For experiments involving the oxidative half-reaction, samples were mixed with an appropriate amount of 1-4 benzoquinone or ubiquinone-1 and controls of fully oxidized or fully reduced by titration with dithionite were also prepared.

2.12. Electron nuclear double resonance (ENDOR) spectroscopy

ENDOR samples were prepared by making the enzyme (at a concentration of ~200 μM) anaerobic by cyclic evacuation and flushing with O_2-scrubbed argon gas for 1 h, followed by reduction under 1 atmosphere of CO for 30 s prior to freezing in a dry ice-acetone bath and storage in liquid N_2. Samples were shipped to the lab of Brian Hoffman at Northwestern University in a liquid N_2 dewar. The data was collected and analyzed by collaborators using a Brüker Instruments ER 300 spectrometer equipped with an ER 035M gaussmeter and HP 5352B microwave frequency counter. Temperature was controlled at 150 K

using a Brüker ER 4111VT liquid N_2 cryostat. 35 GHz pulsed EPR/ENDOR spectra were recorded as reported previously.[46,47]

Chapter 3

Identification of the physiological electron acceptor for CO dehydrogenase and characterization of the oxidative half reaction

3.1. Introduction

Carboxidotrophic bacteria are able to utilize CO as a carbon source and sole energy source for growth. Carbon monoxide oxidation by CO dehydrogenase generates reducing equivalents utilized by the cell to produce ATP and redox molecules for metabolic pathways, which are passed into the electron transport chain. The enzyme has been shown to be localized to the cytosolic side of the bacterial membrane when the enzyme is functional,[48] with the membrane interaction likely mediated by the other proteins encoded by the CO dehydrogenase gene cluster (specifically *coxC* and *coxH* which are likely to have multiple trans-membrane helicies) allowing the enzyme to be "docked" to the membrane and allow for interaction with its physiological electron acceptor.[30]

In previous work by Meyer and coworkers it was suggested cytochrome b_{561} is the physiological electron acceptor for the enzyme.[24] The evidence for this conclusion comes from monitoring whole cell extracts where a peak at 561nm (assigned to cyt b_{561}) was found to be the last reduced peak. This was later investigated further with reconstituted membranes and partial purification of cytochromes with CO dehydrogenase.[49,50] On the other hand, Kim et. at. found

that membranes depleted of quinones prevented the cytochrome reduction and only after addition of quinone to the membranes was reduction of cytochromes re-established.[51]

In the present study we have investigated the rapid reaction kinetics of the reduced CO dehydrogenase with a series of quinones. We find various quinones to serve very effectively as oxidizing substrates for CO dehydrogenase, reacting with reduced enzyme with rate constants large enough to support catalysis. We conclude that ubiquinone is the likely physiological oxidant of CO dehydrogenase. By contrast cytochrome b_{561} is found to not readily accept reducing equivalents from reduced CO dehydrogenase, and we are unable to identify any other cytochrome from *O. carboxidovorans* capable of doing so.

3.2 Results

3.2.1. CO dehydrogenase reactivity toward cytochrome b_{561}

Cytochrome b_{561} was examined for reactivity toward CO dehydrogenase in both steady-state and rapid-reaction experiments. In the assays performed, cytochrome b_{561} in 50 mM HEPES, pH 7.2, containing 0.2% Triton X-100 or N,N-dimethyldodecylamine-N-oxide was made anaerobic by repeated evacuation and flushing with O_2-scrubbed Ar followed by CO bubbling. The activity assay was carried out over 10 min observing total spectral change with an emphasis near 415 nm and 561 nm, Figure 3.1, but no reduction of cytochrome b_{561} was observed in these experiments. Other cytochrome-containing fractions isolated

from soluble and membrane cell fractions included multiple cytochromes *c* and cytochrome *a*, and these were also examined for activity toward CO dehydrogenase; in no case was cytochrome reduction observed. Only when 5 μM 1,4-benzoquinone was added to the assay with cytochrome *c* was reduction observed, as reflected in the absorbance increase at 550 nm and a shift of the Soret band from 410 nm to 415 nm. These results suggest that cytochrome reduction was mediated by the quinone, which served as the proximal oxidant for the enzyme.

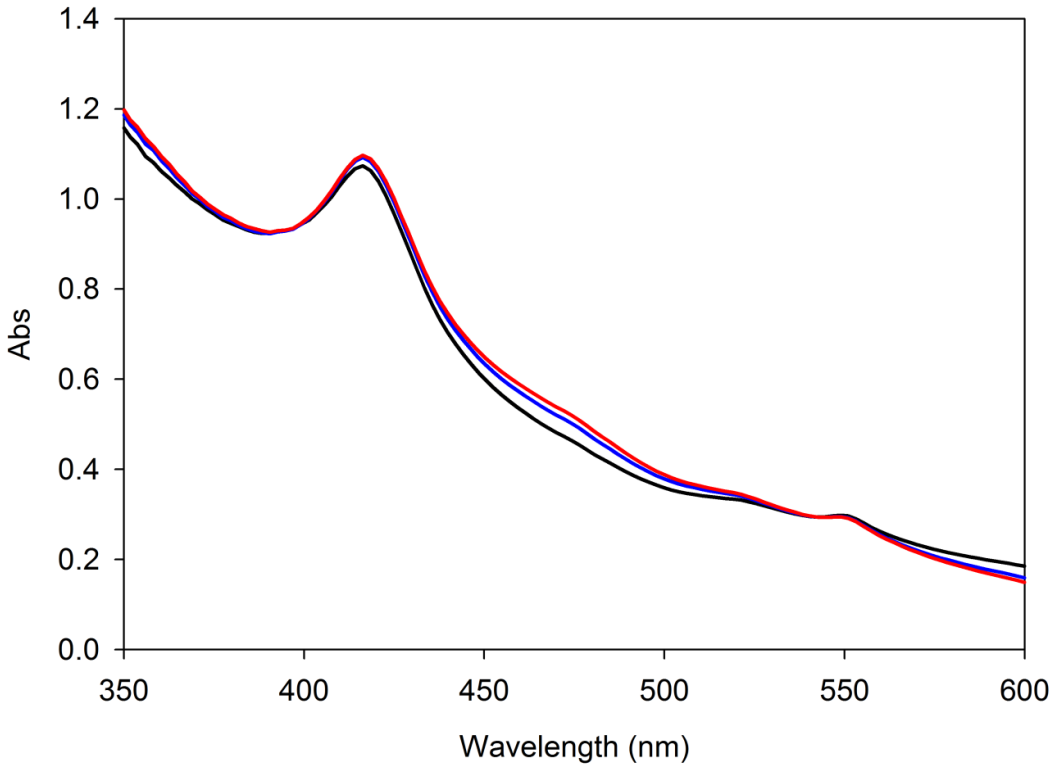

Figure 3.1. Rapid reaction kinetics of CO dehydrogenase and cyt b_{561}

Rapid reaction kinetics using purified cyt b_{561} in 50mM Hepes (pH 7.2) 0.2% Triton X-100 reacted with 5 µM CO dehydrogenase in a stopped flow apparatus. Traces shown are at 1s (black), 250s (blue), and 500s (red). The soret shift from 416nm to 427 nm, or accumulation of a peak at 561 nm of the cyt b_{561} is not observed in the course of the reaction.

3.2.2. Steady state kinetic studies:

Based on the above results suggesting that 1,4-benzoquinone is an oxidizing substrate of CO dehydrogenase, a steady-state analysis was performed using 1,4-benzoquinone as oxidizing substrate. The assay was performed under the standard conditions of 25° C in 50 mM HEPES pH 7.2, with solutions of 8.4 μM to 191 μM 1,4-benzoquinone placed in a serum-stoppered cuvette and bubbled first with argon and then CO to give a concentration of 400 μM. The reaction was followed by the spectral change at 246 nm associated with reduction of the quinone. Significant catalytic rates were observed. A plot, Figure 3.2 and Table 3.1, of observed catalytic velocity versus [1,4-benzoquinone] was hyperbolic and a fit to the data yielded a k_{cat} of 52 s^{-1}, K_m of 16.4 μM and k_{cat}/K_m of 3.19 x 10^6 $M^{-1}s^{-1}$. This is essentially identical to the previously observed k_{cat} of 93.3 s^{-1} (per dimer) using methylene blue as oxidizing substrate, consistent with the previous conclusion that the reductive half-reaction was principally rate-limiting.[34] Ubiquinone-1 was also examined as substrate, but in this case (owing to its limited water solubility) it proved impossible to obtain sufficiently high concentrations of substrate to yield saturating kinetics. A plot of the observed catalytic velocity versus [ubiquinone-1] thus yielded a straight line, Figure 3.3 and Table 3.1, and from the slope a value for the ratio k_{cat}/K_m of 5.81 x 10^4 $M^{-1}s^{-1}$ was obtained. When the steady-state kinetics with ubiquinone-1 were repeated in D_2O, Figure 3.3, a solvent isotope effect of 1.4 was obtained from the ratio of $^{H}(k_{cat}/K_m)/^{D}(k_{cat}/K_m)$.

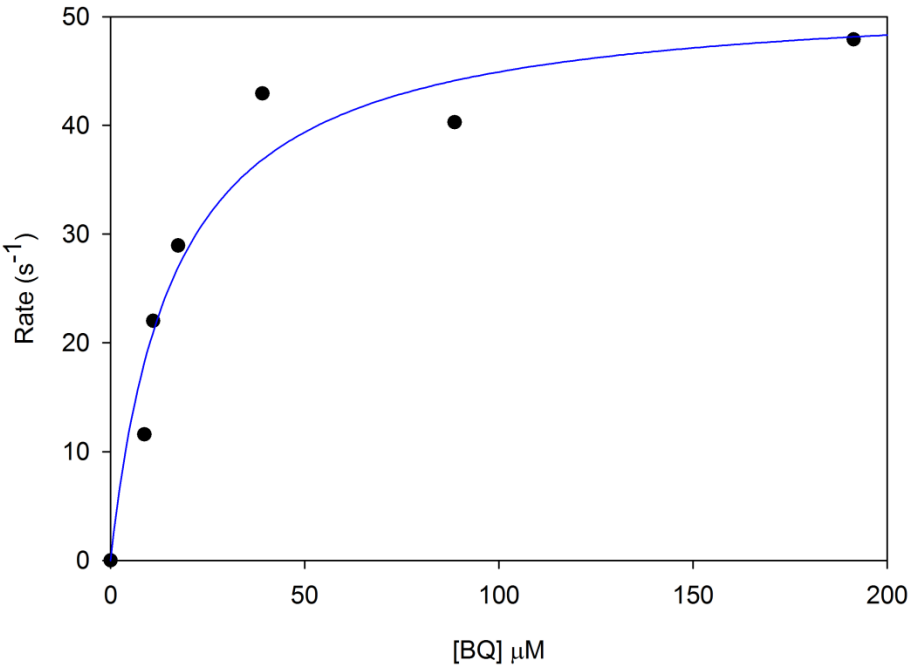

Figure 3.2. Steady state concentration dependence of 1,4-benzoquinone.

Steady state kinetics preformed at 25° C in 50mM HEPES (pH 7.2). The concentration ranges used was 8.4 μM to 191 μM for 1,4-benzoquinone. The reaction was initiated by the addition of 10 μL of 2 μM CO dehydrogenase, and the reaction monitored by the spectral change at 246 over 300 s. Activities were obtained from the initial slopes of each assay, calculated using $\Delta\varepsilon_{247}$=20.2 $mM^{-1}cm^{-1}$. The data was fit to the Michaelis-Menten equation (R^2= 0.946) and yielded a k_{cat} of 104 s^{-1}, K_m of 16.4 μM and k_{cat}/K_m of 6.37 x 10^6 $M^{-1}s^{-1}$

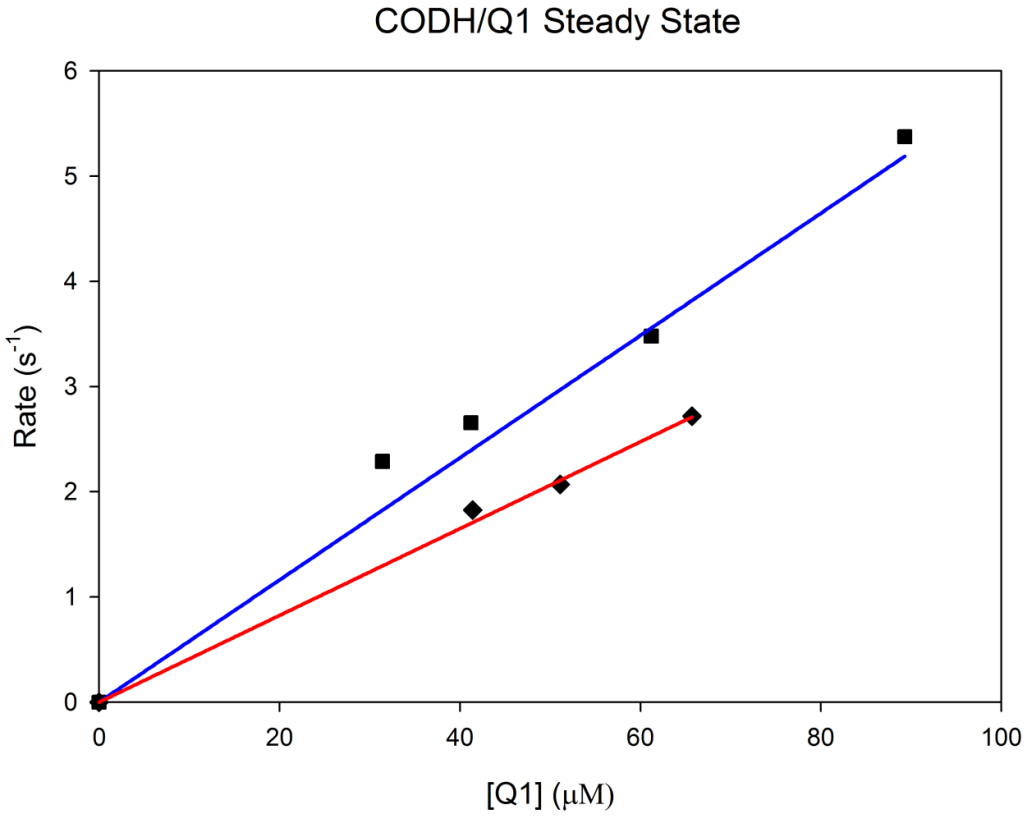

Figure 3.3. Ubiquinone-1 steady state activities in H_2O and D_2O solvent

Ubiquinone-1 steady state kinetics was performed at concentrations from 11 μM to 97 μM. The reaction was initiated by the addition of 10 μL of 2 μM CO dehydrogenase, and the reaction monitored by the spectral change at 275 nm over 300 s in 50 mM HEPES (pH7.2 or pD 7.6) at 25° C. Activities were obtained from the initial slopes of each assay calculated using $\Delta\varepsilon_{278}$=14.7 $mM^{-1}cm^{-1}$ in H_2O (■) and D_2O (♦). The straight line represents the low substrate, k_{cat}/K_m, portion of the Michaelis-Menten equation and determined to have a k_{cat}/K_m of 5.81 x 10^4 $M^{-1}s^{-1}$ in H_2O and 4.13 x 10^4 $M^{-1}s^{-1}$ in D_2O, a solvent isotope effect of 1.4 was obtained from the ratio of $^{H}(k_{cat}/K_m)/^{D}(k_{cat}/K_m)$.

Table 3.1 Kinetic parameters of CO dehydrogenase oxidation by various quinones.

	K_d (μM)	k_{ox} (s^{-1})	k_{ox}/K_d ($M^{-1}s^{-1}$)	K_m (μM)	k_{cat} (s^{-1})	k_{cat}/K_m ($M^{-1}s^{-1}$)	KIE
1,4-benzoquinone	47.6	125.1	2.60×10^6	16.4	52	3.19×10^6	
1,4-naphthoquinone	140	38.1	2.72×10^5				
1,2-naphthoquinone-4-sufonic acid			1.31×10^5				
Ubiquinone-1 H20			2.88×10^5			2.9×10^4	1.4
Ubiquinone-1 D20						2.07×10^4	

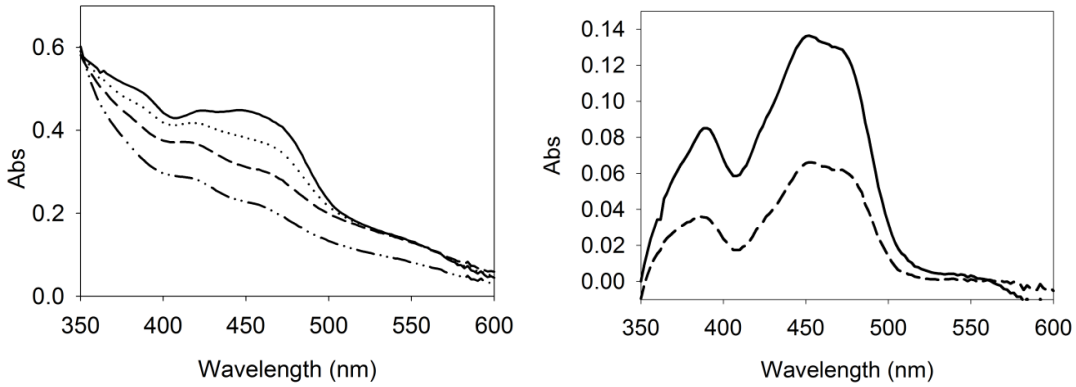

Figure 3.4. Diphenyliodonium chloride inhibition of CO dehydrogenase.

Left, The spectral change over the course of inhibition of CO dehydrogenase in 50 mM HEPES, pH 7.2, with diphenyliodonium chloride. Spectra are for oxidized CO dehydrogenase (—), dithionite-reduced CO dehydrogenase (− · · —), air oxidized CO dehydrogenase following diphenyliodonium chloride inhibition (− −), and diphenyliodonium chloride-inhibited CO dehydrogenase after 18hrs (· · · ·).

Right, The oxidized-minus-inhibited difference spectrum following diphenyliodonium chloride inhibition (—) and after an 18 hr incubation (− −).

3.2.3. Inhibition of quinone reduction by diphenyliodonium ion

In CO dehydrogenase, as with other enzymes of the XOR family, reducing equivalents enter at the molybdenum center in the reductive half of the catalytic sequence, pass through a proximal then distal [2Fe-2S] cluster and leave via the FAD cofactor.[7] In order to establish that quinone substrates interacted with CO dehydrogenase at its FAD site, the enzyme was reacted with diphenyliodonium chloride to covalently modify the FAD and render the cofactor redox-inert.[45] Treatment of enzyme in this way lowered the steady state rates of ubiquinone-1 reduction by 83% and methylene blue by 80%; modification of the flavin was confirmed by comparing the absorption spectrum of the reoxidized, modified enzyme with that of the original (Figure 3.4). The unmodified minus modified difference spectra revealed features at 370 nm and 450 nm constant with flavin modification seen in xanthine oxidase (Figure 3.4).[45] With the modified enzyme, reoxidation of the iron-sulfur clusters is observed after exposure to air, while the additional absorbance increase expected for reoxidation of the FAD is not observed. The reaction was carried out to longer time periods in order to achieve a greater degree of inhibition, but no further inhibition was observed. The incomplete inactivation was most likely due to slow reversal of the covalent modification in air. We observe, for example, that CO dehydrogenase inhibited with diphenyliodonium chloride slowly regained activity over time, suggesting that the inhibited flavin-diphenyliodonium chloride enzyme complex was slowly returned back to functional enzyme. Consistent with this, the absorbance of

oxidized FAD is slowly recovered over the next 18 hr, reflecting the slow breakdown of the flavin-diphenyliodonium chloride complex to yield the oxidized cofactor[45].

3.2.4. Oxidative-Half Reaction of CO dehydrogenase with Quinone Substrates

The rapid reaction kinetics of the reoxidation of reduced CO dehydrogenase by several quinones was next examined by stopped-flow spectrophotometry at 25° C, following the reoxidation of enzyme at 450 nm. The substrates used were 1,4-benzoquinone, 1,4-naphthoquinone, 1,2-naphthoquinone-4-sulfonic acid and ubiquinone-1. Figure 3.5 shows a typical time course for the reaction with 25 μM 1,4-benzoquinone with 5 μM CO dehydrogenase after mixing in the stopped flow apparatus. At low substrate concentrations the reaction appeared biphasic with apparent rate constants of 37 s^{-1} for the first phase (with an associated absorbance change of 0.01 OD, 24% of the total absorbance change) and 3.33 s^{-1} for the second (with amplitude of 0.03 OD, 73% of the total absorbance change). (A third phase was sometimes observed at low substrate concentrations, with a rate constant 0.5 s^{-1} and absorbance change of ~0.001 OD, 2% of the total absorbance change, that was attributed to oxygen contamination. This phase was neglected on the basis of the very small absorbance change associated with it.) The overall kinetic complexity of the reaction is a reflection of the fact that three equivalents of quinone must react with the fully reduced enzyme in turn for full reoxidation. We

attribute the first phase to the reaction of fully reduced (*i.e.*, six-electron-reduced) CO dehydrogenase with a first equivalent of 1,4-benzoquinone to yield four-electron reduced enzyme and 1,4-benzoquinol, and the second rate constant the subsequent reaction of four-electron reduced enzyme with two additional equivalents of 1,4-benzoquinone in turn (which are kinetically unresolved). At higher substrate concentrations, the amplitude of the faster process increases at the expense of the slower, the latter eventually disappearing by 500 μM. Plots of the observed rate constant versus [1,4-benzoquinone] were hyperbolic for both phases of the reaction; the first phase, Figure 3.6, yield a k_{ox} of 125.1 s^{-1}, K_d of 48 μM and k_{ox}/K_d (*i.e.*, the slope of the plot of k_{obs} versus [1,4 BQ]) of 2.60 x 10^6 $M^{-1}s^{-1}$, while the second phase show a k_{ox} of 32.7 s^{-1} and K_d of 154 μM. Again, the second phase was only clearly resolved below 500 μM 1,4-benzoquinone when 5 μM enzyme is used.

The reaction of reduced CO dehydrogenase with 1,2-naphthoquinone-4-sulfonic acid was also biphasic, with amplitudes of 0.02 OD (28% of the total observed spectral change) seen for the first phase and 0.04 OD (57% of the total spectral change) for the second when 5 μM CO dehydrogenase was used. A third very slow phase (0.01 OD, 14% of the total spectral change) was observed that was attributed to photosensitivity of the quinone, as confirmed by monitoring the spectral change of 1,2-naphthoquinone-4-sulfonic acid alone in the observation cell of the stopped-flow apparatus. This phase became negligible at substrate concentrations above 125 μM owing to the short time scale of the

reaction. Due to the high extinction of 1,2-naphthoquinone-4-sulfonic acid, concentrations under 1 mM had to be used and it was not possible to reach saturating concentrations; only the ratio k_{ox}/K_d could be obtained from the linear plot, Figure 3.6, of k_{obs} versus [1,2-naphthoquinone-4-sulfonic acid], with values of 1.31 x 10^5 $M^{-1}s^{-1}$ and 3.90 x 10^4 $M^{-1}s^{-1}$ obtained for the faster and slower phases, respectively.

1,4-naphthoquinone also exhibited biphasic behavior, with amplitudes of 0.04 OD (40% of the total observed spectral change) and 0.06 OD (60% of the observed spectral change) for the first and second phases, respectively, with 5 μM enzyme. 1,4-naphthoquinone (which is structurally similar to menaquinone) yielded somewhat slower kinetics than seen with 1,4-benzoquinone, with k_{ox} = 38.1 s^{-1}, K_d = 140 μM , and k_{ox}/K_d = 2.72 x 10^5 $M^{-1}s^{-1}$ for the faster phase of the reaction, Figure 3.6; the slower phase gave k_{ox} = 6.0 s^{-1} , K_d 213 μM and k_{ox}/K_d = 2.82 x 10^4 $M^{-1}s^{-1}$.

Ubiquinone-1 also showed biphasic behavior with amplitudes of 0.02 OD (14% of the total observed spectral change) and 0.12 (86% of the total spectral change) OD for the first and second phases, respectively, with 5 μM CO dehydrogenase. Due to the limited solubility of ubiquinone-1 it was again not possible to approach saturating conditions, and only a ratio k_{ox}/K_d could be determined from the slope of the linear plot of k_{obs} versus [ubiquinone-1], with values of 2.88 x 10^5 $M^{-1}s^{-1}$ and 1.99 x 10^4 $M^{-1}s^{-1}$ obtained for the faster and slower phases, respectively. Plots of observed rate constant versus [quinone] for

each substrate is shown in Figure 3.6, with the kinetic parameters thus determined summarized in Table 3.1. For the purposes of comparison, attention was focused on the faster phases of the overall reaction which reflected the reaction of fully reduced enzyme with the first equivalent of quinone in the course of reoxidation and thus represented the intrinsic reactivity of the fully reduced flavin site with quinone. It was evident that of the three quinones examined, 1,4-benzoquinone (which is structurally similar to ubiquinone) was the most effective substrate having a k_{ox}/K_d an order of magnitude higher than 1,4-naphthoquinone or 1,2-naphthoquinone-4-sulfonic acid.

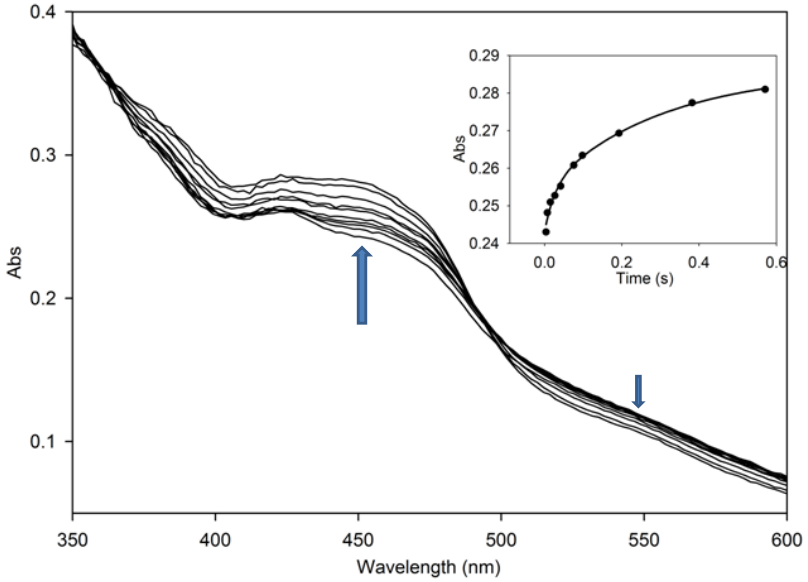

Figure 3.5. Oxidation of reduced CO dehydrogenase by 25μM 1,4-benzoquinone.

Oxidation of dithionite-reduced 5 μM CO dehydrogenase by 1,4-benzoquinone in 50 μM HEPES, pH 7.2 25° C, over 0.6 s. The traces shown are those recored at 0.004 s, 0.007 s, 0.015 s, 0.027 s, 0.042 s, 0.076 s, 0.098 s, 0.0193 s, 0.0382 s and 0.0571 s increasing in absorbance from 0.004 s to 0.0571 s at 450 nm. *Inset*, Time course of absorbance change at 450 nm over 0.6 s (absorbance measurements shown are for 0.004 s, 0.007 s, 0.015 s, 0.027 s, 0.042 s, 0.076 s, 0.098 s, 0.0193 s, 0.0382 s and 0.0571 s) during the course of CO dehydrogenase oxidation. Fits to the data yield observed rate constants of 37 s^{-1} for the first phase and 3.3 s^{-1} for the second phase (with an R^2 value for the fit of 0.993).

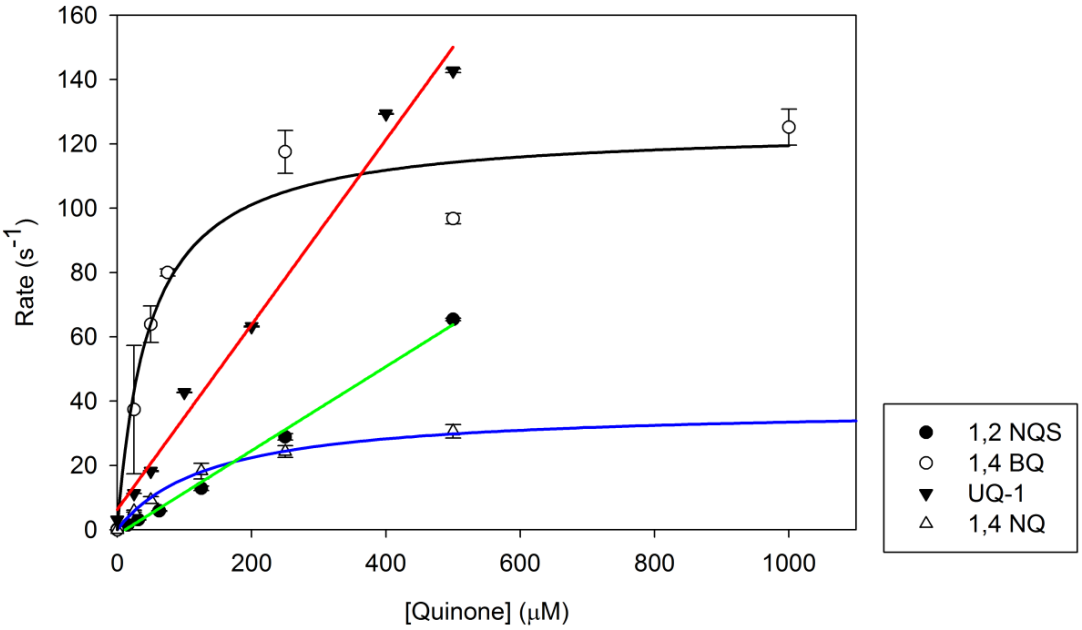

Figure 3.6. Substrate concentration dependence of reoxidation of dithionite-reduced CO dehydrogenase by quinones.

Plots of k_{fast} *versus* [quinone] for the reaction of 5 µM enzyme with ubiquinone-1 (▼, red fit line) and 1,2-naphthoquinone-4-sulfonic acid (●, green fit line) in 50 mM HEPES, pH 7.2, 25° C. Solid Line, fit with a linear equation using SigmaPlot (Systat Software, Inc.). The ratio k_{ox}/K_d (corresponding to the second-order reaction of reduced enzyme with substrate in the low-[Q] regime) was determined by the slope of the fitted line, which for ubiquinone-1 and 1,2-naphthoquinone-4-sulfonic acid were 2.88 x 10^5 $M^{-1}s^{-1}$ (R^2= 0.990) and 1.31 x 10^5 $M^{-1}s^{-1}$ (R^2= 0.995), respectively.

Plots of k_{fast} *versus* [quinone] for the reaction of 5 µM enzyme with 1,4-benzoquinone (○, black fit line) and 1,4-naphthoquinone (Δ, blue fit line) in 50 mM HEPES, pH 7.2, 25° C, fit using the hyperbolic equation $k_{obs} = k_{ox}[Q]/(K_d + [Q])$ using SigmaPlot, where k_{ox} is the limiting rate constant for reoxidation at high [Q] and K_d is the dissociation constant for substrate binding. Kinetic parameters thus determined for 1,4-benzoquinone are k_{ox}, 125.1 s^{-1}, K_d, 46.7µM, k_{ox}/K_d, 2.60 x 10^6 $M^{-1}s^{-1}$ (line fit R^2= 0.955) and for 1,4-napthoquinone are k_{ox}, 38.1 s^{-1}, K_d, 140 µM, and k_{ox}/K_d of 2.72 x 10^5 $M^{-1}s^{-1}$ (line fit R^2= 0.999).

3.2.5. Titration of CO dehydrogenase with oxidized and reduced quinone

In order to establish the affinity of CO dehydrogenase for 1,4-benzoquinone, titrations of CO dehydrogenase with oxidized and reduced 1,4-benzoquinone were carried out. Figure 3.7 shows the titration of oxidized 1,4-benzoquinone with 8 μM CO dehydrogenase, with the greatest spectral change seen at 424 nm. Figure 3.7 shows a plot of the change in absorbance at 424 nm *vs.* [1,4-benzoquinone] from which a K_d of 100 μM can be determined. A comparison with the kinetically determined K_d for binding of oxidized 1,4-benzoquinone with reduced CO dehydrogenase of 48 μM indicates that oxidation of the enzyme flavin reduces affinity for the quinone by a factor of two. Titration of oxidized CO dehydrogenase with pre-reduced 1,4-benzoquinol under anaerobic conditions yielded an oxidized minus-reduced difference spectrum indicating that the FAD and Fe-S centers became fully reduced, as reflected by bleaching at 450 nm and 550 nm.

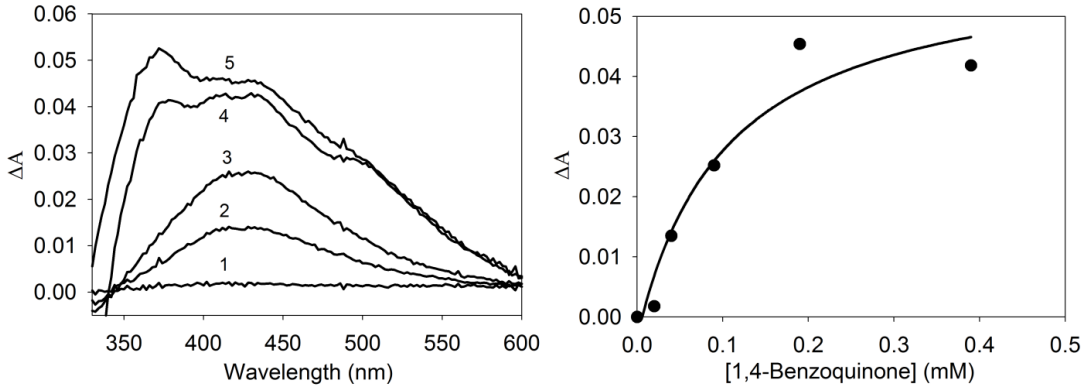

Figure 3.7. Titration of oxidized CO dehydrogenase with oxidized 1,4-benzoquinone.

Left, Difference spectra of CO dehydrogenase with bound 1,4-benzoquinone in 50 mM HEPES, pH 7.2, minus oxidized CO dehydrogenase when CO dehydrogenase is titrated with oxidized 1,4-benzoquinone. Additions of 1,4 benzoquinone yielded final concentrations of 20 μM (1), 40 μM (2), 90 μM (3), 190 μM (4), 390 μM(5).

Right, concentration dependence of the spectral change at 424 nm produced by 1,4-benzoquinone titration with CO dehydrogenase. K_d was found to be 104 μM, determined by a fit using the hyperbolic equation $A_{obs}=(\Delta A_{max} \cdot x)/(K_d+x)$ (R^2= 0.9359).

3.3. DISCUSSION

Here we have examined the reaction of reduced CO dehydrogenase with several cytochromes and quinones in an effort to determine the oxidizing substrate for the enzyme. Having failed in an exhaustive effort to identify a cytochrome capable of being effectively reduced by CO dehydrogenase, we find that several quinones are very effective substrates, rapidly oxidizing reduced CO dehydrogenase under anaerobic conditions. 1,4-benzoquinone is found to be the most effective oxidizing substrate, with a k_{ox} of 125.1 s^{-1} at pH 7.2, 25° C for the fastest phase of enzyme reoxidation. The multiple phases observed in the oxidative half-reaction kinetics seen here are attributed to the necessarily sequential nature of the reaction of fully (six-electron) reduced enzyme with three successive equivalents of quinone.

Although 1,4-benzoquinone was the most effective (and also most soluble) of the quinones tested, ubiquinone-1 was also a fairly effective substrate, but due to its low solubility in water only k_{ox}/K_d, 2.88 x 10^5 $M^{-1}s^{-1}$ and k_{cat}/K_m, 2.9 x 10^4 $M^{-1}s^{-1}$ could be determined experimentally – both parameters were approximately an order of magnitude slower than seen with 1,4-benzoquinone, k_{ox}/K_d, 2.60 X 10^6 $M^{-1}s^{-1}$. A similar situation has been seen in chromate reductase, a soluble quinone-reducing protein that best utilizes 1,4-benzoquinone over ubiquinone-1.[52] Both 1,4-naphthoquinone and 1,2 naphthoquinone-4-sulfonate were poorer oxidizing substrates for CO dehydrogenase, suggesting that the structurally related menaquinone is a less likely physiological substrate for the enzyme than

ubiquinone. In order to establish that the oxidative half reaction takes place at the FAD cofactor, CO dehydrogenase was reacted with diphenyliodonium chloride to covalently modify the FAD. This modification has been shown by Chakraborty et. al. to render the FAD redox-inert. Figure 3.8 shows the various types of adducts that can be formed, and based on solvent accessibility it is likely that adduct *C* or *D* is the major product formed during inactivation of CO dehydrogenase. The low solvent accessibility and instability of this adduct led to incomplete and un-stable inactivation, with the enzyme spontaneously recovering activity over time. Nevertheless, this inhibition was sufficient to establish quinones reacted with the enzyme at the FAD site to the quinones.

No semiquinone EPR signal was observed in EPR experiments monitoring catalytic enzyme turnover, and it appears that the principal oxidizing event is an effective two-electron process, Figure 3.9. Finally, given the overall effectiveness of quinones as substrate, we conclude that one or another component of the quinone pool of *O. carboxidovorans*, most likely ubiquinone, constitutes the proximal oxidizing substrate for CO dehydrogenase, and that cytochromes become reduced only subsequent to the introduction of reducing equivalents into the quinone pool. This finding establishes a new category of oxidizing substrate for the xanthine oxidase family of enzymes adding to the unique chemistry, structure and function of CO dehydrogenase.

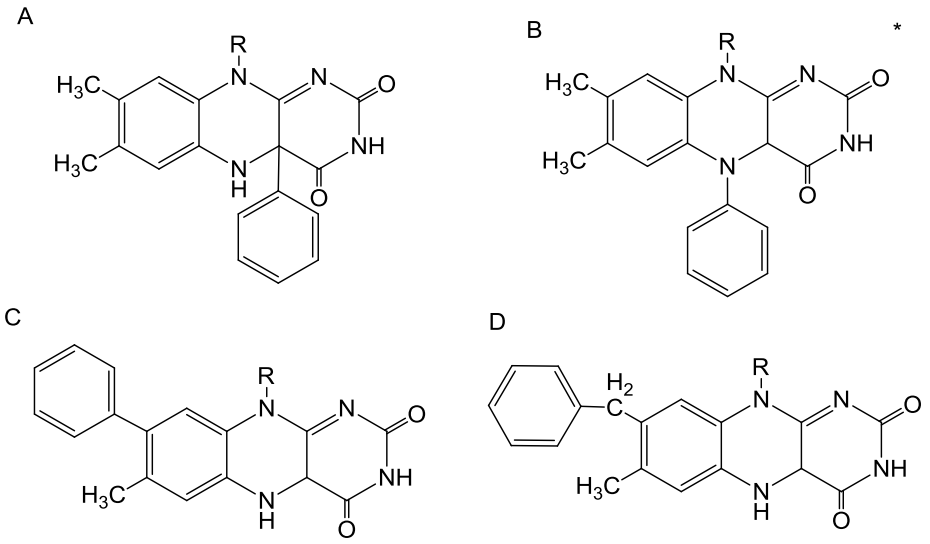

Figure 3.8. Diphenyliodonium cloride- FAD adducts

Flavin-phenyl adducts characterized by Chakraborty et. al. indicates possible reaction sites and products formed when FAD is inhibited by diphenyliodonium cloride. Structure B was characterized to be an unstable addition product.

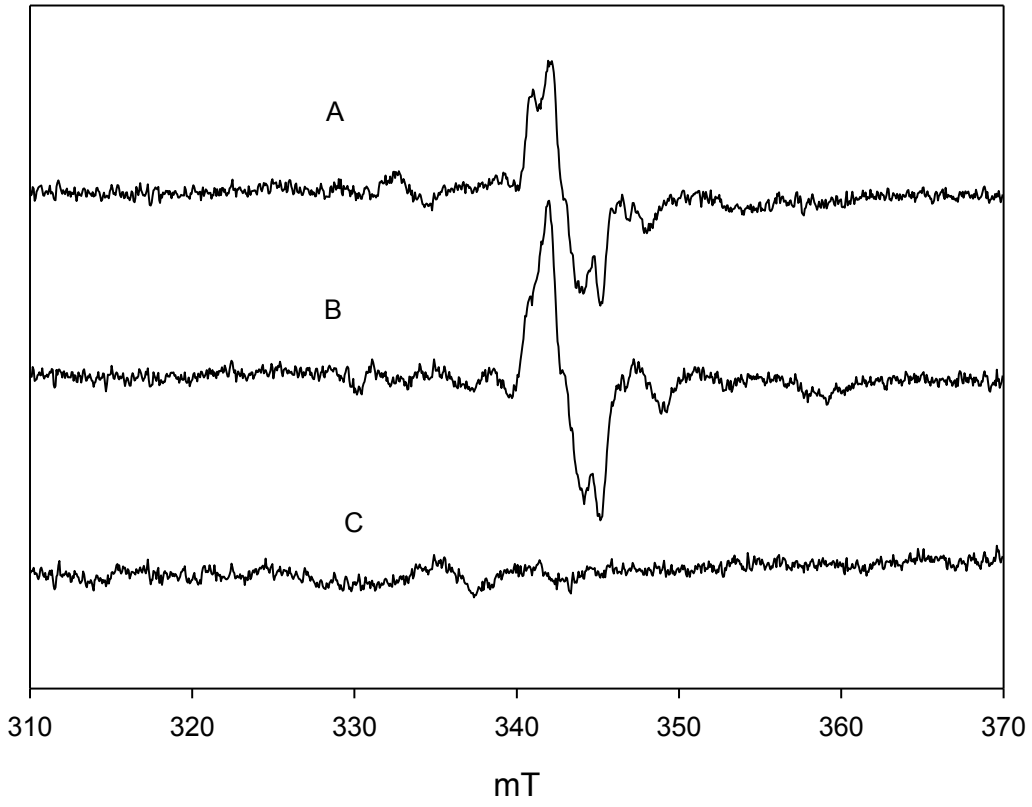

Figure 3.9. Electron paramagnetic resonance spectroscopy of CO dehydrogenase reacted under various conditions.

Samples were made in 50 mM Hepes (pH 7.2) and fully reduced with dithionite (A), re-oxidized with a half equivalence of ubiquinone-1 (B) or 12 equivalence of ubiquinone-1 (C).

The spectra were obtained at 150 K, 9.5 GHz microwave frequency, 10 milliwatt microwave power and 5 Gauss modulation amplitude. Signal seen is consistent with a dithionite reduced inactive molybdenum center. No formation of a semi-quinone signal present.

Chapter 4

Substitution of silver for copper into the active site of CO dehydrogenase

4.1 Introduction

Carbon monoxide dehydrogenase is capable of catalyzing the oxidation of carbon monoxide at a unique molybdenum and copper center. Cyanide, although isoelectric and isosteric to carbon monoxide, has a disastrous effect at the metal center removing the copper and μS, Figure 4.1, to form the inactive tri-oxo molybdenum species. Using this attribute it was shown by Resch et. al. that the active site can be stripped of the μS and copper and then reassembled through a reconstitution procedure that first replaces the bridging μS followed by the copper to re-form a fully functional active site, described further in Chapter 2.[43] Using this technique we hoped to exchange the native copper for a different metal in hopes of trapping an intermediate in the reaction or perturbing the reaction in such a way to gain insight into how the native active site is able to perform a reaction that is otherwise difficult to accomplish. In searching for a suitable metal for replacement atomic radii, oxidation state, *d*-orbital configuration and preferred coordination geometry needed to be taken into account, with this in mind silver was selected as a suitable substitute to copper. We report here the substitution

of silver for copper in the binuclear cluster, yielding a molybdenum- and silver-containing enzyme that retains the ability to oxidize CO.

4.2 Results

4.2.1 EPR spectroscopy

The EPR spectrum of CO-reduced native CO dehydrogenase is shown in Figure 4.2 with simulations. The importance of using CO as a reductant ensures that only the functional enzyme is reduced and rendered EPR active. The spectrum shows strong super-hyperfine coupling to the I=3/2 ^{63,65}Cu nuclei in the native enzyme, with $\mathbf{g}_{1,2,3}$ = [2.0010, 1.9604, 1.9549] and $|\mathbf{A}_{1,2,3}(^{63,65}\text{Cu})|$= [117, 164, 132] MHz, as reported with previous work.[34] By comparison, as seen in Figure 4.2, treatment of the silver-substituted enzyme with CO yielded an EPR spectrum exhibiting doublets rather than quartets due to strong super-hyperfine coupling to the ^{107,109}Ag nucleus (I = ½ nucleus). Simulation of the EPR signal using the EasySpin software package, Figure 4.2 and Table 4.1, for the Ag-substituted enzyme yielded $\mathbf{g}_{1,2,3}$ = [2.0043, 1.9595, 1.9540] and $|\mathbf{A}_{1,2,3}(^{107,109}\text{Ag})|$= [81.98, 78.85, 81.89] MHz, Table 4.1.[53] The $\mathbf{g}_2$ and $\mathbf{g}_3$ values for the silver-substituted enzyme are comparable to those seen with the native, copper containing enzyme, but g_1 differs to a rather greater degree from the value of 2.0010 seen with the native copper-containing enzyme.[34] Samples prepared in D_2O HEPES (pD 7.2) showed only very slight line width narrowing, with values of 0.051 mT and 0.048 mT for the H_2O and D_2O samples,

respectively indicating weak if any proton super-hyperfine coupling in the signal. Reduction of the enzyme by dithionite or ^{13}CO also yields signals identical to the CO reduced enzyme. An observation of great importance is the lack of any observable EPR signal arising from the native, copper-containing enzyme in the EPR signal of the silver-substituted form (the high-field features in both the native and silver substituted enzyme are due to hyperfine coupling to the I = 5/2 $^{95,97}Mo$ nuclei, which have a combined natural abundance of 25%). This indicates the absence, to within the detection limits of the experiment, of copper in the enzyme active site.

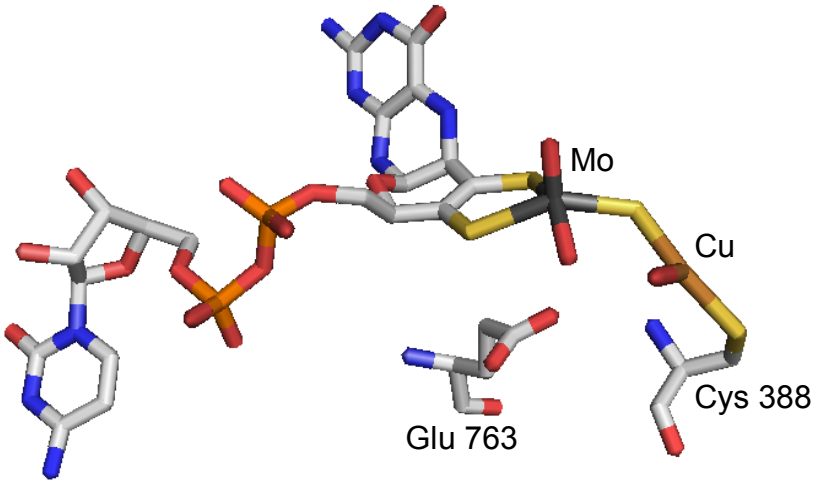

Figure 4.1. Active site of CO dehydrogenase

The active site of CO dehydrogenase was rendered using Protein Data Bank entry 1N5W. Atom colors are CPK with molybdenum in grey and copper in brown coordinated by Cys_{388}.

A.

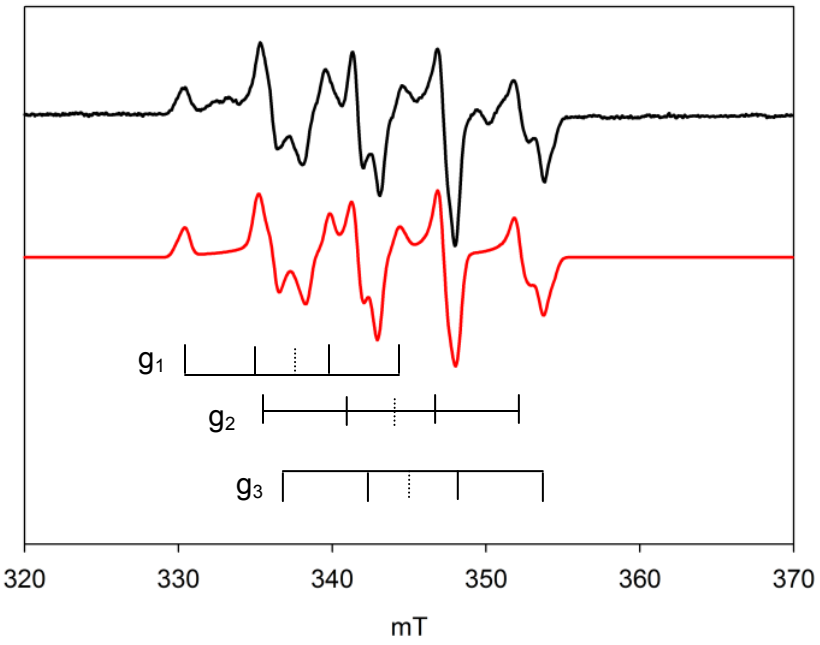
g1
g2
g3
320
330
340
350
360
370
mT

B.

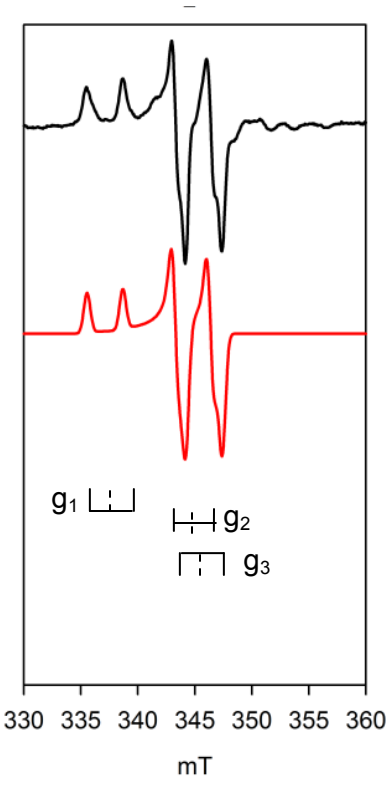
g1
g2
g3
330
335
340
345
350
355
360
mT

C.

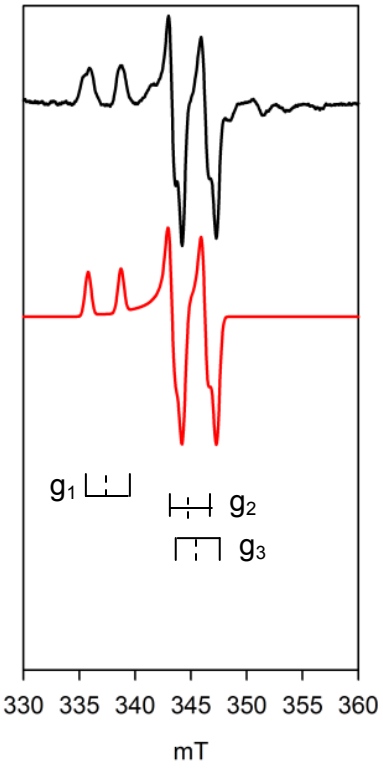
g1
g2
g3
330
335
340
345
350
355
360
mT

Figure 4.2. EPR spectra of CO reduced CO dehydrogenase.

Samples were prepared as follows (all in 50mM HEPES, pH 7.2): *A*, 100μM Cu-CO dehydrogenase reduced with excess CO (Black), simulation below(Red) with parameters $\mathbf{g}_{1,2,3}$ = [2.0010, 1.9604, 1.9549]; $|\mathbf{A}_{1,2,3}(^{63,65}\text{Cu})|$ = [117, 164, 132] MHz; *B*, Ag substituted CO dehydrogenase with excess CO (Black), simulation below (Red) with parameters $\mathbf{g}_{1,2,3}$ = [2.0043, 1.9595, 1.9540]; $|\mathbf{A}_{1,2,3}(^{107,109}\text{Ag})|$ = [82, 79, 82] MHz; *C*, Ag substituted CO dehydrogenase with excess CO in the presence of D_2O (Black), simulation below(Red) with parameters $\mathbf{g}_{1,2,3}$ 2.0032, 1.9596, 1.9539; $|\mathbf{A}_{1,2,3}(^{107,109}\text{Ag})|$ = [75, 77, 78] MHz.

The EPR instrument settings were: 9.456 GHz microwave frequency; 10 milliwatt microwave power for the Cu containing sample and 4 mW power for the Ag containing sample; 5 Gauss modulation amplitude for the Cu containing sample and 2 Gauss modulation amplitude for the Ag containing sample; 150 K.

Table 4.1. EPR simulation parameters

	Cu-CODH	**Ag-CODH H_2O**	**Ag-CODH D_2O**
$\mathbf{g_1}$	2.0010 *	2.0043	2.0032
$\mathbf{g_2}$	1.9604 *	1.9595	1.9596
$\mathbf{g_3}$	1.9549 *	1.9540	1.9539
$\lvert\mathbf{A_1}\rvert$(MHz)	117 *	81.98	75.05
$\lvert\mathbf{A_2}\rvert$(MHz)	164 *	78.85	77.35
$\lvert\mathbf{A_3}\rvert$(MHz)	132 *	81.89	78.02

* From Zhang et. al.[34]

4.2.2. Steady state kinetics

Steady-state kinetics, preformed under anaerobic conditions, were well-behaved and yielded straight lines over 300 s at each CO concentration used. The velocities at each CO concentration were averaged and plotted against CO concentration, Figure 4.3. The data was fit with a hyperbola to yield a k_{cat} of 8.2 s^{-1} (per active site) and a K_m, 2.95 μM, with $k_{cat}/K_m = 2.78 \times 10^6$ $M^{-1}s^{-1}$. These values may be compared with the values obtained with native enzyme, Table 4.2, of where k_{cat}, K_m, and k_{cat}/K_m had values of 46.7 s^{-1}, 10.7 μM, and 4.35×10^6 $M^{-1}s^{-1}$ respectively, indicating that the silver-substituted CO dehydrogenase, while lower in activity than the native enzyme, indeed retains significant catalytic activity.[34]

4.2.3. Rapid Reaction Kinetics

The reduction of CO dehydrogenase by CO under anaerobic conditions was next examined by stopped-flow spectrophotometry, following the bleaching of CO dehydrogenase at 450 nm upon reduction of the Fe/S and FAD centers of the enzyme. At all CO concentrations used over the range 6 to 500 μM, well-behaved single-exponential transients were observed, with absorbance changes of a magnitude consistent with the overall functionality of the enzyme defined independently, k_{obs} was obtained from exponential fits to the data. Figure 4.3 shows a plot of k_{obs} *vs.* [CO] for the reaction as carried out at 50 mM HEPES, pH 7.2, where it can be seen that, as with the native enzyme, the rate constant for

enzyme reduction is independent of [CO] (presumably due to a prior rapid-equilibrium binding step). The k_{red} of 8.1 s^{-1} is in good agreement with the steady-state k_{cat} of 8.2 s^{-1}. Again, the results indicate the reductive half-reaction is overall rate-limiting in catalysis, as is seen with the native copper-containing enzyme, Table 4.2.[34]

The temperature dependence of the rate of enzyme reduction over the range 5 °C to 30 °C was monitored in 50 mM HEPES, pH 7.2, using 500 μM CO (after mixing). Rate constants obtained from exponential fits to the kinetic transients at each temperature were averaged and an Arrhenius plot of $\log(k_{obs})$ vs. 1/T, Figure 4.4, to obtain an effective activation energy (E_a) of 42.7 kJ/mole; an Eyring plot, Figure 4.4, of the same data yielded an enthalpy and entropy of activation ($\Delta H^{\ddagger}$ and $\Delta S^{\ddagger}$) of the transition state yielded values of 40.2 kJ/mol and -94.4 J/K•mol, respectively. The value for $\Delta H^{\ddagger}$ is in excellent agreement with the value for E_a of 42.7 kJ/mol, given that RT = 1.7 kJ/mol at room temperature, and compares to an E_a of 47.8 kJ/mol for the native copper containing enzyme, Table 4.3. While the E_a for the silver- substituted enzyme is lower than that of the native enzyme there is a greater entropic cost involved in the reaction indicated by a lower $\Delta S^{\ddagger}$ of -94.4 J/K•mol compared to -60.4 J/K•mol for the native enzyme. The greater cost may arise from the coordination of CO, where in the native enzyme the coordination likely releases a coordinated water at the copper site. The silver likely does not have anything coordinated, as evident by the dithionite reduced EPR spectra, Figure 4.4.

A.

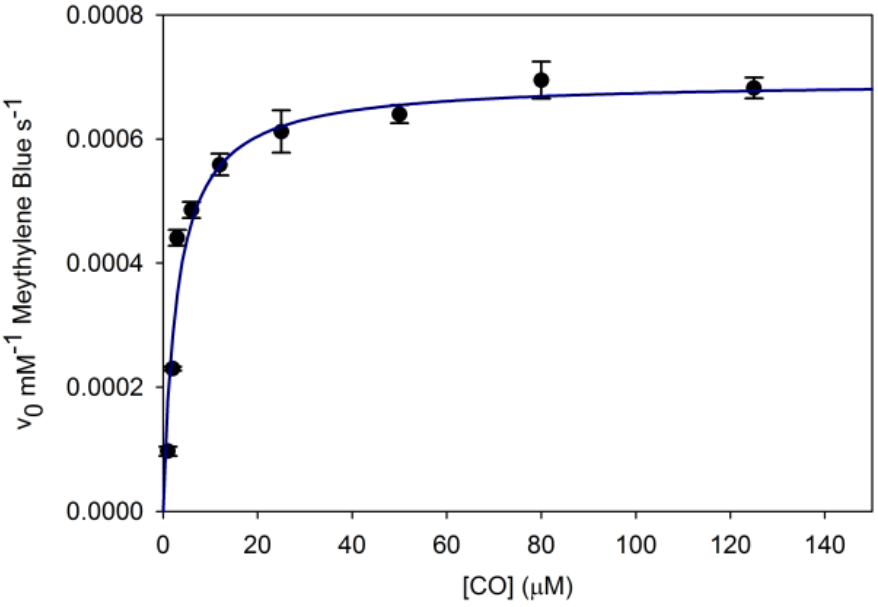
0.0008
0.0006
0.0004
0.0002
0.0000
v_0 mM^{-1} Meythylene Blue s^{-1}
0
20
40
60
80
100
120
140
[CO] (μM)

B.

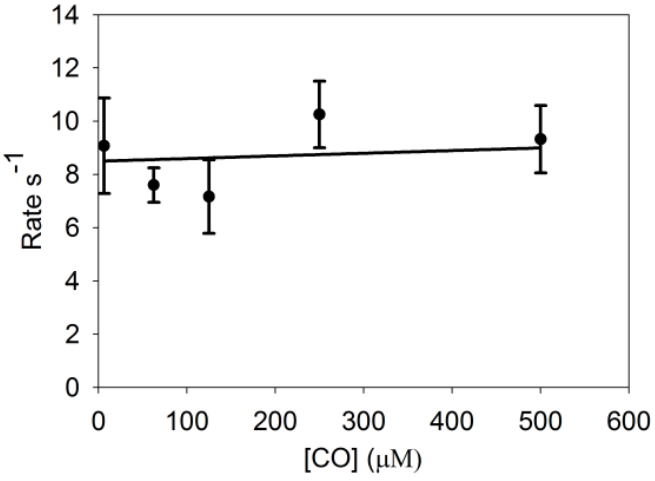
14
12
10
8
6
4
2
0
Rate s^{-1}
0
100
200
300
400
500
600
[CO] (μM)

Figure 4.3. Kinetic Data for Ag substituted CO dehydrogenase.

A, Steady state CO concentration dependence of Ag substituted CO dehydrogenase using methylene blue as an electron acceptor in 50 mM potassium phosphate buffer, pH 7.2, at 25 °C. Plot of the initial rate, following methylene blue reduction at 615 nm after mixing a final concentration of 82.0 nM CO dehydrogenase with CO dissolved (1-500μM) in methylene blue, versus [CO]. Data was fit with the Michaelis–Menten equation using Sigma Plot (R^2 = 0.95) to give a k_{cat} of 8.2 s^{-1} and K_m of 2.95 μM.

B, Rapid reaction kinetic plots of the rate k_{obs} following the reduction of 5μM CO dehydrogenase at 450 nm versus [CO], from 3 μM to 500 μM, in 50 mM HEPES, pH 7.2, at 25 °C. Since the data observed has no concentration dependence saturating substrate conditions are assumed and apparent k_{red} was estimated to be 8.1 s^{-1}.

Table 4.2. Summary of kinetic parameters

	Cu-CODH	Ag-CODH
k_{cat} (s^{-1})	46.7*	8.2
K_m (μM)	10.7*	1.91
k_{red} (s^{-1})	51*	8.1
K_d (μM)	ND*	ND

* From Zhang et. al. [34]

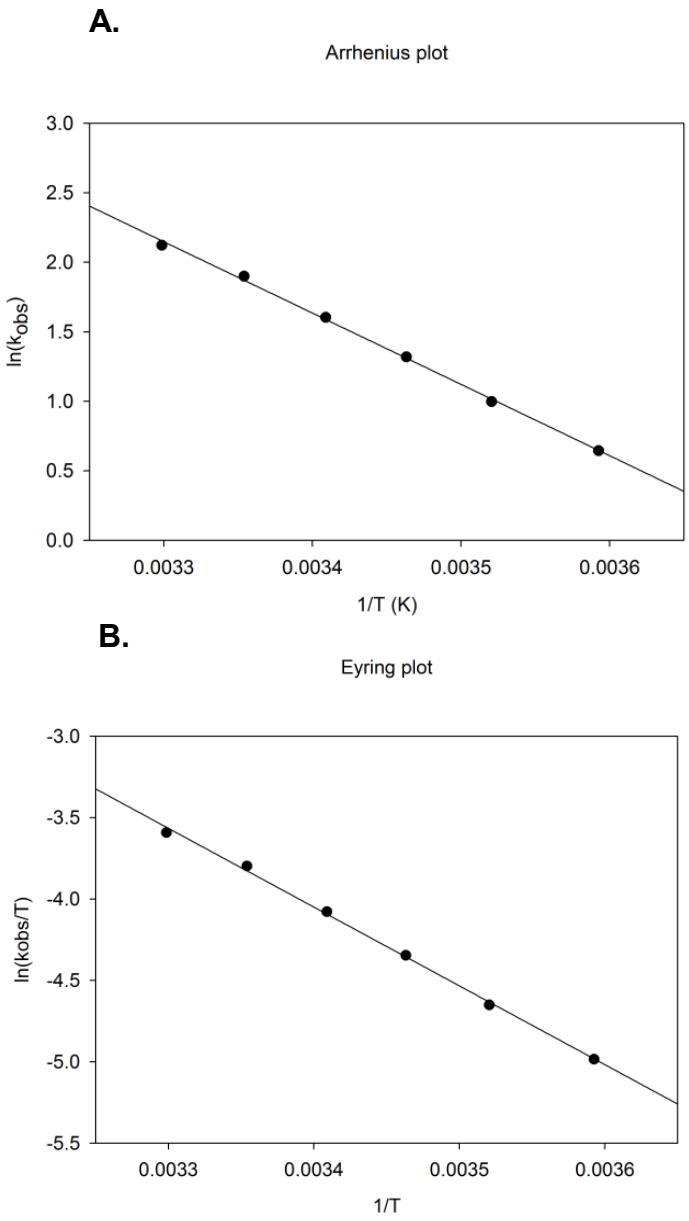

Figure 4.4: Temperature dependence of Ag-CO dehydrogenase reduction by CO

Temperature dependence of the Ag substituted CO dehydrogenase reduction by CO. Rates were obtained from 5 – 30 °C using 5 µM CODH reduced with 500 µM CO. Observed rates were plotted in Arrhenius (*A*) and Erying (*B*) plots for the determination of activation energy of CODH reduction.

Table 4.3. Activation energy parameters of CO dehydrogenase

	Cu-CODH (pH7.2)*	Ag-CODH (pH7.2)
E_a	47.8	42.65
$\Delta H^{\ddagger}$, kJ/mole	45.4	40.23
$\Delta S^{\ddagger}$, J/K•mole	-60.4	-94.4
$\Delta G^{\ddagger}$, kJ/mole	63.4	68.4

* From Zhang et. al.[34]

4.3 Discussion

In the present work, we have developed a protocol for incorporating silver into the active site of CO dehydrogenase in place of the naturally-occurring copper, and demonstrated that the silver-substituted enzyme thus obtained remains reducible by CO and exhibits an EPR signal that, apart from doublets due to ^{107,109}Ag rather than quartets due to ^{63,65}Cu, is strongly reminiscent of the EPR signal seen with native enzyme upon reduction by CO. Although the coupling of silver nucleus appears weaker ($|\mathbf{A}_{avg}|$ of 76 MHz for silver compared to 130 MHz for copper) this is expected given the weaker nuclear bohr magneton (^{107}Ag = -0.227, ^{109}Ag = -0.262, ^{63}Cu = +1.484, ^{65}Cu = +1.588) and is comparable to the differences observed in Cu-TPP (5,10,15,20-Tetraphenyl-21H,23H-porphine) and Ag-TPP complexes, Table 4.4.[54] There is a modest shift in $\mathbf{g}_1$ value upon silver-substitution (2.0043, as compared with 2.0010 for the copper containing), but no substantial change in the $\mathbf{g}_2$ and $\mathbf{g}_3$ value is observed. Overall, the EPR results indicate a similar coordination environment in the silver-substituted enzyme to that seen in the native form.

Steady-state kinetics studies show a five-fold reduction in both k_{cat} and K_m relative to the native system. No dissociation constant, K_d, could be determined through rapid reaction kinetics due to rapid formation of a complexed CO prior to catalysis. The observed limiting k_{red}, 8.1 s^{-1}, correlates well with the k_{cat} of 8.2 s^{-1} obtained by steady-state kinetics, indicating (as with the native enzyme) the rate-limiting step is in the reductive-half reaction of the overall catalytic cycle.[34]

Given the nature of the metal replacement, and the metal's interaction with substrate, the observed slower kinetics is not unexpected if the role of the active site copper is to bind and activate the CO for oxidation by nucleophillic attack at the copper site. The degree of back-bonding from the metal to the π* orbital of CO influences the strength of the CO triple bond, with stronger back-bonding strengthening the metal-C bond weakening the C-O bond. It is known that silver carbonyl complexes have much less back-bonding than the corresponding copper complexes.[55,56] The stretching frequency is increased when CO becomes more of a σ donor, from 2143 cm^{-1} up to 2204 cm^{-1} (depending on the other ligands to the metal) for the free carbon monoxide and silver carbonyl complex, strengthening the CO bond.[7] This difference observed between copper and silver is the result of the a lower ^1D state ($4d^9 5s^1$) for copper than for silver (75 kcal/mol and 131 kcal/mol respectively above the ground state) causing less sd_σ hybridization and therefore significantly less π* back donation for silver than copper.[55] As a result, the bound CO is expected to be less susceptible to nucleophillic attack with silver relative to copper.

Using the reported differences in metal carbonyl stretching frequencies a role for copper can be established where CO initially binds to the copper, displacing a water, and is activated for nucleophillic attack by the equatorial oxo ligand of molybdenum (which is orientated toward the proposed CO binding site) at the carbon through the effects of π* back donation from copper weakening the CO bond, Figure 4.5.

Table 4.4. Cu vs. Ag coupling to TPP

	Nuclear g_n	a_{iso}/e^-(mT)	Cu/Ag-TPP (MHz)	CODH (MHZ)
^{65,65}Cu	1.484/1.588	213.9/228.9	a_{iso} = 274	a_{iso} = 137
^{107,109}Ag	-0.227/-0.262	-65.33/-75.25	a_{iso} = 117/130	a_{iso} = 88
Ratio	-6.537/-6.061	-3.27/-3.04	2.34	1.56

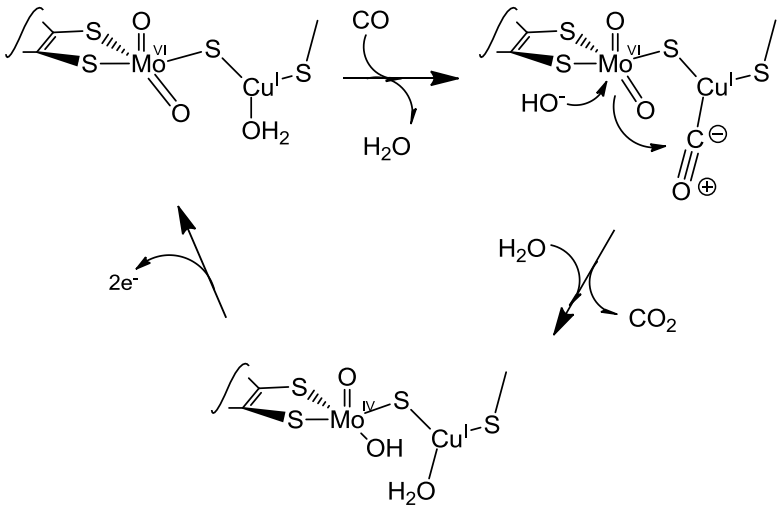

Figure 4.5 Minimal reaction mechanism of CO dehydrogenase

Chapter 5

Electron nuclear double resonance studies of CO dehydrogenase; evidence for a Michaelis complex intermediate

5.1. Introduction

The binuclear cluster of CO dehydrogenase is the site at which CO is oxidized and has the structure shown in Figure 5.1, with the two transition metals linked by a μ-sulfido bridge.[28] In the course of reduction of the enzyme by excess CO, the binuclear cluster exhibits a Mo(V) EPR signal with $\mathbf{g}_{1,2,3}$ = [2.0010, 1.9604, 1.9549] and large hyperfine coupling to the $I = {}^3/_2$ ^{63,65}Cu nuclei, $|\mathbf{A}_{1,2,3}(^{63,65}\text{Cu})|$ = [117, 164, 132] MHz.[57] The signal exhibits no proton super-hyperfine structure and is unchanged when the sample is prepared in D_2O, but modest line-broadening is observed when ^{13}CO is used as substrate suggesting coupling to the carbon atom derived from substrate.[57]

Both the μ-sulfido ligand and the Cu(I) ion of the binuclear cluster can be removed by treating the enzyme with cyanide, and a reconstitution protocol has been developed using Cu^{I}•thiourea as the copper source as described in Chapter 2.[12] Alternatively, when Ag^{I}•thiourea is used the Ag(I) ion is reconstituted into the active site.[58] The Ag(I) substituted enzyme remains active and is reduced by CO

with a limiting rate constant of 8.2 s^{-1}, as compared with 51 s^{-1} for the native Cu-containing form of the enzyme.[58] In the course of reduction by CO, the Ag(I) substituted form of the enzyme also exhibits a characteristic EPR signal, with $\mathbf{g}_{1,2,3}$ = [2.0043, 1.9595, 1.9540] and with strong coupling to the I = ½ ^{107,109}Ag nuclei with $|\mathbf{A}_{1,2,3}(^{107,109}\text{Ag})|$ = [82, 79, 82] MHz.

Several structures can be envisaged for the EPR-active Mo(V) form of the native copper-containing CO dehydrogenase, as illustrated in Figure 5.2. Structure A is the Mo(V)-containing analog of a proposed Mo(IV)-containing intermediate in the reaction of enzyme with CO based on the 1.1-Å resolution structure of the enzyme in complex with *n*-butylisonitrile, in which the inhibitor is found to insert between the S-Cu bond of the μ-sulfido bridge (Figure 2, Structure A_1).[28] The Mo(V) species would be formed from an initial Mo(IV) species by transfer of one electron from the binuclear cluster to the other redox-active centers of the enzyme prior to completion of the reaction (in a manner analogous to generation of the "very rapid" Mo(V) species seen with xanthine oxidase[59,60,61]). Structure B represents an alternate reaction intermediate proposed on the basis of density functional studies of the binuclear center,[41,62] with the Mo(V) species again generated by one-electron oxidation of a Mo(IV) species. Structure C is a Mo(V)-containing analog of the presumed complex of CO with oxidized enzyme that is believed to represent the initial intermediate in catalysis. Here, the CO is coordinated to the Cu(I) with a residual electron remaining in the binuclear center after reaction with a prior equivalent of CO (in this case, partial reduction of the

center would have occurred by reaction of a prior equivalent of CO). In all three structures, the molybdenum is formally Mo(V) and the copper is Cu(I).

To discriminate among these structural alternatives and gain insight into the mechanism of CO oxidation, we have used 35 GHz pulsed-ENDOR spectroscopy to determine the ^{13}C, $^{95,97}Mo$, and $^{63,65}Cu$ hyperfine coupling tensors and the $^{63,65}Cu$ quadrupole coupling interaction for $^{12,13}CO$-reduced CO dehydrogenase. The measured ^{13}C-hyperfine coupling is compared with reported ^{13}C-coupling for paramagnetic Mo(V) species observed with other members of the xanthine oxidase family, and the magnitude *and* sign of the $^{63,65}Cu$ couplings are compared with those of other Cu centers. The combination of these measurements with previously measurements of xanthine oxidase structures discriminates among the potential structures for the intermediate (Figure 5.2), and support a spin-delocalized [Mo(V)-(μ-S)-Cu(I)] structure that has CO coordinated to Cu(I). This species represents a paramagnetic analog of the initial [Mo(VI)-μS-Cu(I)•CO] Michaelis complex of the catalytic cycle, from which a catalytic sequence can be developed.

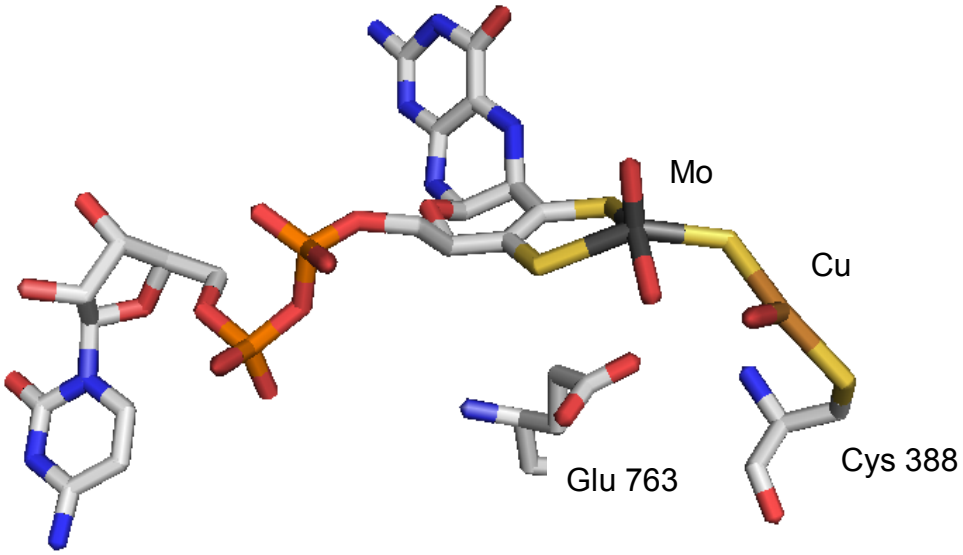

Figure 5.1. Active site of CO dehydrogenase

The active site of CO dehydrogenase was rendered using Protein Data Bank entry 1N5W. Atom colors are CPK with molybdenum in grey and copper in brown coordinated by Cys_{388}.

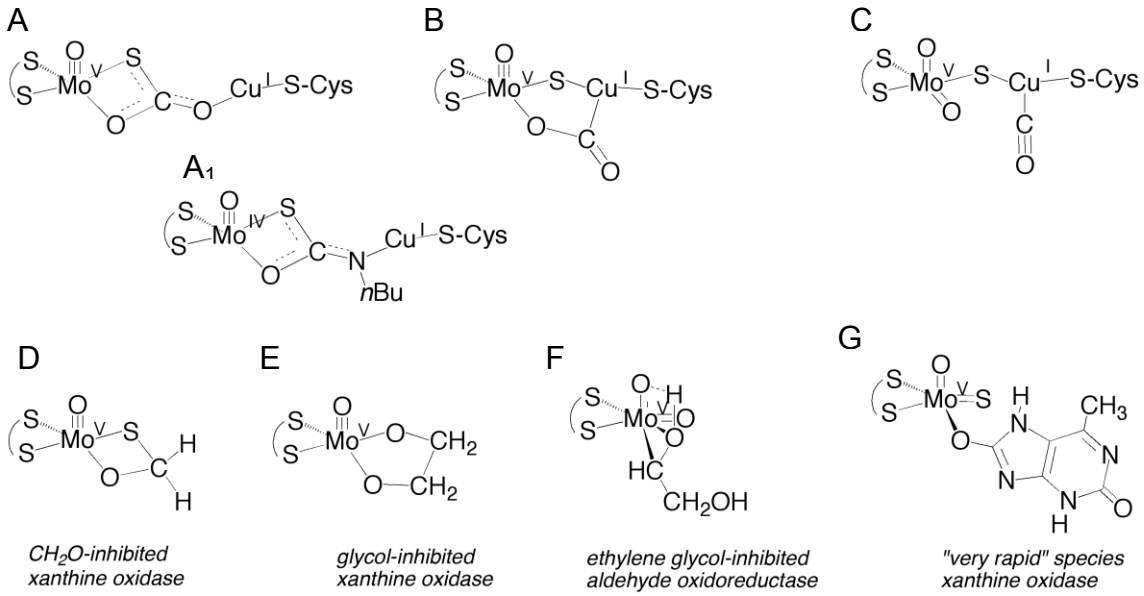

Figure 5.2. Possible structures for the EPR-active species seen with CO dehydrogenase

Possible structures for the EPR-active species seen with CO dehydrogenase (A-C), and structures of various relevant EPR-active Mo(V) species observed with the related enzyme xanthine oxidase (D-G).

5.3. Results

X-band (~ 9.5 GHz) EPR spectra of CO-reduced CO dehydrogenase (native and Ag substituted) were collected for samples prepared with ^{12,13}CO in 50 mM HEPES buffer, pH 7.2 at 150 K (Figure 5.3). The EPR spectrum of the binuclear center of the enzyme generated with ^{12}CO (black line) shows a well-resolved structure centered around *g* ~1.96 with complex multiplet features due to hyperfine interactions with both Mo [$I(^{95,97}\text{Mo}) = 5/2$; 25 % natural abundance] and Cu [$I(^{63,65}\text{Cu}) = 3/2$; 100 % natural abundance] or Ag [$I(^{107,109}\text{Ag}) = 1/2$; 100 % natural abundance] nuclei in the native and Ag substituted enzyme respectively. For the native enzyme, the 150 K spectrum was well reproduced (red dashed line) with the following spin-Hamiltonian parameters; **g** = [2.002, 1.958, 1.953], $|\mathbf{A}(^{63,65}\text{Cu})|$ = [117, 164, 132] MHz, values, corresponding to $|a_{iso}(^{63,65}\text{Cu})|$= 138 MHz, with small anisotropic coupling **T** = [-21, 26, -7] having a maximum anisotropic coupling, $|T_{max}(^{63,65}\text{Cu})|$ = 26.4 MHz.[57] The g values, all being $\leq g_e$, indicate that the EPR signal arises from a Mo(V) rather than Cu(II) species, consistent with the known constitution of the binuclear center, with Mo(VI) and Cu(I) in the fully oxidized state.[31]

This conclusion is supported by contrasting the nearly isotropic ^{63,65}Cu, hyperfine tensor with the highly anisotropic hyperfine coupling observed for Cu(II) systems;[63] it is confirmed below by ENDOR measurements which determine both the magnitude *and* sign of the ^{63,65}Cu couplings. When the binuclear signal is

generated using ^{13}CO, the spectrum shows significant line broadening (Figure 5.3) due to unresolved hyperfine coupling to the ^{13}C in the native enzyme, as previously reported.[64] This is in contrast to what is observed with the silver substituted enzyme, where only minimal line broadening is observed indicating little or no coupling to the ^{13}C nucleus. Further discussion will be limited to CO coupling to cooper in the native enzyme.

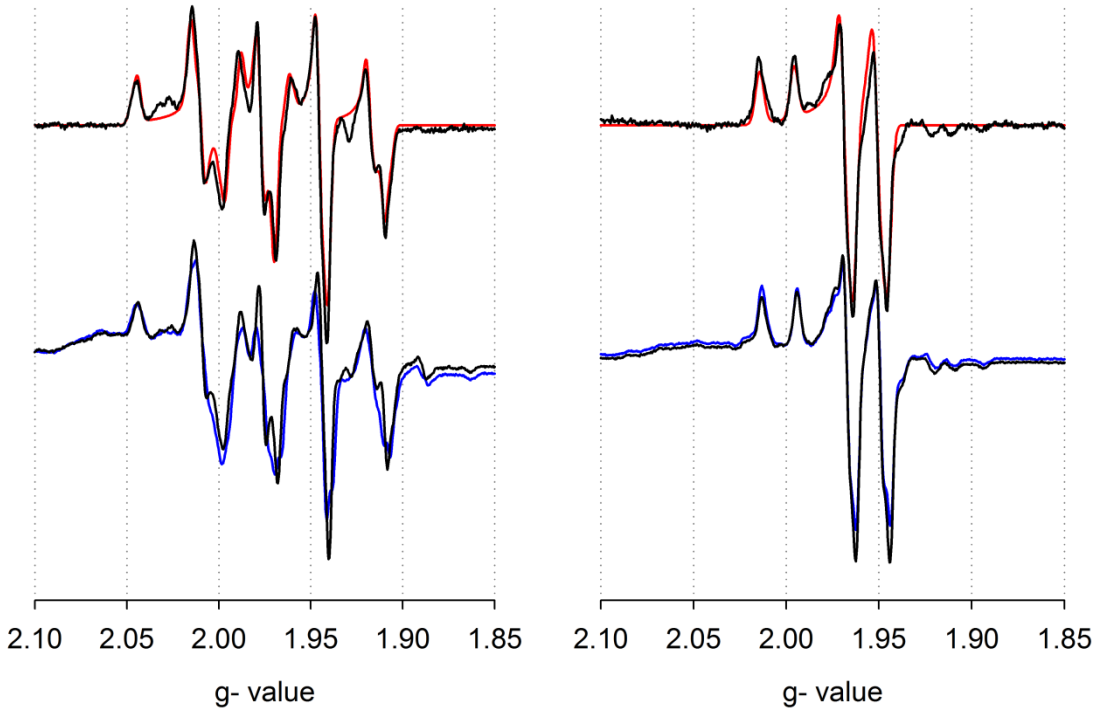

Figure 5.3. 9 GHz X-band EPR spectra of copper- or silver- containing CO dehydrogenase reduced with ^{12}CO or ^{13}CO

A. ^{12}CO-reduced CO dehydrogenase in 50 mM HEPES, pH 7.2, with simulation in red; *B*. ^{12}CO-reduced CO dehydrogenase in 50mM HEPES, pH 7.2 (black) and ^{13}CO-reduced CO dehydrogenase in 50mM HEPES, pH 7.2 (blue); *C*. ^{12}CO-reduced silver- substituted CO dehydrogenase in 50 mM HEPES, pH 7.2, with simulation in red; D. ^{12}CO-reduced silver- substituted CO dehydrogenase in 50 mM HEPES, pH 7.2, and ^{13}CO-reduced silver- substituted CO dehydrogenase in 50mM HEPES, pH 7.2 (blue).

The EPR instrument settings were: 9.45 GHz microwave frequency; 4 milliwatt microwave power; 5 Gauss modulation amplitude; 150 K.

The 35 GHz Echo-detected EPR spectrum at 2 K is shown in Figure 5.4 for the native, copper- containing, enzyme. In addition to the signal from the binuclear center, the spectrum shows signals from the two [2Fe-2S] centers of the enzyme, Figure 5.5, a proximal cluster ~ 15 Å from the molybdenum center (designated Fe/S I), and a second more distal one ~ 25 Å away (Fe/S II).[65,66] The g tensors of these centers are approximately; **g**(Fe/S I) = [2.000, 1.938, 1.919] and **g**(Fe/S II) = [2.08, 1.998, 1.900]. At 150 K, the EPR signals arising from the iron-sulfur centers relax very fast and are not detected, behavior that is typical of the iron-sulfur clusters in this family of molybdenum-containing enzymes.

Although the EPR signal from the [2Fe-2S] centers overlaps that of the binuclear center, this causes no problem for ENDOR measurements. ^{13}CO signals are identified by comparing centers prepared with $^{13/12}$CO, and the [2Fe-2S] centers give no ENDOR response in the vicinity of ^{63,65}Cu ENDOR transitions.[67]

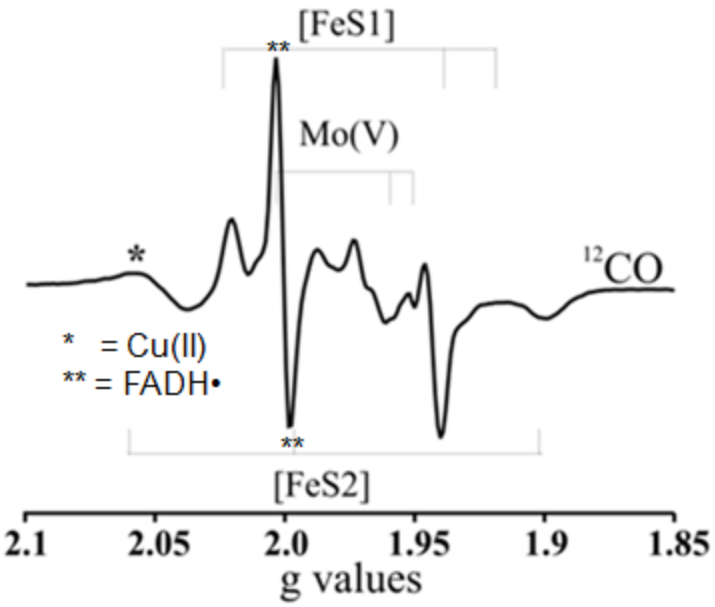

Figure 5.4. 35 GHz Echo-detected 2K spectrum of CO dehydrogenase

35 GHz EPR spectra of the binuclear signal (black solid line) in H_2O buffer at 2 K. *Conditions:* two-pulse echo, π-pulse length = 80 ns, τ = 600 ns, repetition time = 50 ms, microwave frequency = 34.8 GHz, T = 2 K. The 'braces' show the field values for the canonical g-values of the Fe/S clusters. The asterisk denotes the signal of adventitious Cu(II) in the signal, and the double asterisk the isotropic signal of FADH• from the enzyme, with g = 2.00.

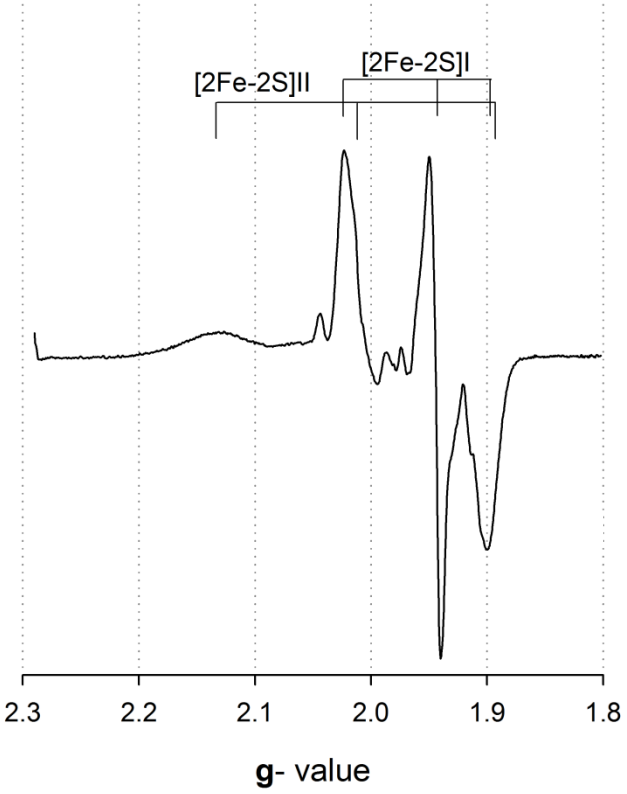

Figure 5.5. 9 GHz EPR spectrum of the two [2Fe-2S] clusters of CO dehydrogenase.

Low temperature (18K) spectrum of CO dehydrogenase fully reduced with dithionite so no contribution from the Mo/Cu active site or flavin semiquinone is observed, with two overlapping Fe/S clusters. *B*. Low temperature (18K) spectrum of xanthine dehydrogenase with two overlapping Fe/S clusters. The g tensors of these centers are approximately; **g**(Fe/S I) = [2.000, 1.938, 1.919] and **g**(Fe/S II) = [2.08, 1.998, 1.900].

The EPR instrument settings were: 9.45 GHz microwave frequency; 4 milliwatt microwave power; 5 Gauss modulation amplitude;

Davies ENDOR spectra of the binuclear center of the native CO dehydrogenase, recorded at 2 K and taken at g = 1.971, are shown in Figure 5.6 (*top*) for samples of the native enzyme reduced by ^{12,13}CO. The υ^+ = 23 MHz branch of the ^{13}C doublet ($\nu^{\pm}(^{13}C) = |A(^{13}C)/2 \pm \nu\ (^{13}C)|$) from ^{13}CO is evident. Assignment as ν^- would yield a hyperfine coupling too large to be compatible with the X-band EPR spectra. At the field of observation, $\nu^+(^{13}C)$ is ~13.5 MHz, yielding $A(^{13}C)$ ~ 19 MHz for the ^{13}C-hyperfine coupling. The ENDOR intensity in the 9-16 MHz region for both labeled and unlabeled samples can be assigned to amide ^{14}N features from the two [2Fe-2S] clusters, whose EPR signals overlap the Mo(V) EPR signal at low temperature (Figure 5.5). Subtraction of the ^{12}CO background (black line) from the ^{13}CO spectrum (red line) of the binuclear cluster more clearly shows the ν^+ peak (red dotted line), but also reveals the ν^- branch of the ^{13}C-doublet (relaxation effects lead to the reduced intensity for ν^-). Figure 5.6 (*bottom*) shows a 2-D field-frequency plot of the background-subtracted Davies ^{13}C-ENDOR spectra for the binuclear cluster of CO dehydrogenase reduced by ^{13}CO, recorded at selected magnetic fields across the EPR envelope. The frequencies of the ^{13}C doublet remain essentially constant over the entire absorption envelope, and the pattern can be simulated by the hyperfine tensor, $\mathbf{A}(^{13}C)$ = [16.7, 16.5, 18.8] MHz. The ^{13}C hyperfine tensor is thus dominated by an isotropic coupling of $a_{iso}(^{13}C)$ = 17.33 MHz, with an extremely small anisotropic term that approximates the dipolar form: **T** = [-*T*, -*T*, 2*T*] where *T* = 0.73 MHz. These results are summarized in Table 5.1. The complete 2-D field

frequency pattern for the silver substituted CO dehydrogenase, Figure 5.7, indicated no ^{13}C coupling in agreement with the observed EPR spectrum.

Figure 5.8 shows a 2-D field-frequency plot of Davies ENDOR spectra collected over the frequency range of 30-100 MHz at multiple field settings across the EPR envelope for the spectrum seen with native enzyme reduced by ^{12}CO. At all magnetic field settings the spectra exhibit a strong ^{1}H-ENDOR response arising from weakly coupled proton(s) without well-resolved structure. These ^{1}H-ENDOR features overlap with ENDOR features attributable to $^{95,97}Mo$ (I = 5/2), isotopes that together account for 25 % of the total isotopic abundance. These features are similar to those that have been seen previously in the ENDOR spectrum of the formaldehyde-inhibited Mo(V) signal of xanthine oxidase.[68] Because of the poor resolution and low natural abundance, combined with the additional complexity arising from strong quadrupolar coupling in the case of ^{97}Mo, no attempt has been made to simulate this pattern. However, its overall character indicates that the isotropic hyperfine coupling for molybdenum, $a_{iso}(^{95,97}Mo)$, is roughly 75-125 MHz. [69]

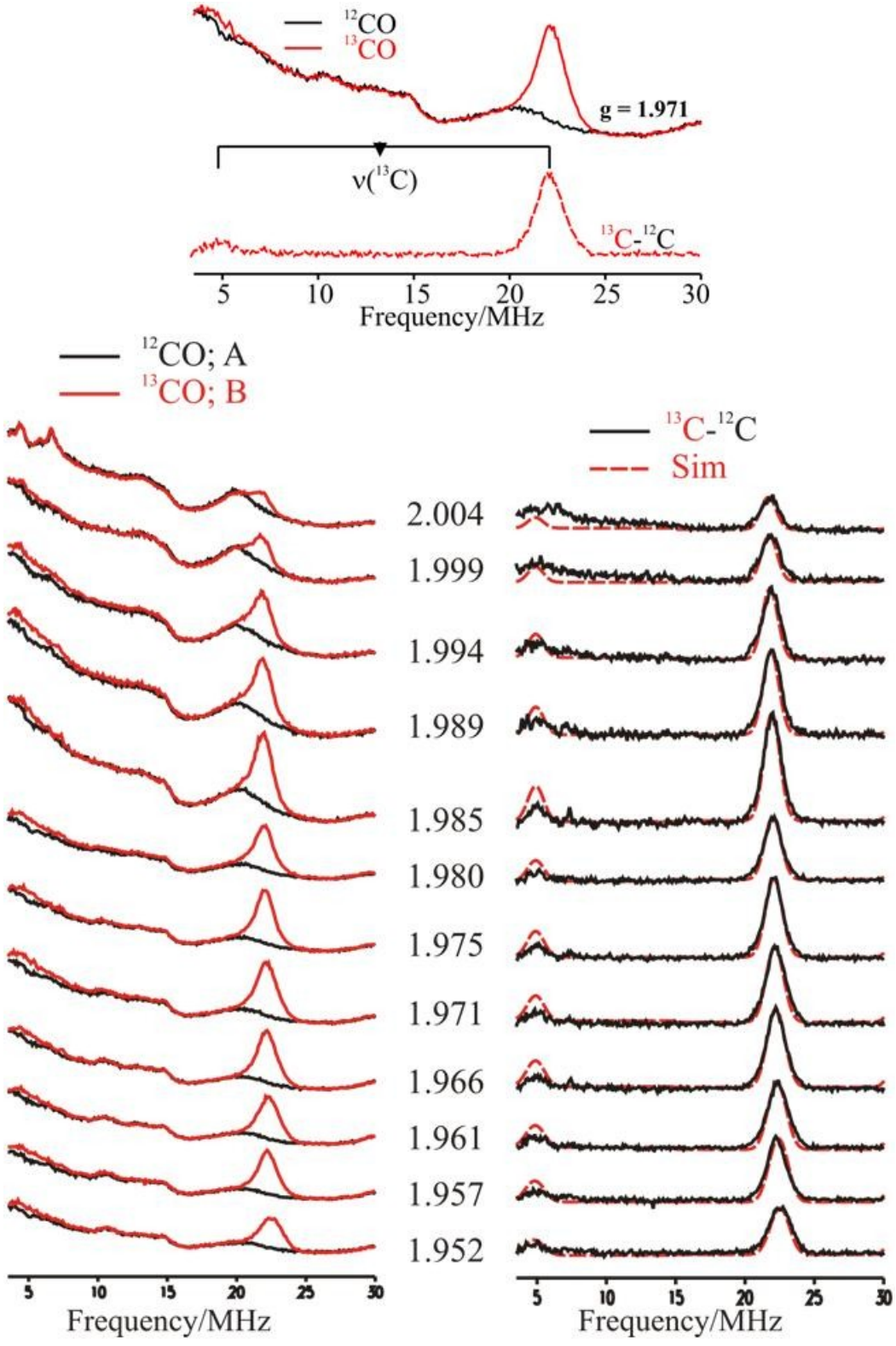
12CO
13CO
g = 1.971
ν(13C)
13C-12C
5
10
15
20
25
30
Frequency/MHz
12CO; A
13CO; B
13C-12C
Sim
2.004
1.999
1.994
1.989
1.985
1.980
1.975
1.971
1.966
1.961
1.957
1.952
5
10
15
20
25
30
Frequency/MHz
5
10
15
20
25
30
Frequency/MHz

Figure 5.6. Davies ^{13}C-ENDOR spectra of the molybdenum- and copper-binuclear center of CO dehydrogenase

Top: Davies ^{13}C-ENDOR spectra of the binuclear signal measured at g = 1.971. The red dotted line shows the ^{13}C hyperfine coupling, obtained by subtracting the spectrum of ^{12}CO (black line) from that of ^{13}CO (red line) in H_2O. The black horizontal bar connects the ^{13}C peaks centered at $\nu(^{13}C)$ and separated by **A**(^{13}C). The low intensity of the low-frequency partner common in Q-band ENDOR.

Bottom: Experimental (left) and simulated (right) 2-D field-frequency plot of Davies ^{13}C-ENDOR spectra of the binuclear signal reduced with ^{12}CO **(**black lines) and ^{13}CO **(**red lines) in H_2O: *Conditions: (left):* π-pulse length = 120 ns, τ = 600 ns, repetition time = 40 ms, average microwave frequency = 34.783 GHz, T = 2 K; (*right):* red dashed lines are simulated spectra overlaid on the background subtracted (black lines) experimental spectra. The amplitudes of the simulated u^- (^{13}C) signals are multiplied by 1/3 to reflect the low-intensities due to relaxation effects.

Conditions: π-pulse length = 120 ns, τ = 600 ns, repetition time = 40 ms, microwave frequency = 34.795 GHz, T = 2 K.

Table 5.1. Spin Hamiltonian parameters used to simulate[a] the 2-D ENDOR patterns of ^{13}C and $^{63,65}Cu$ nuclei of Cu-CO dehydrogenase.

Nuclei	A_1	A_2	A_3	a_{iso}	**T**
^{13}C	+16.7	+16.5	+18.8	+17.33	[-.6, -.8, 1.5]
$^{63,65}Cu$ (ENDOR)[b]	+148	+148	+148	+148	[-20.7, +26.4,-5.7]
$^{63,65}Cu$ (EPR)	117	164	132	+137.6	~0
$^{95,97}Mo$ (ENDOR)				75-100	

[a] Simulations employed **g** = [2.002, 1.958, 1.953] and the hyperfine couplings are in MHz.

[b] Quadrupole splitting for $^{63,65}Cu$ (I = 3/2) are not observed, their inclusion had no effect on simulations, so were not incorporated.

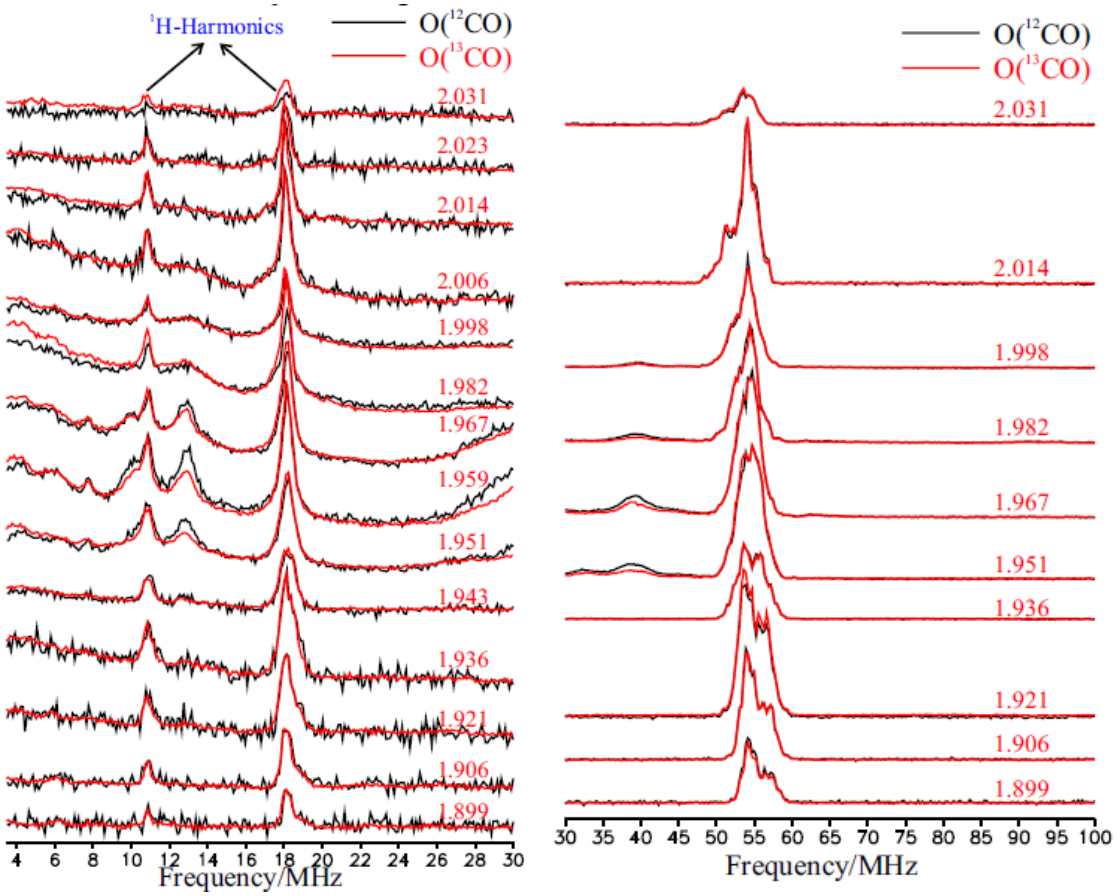

Figure 5.7 Davies ^{13}C-ENDOR spectra of the molybdenum- and silver- binuclear center of CO dehydrogenase.

2-D field-frequency plot of Davies ^{13}C-ENDOR spectra of the silver-molybdenum- binuclear signal. CO dehydrogenase partially reduced with ^{12}Co in black and ^{13}CO in red. The low intensity of the low-frequency partner common in Q-band.

The hyperfine tensor measured in the X-band EPR spectrum from the overlapping splittings of ^{63}Cu,(69 %) and ^{65}Cu (30 %), predicts the presence of a Q-band ^{63,65}Cu ENDOR response from the $\nu^{+}(^{63,65}\text{Cu})$ manifold in the frequency range, ~ 75-100 MHz. The Q-band ENDOR spectra taken at 2 K exhibit the predicted response, with $\nu^{+}(^{63,65}\text{Cu}) \sim 90$ MHz (Figure 5.8, blue horizontal bar) corresponding to a hyperfine coupling of $|A(^{63,65}\text{Cu})| = 148$ MHz, within the range of values expected from the EPR-derived hyperfine tensor. The signals are exceedingly sharp compared to those seen for a Cu(II) protein;[70] and there is no evidence in the ENDOR spectra for the significant quadrupolar coupling to the $I = 3/2$ nuclear spin of ^{63,65}Cu seen in the protein.

The frequency of this ^{63,65}Cu signal remains constant as the field is moved towards g_2 and g_3, indicating that the hyperfine interaction is isotropic within experimental error, with $a_{iso}(^{63,65}\text{Cu}) = +148$ MHz, quite consistent with that obtained from the 150 K continuous-wave EPR spectrum, $|a_{iso}| = 136.7$ MHz. There is no detectable dipolar component in the 2 K ENDOR spectra, but the spectra collected towards the high field/low-g-value edge of the EPR spectrum do show a 'tailing' towards higher frequency that may reflect a minimal heterogeneity in the geometry at Cu(I). This is compatible with an assignment of the minor differences between the 150 K EPR simulations and the 2 K ENDOR results to slight changes in the geometry at Cu(I) with cooling; note that considerable changes in the geometry of a diatomic bound to a metal ion upon

cooling, in analogy to the Cu-CO, are well known.[71] For consistency, the ENDOR-derived values for ^{63,65}Cu will be used in the following discussion.

Signs for the hyperfine tensors, which are not available from EPR measurements, were determined from the ENDOR spectra of the binuclear cluster (more specifically, the sign of $g_{Nuc}A_{Nuc}$) using the Pulse-Endor-SaTuration-REcovery (PESTRE) protocol, a pulse multi-sequence comprised of multiple Davies ENDOR sequences.[72,73] Figure 5.9 shows the PESTRE measurements obtained at g = 1.975 for the υ^+ branches of the ^{13}C and ^{63}Cu-ENDOR responses, where relatively sharp ENDOR responses for ^{13}C and ^{63,65}Cu nuclei are observed. In phase I of the PESTRE traces (no radio frequency illumination), the υ^+ branches of the ^{13}C and ^{63,65}Cu have reached the steady-state electron spin-echo baseline; in phase II, radio frequency excitation is applied and converts the spin populations and spin-echo response to their steady-state ENDOR values; in phase III (again in the absence of radio frequency illumination), the electron-nuclear spin populations give rise to a spin-echo signal denoted as the dynamic reference level, which relaxes to the BSL. In phase III, the υ^+ signals of ^{13}C (red line) and ^{63}Cu (blue line; inset) both relax to the spin-echo baseline 'from below', behavior that unambiguously establishes that both **A**(^{13}C) and **A**(^{63,65}Cu) are positive.

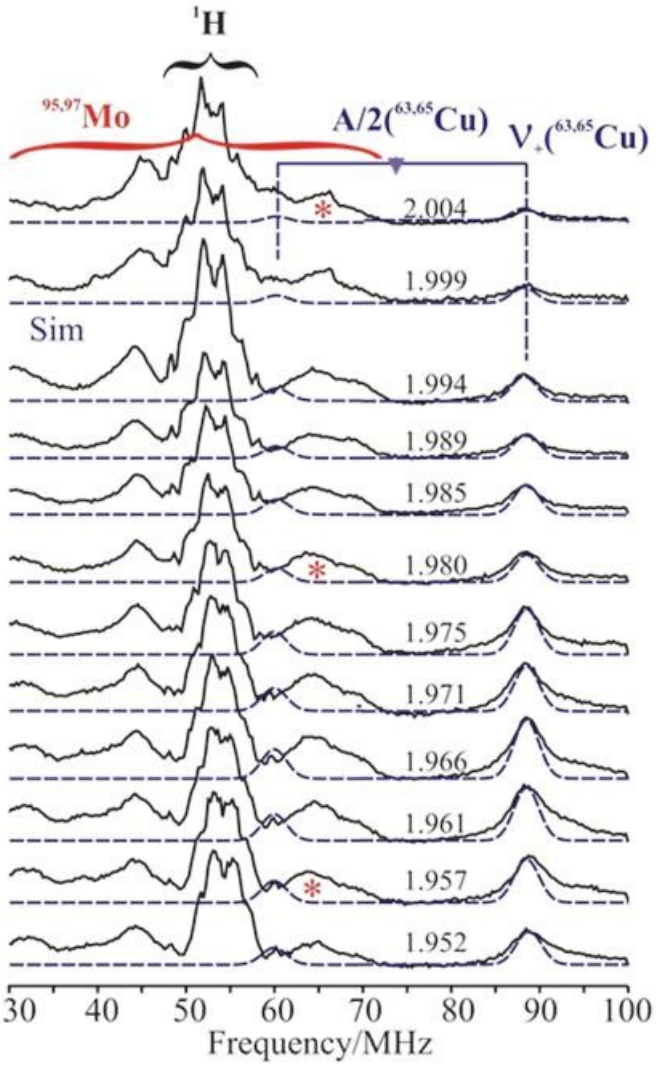

Figure 5.8. 2-D field-frequency plot of broad-band Davies ENDOR spectra of the molybdenum- and copper- binuclear signal reduced by ^{12}CO.

The black brace encompasses the frequency range of ^{1}H signals; the red brace encompasses the frequency range of ^{95,97}Mo signals, with the (*) in representative spectra identifying resolved ^{95,97}Mo signals. Blue 'goalpost' connects the ^{63,65}Cu peaks at $\nu^{+}(^{63,65}\text{Cu}) \sim 87$ MHz and $\nu^{-}(^{63,65}\text{Cu}) \sim 60$ MHz; the center frequency is A(^{63,65}Cu)/2 and separation is 2ν(^{63,65}Cu). Blue dotted lines are simulations of the ^{63,65}Cu spectra, where the amplitudes of the υ^{-} branches are multiplied by ½ to reflect their low intensities.

Conditions: π-pulse length = 120 ns, τ = 600 ns, repetition time = 40 ms, microwave frequency = 34.772 GHz, T = 2 K.

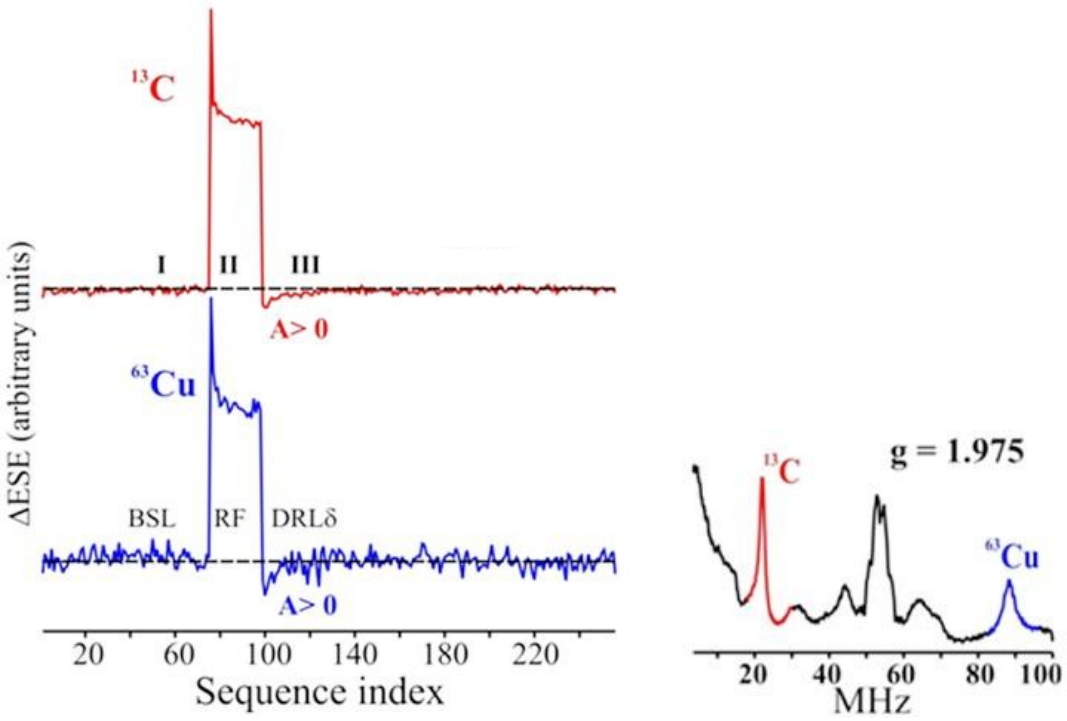

Figure 5.9. PESTRE protocol spectra of the molybdenum- and copper-containing CO dehydrogenase

Pulse-Endor-SaTuration-REcovery (PESTRE) protocol, a pulse sequence comprised of multiple Davies ENDOR sequences, spectra measured at the υ^+ peaks of the ^{13}C and ^{63,65}Cu nuclei (left; indicated as red and blue lines) of the binuclear signal. The RF frequencies and the g value at which PESTRE experiments were carried out are given in the left figure

Conditions: π-pulse length = 120 ns, τ = 600 ns, repetition time = 40 ms, t_{RF} = 20 μs, microwave frequency = 34.795 GHz, T = 2 K.

5.4. Discussion

The aim of the present investigation is to determine the structure of the species that gives rise to the EPR signal seen upon partial reduction of CO dehydrogenase with CO to elucidate the reaction mechanism of the enzyme. The most remarkable EPR/ENDOR feature of this species is the large and positive *isotropic* hyperfine coupling to copper, with $a_{iso}(^{63,65}Cu)$ = +148 MHz, with negligible anisotropic hyperfine coupling to the I = 3/2 nuclear spin. Whereas the magnitude of $a_{iso}(^{63,65}Cu)$ is, consistent with the X-band EPR, as is the finding of minimal anisotropy, the ENDOR measurements now show that the observed isotropic copper hyperfine coupling is *opposite in sign* to that of d^9 Cu(II) centers with an unpaired electron in a ($d\sigma^*$) orbital. Moreover, the small-to-vanishing anisotropic component seen with CO dehydrogenase contrasts sharply with the anisotropy in such Cu(II) centers, where large *negative* isotropic *and negative* anisotropic ^{63,65}Cu couplings are typically observed: $a_{iso}(^{63,65}Cu) \sim T(^{63,65}Cu) \sim$ -[150-200] MHz;[74-76] for a type 2 copper center, $a_{iso}(^{63,65}Cu) \sim T(^{63,65}Cu) \sim$ -70 MHz for a type I Cu[77,78]. The copper hyperfine couplings in CO dehydrogenase are instead consistent with a d^{10} Cu(I) ion whose closed-shell electronic configuration acquires a large *positive* a_{iso} from delocalization of the electron spin in the 'Mo(V) SOMO' over the entire [Mo(V)-(μ-S)-Cu(I)] unit, into the 4*s* orbital of copper.

In support of this assignment, we observe that the Cu(I) hyperfine coupling seen here is quite similar to that of Cu(I) in an inorganic model compound prepared by Gourlay *et al.,*[79] which mimics the structure and spectroscopic properties of the paramagnetic active site of CO dehydrogenase: [$Tp^{iPr}Mo^{(V)}$(O)(OAr)(μ-S)$Cu^{(I)}$(Me_3tcn)] (where Tp^{iPr} = hydrotris(3-isopropylpyrazol-1-yl)borate; OAr = 3,5-(di-*t*-butyl)phenolate; Me_3tcn = 1,4,7-trimethyl-1,4,7-triazacyclononane). The isotropic Cu(I) hyperfine interaction, $|a_{iso}(^{63,65}Cu)|$ ~159 MHz, observed for this model is quite similar in magnitude to $a_{iso}(^{63,65}Cu)$ = +148 MHz seen with CO dehydrogenase. Calculations on the model have confirmed that the remarkably large values of a_{iso} reflect a strong covalent delocalization of the SOMO through the bridging sulfido.

The hyperfine coupling to ^{13}C in the EPR signal manifested by ^{13}CO-reduced CO dehydrogenase also is distinctive in being highly isotropic. The isotropic coupling, $a_{iso}(^{13}C)$ = +17.4 MHz, is intermediate between the values observed to date for carbon-containing ligands to a paramagnetic Mo(V) center: $a_{iso}(^{13}C)$ = +43.8 MHz for formaldehyde-inhibited xanthine oxidase[68,80,81,32] and $|a_{iso}(^{13}C)|$ = 7.9 MHz for the 'very rapid' Mo(V) intermediate trapped with that enzyme.[60,82] Additionally, the anisotropic component seen here with CO dehydrogenase, T = 0.73 MHz[83], is smaller than that observed in the formaldehyde-inhibited xanthine oxidase (T = 3.8 MHz) and slightly smaller than that observed in the 'very rapid' intermediate (T = 1.15 MHz). We therefore argue

that this small isotropic ^{13}C coupling is unlikely to arise from a species with a Mo-C bond.

One possible assignment for the state studied here is Structure A of Figure 5.2. Our recent $^{1,2}H$ and ^{13}C-ENDOR study of the formaldehyde-inhibited Mo(V) of xanthine oxidase[68,81,84] has shown that it possesses the core of four-membered ring structure D, with a Mo-C distance of 2.76 Å in the DFT-optimized geometry.[68,84] This structure resembles that of structure A' (Figure 5.2), found by X-ray diffraction of *n*-butylisonitrile-inhibited CO dehydrogenase (with a Mo-C distance of 2.63 Å)[28]. The planar geometry of the related Structure D, with short Mo-C distance within the ring, favors strong covalent spin delocalization via the Mo-O-C linkage or a strong "transannular hyperfine interaction" between Mo(V) d_{xy} orbital and carbon 2s orbitals, resulting in an extremely large hyperfine coupling to the ^{13}C of formaldehyde, with a_{iso} = 44.6 MHz.[68] The significantly smaller hyperfine coupling for ^{13}C seen here with CO dehydrogenase thus argues against Structure A of Figure 5.2 being responsible for the observed EPR signal.

A second possible assignment of the Mo(V) species studied here is the five-membered metallacyclic ring of Structure B (Figure 5.2), the closest established analogue of which is the species giving rise to the "glycol-inhibited" Mo(V) EPR signal of desulfo xanthine oxidase (Figure 5.2, Structure E). The $^{1,2}H$-ENDOR results for the "glycol-inhibited" species were interpreted in terms of

a five-membered (Mo-O-C-C-O) metallocyclic structure.[68,81] The paramagnetic Mo(V) species giving rise to the "very rapid" EPR signal seen with xanthine oxidase also has a Mo-O-C unit analogous to that of Structure B. Here, the slow substrate 2-hydroxy-6-methylpurine[59] is bound to the Mo(V) ion via the equatorial oxygen atom after being incorporated into product as a hydroxyl group.[60,85] When the C-8 position of 2-hydroxy-6-methylpurine is labeled with ^{13}C, a_{iso} for the "very rapid" signal is 7.9 MHz[68], while a_{iso} for the ^{13}C of glycol in the glycol-inhibited signal a_{iso} is even smaller at 6.2 MHz (Shanmugam *et al.*, unpublished). In both cases, the ^{13}C hyperfine coupling is weak because there is no direct bonding of carbon to Mo(V) and the Mo-C distance is long (~ 3.4 Å), precluding strong overlap between Mo(V) d_{xy} and carbon 2s orbitals. DFT results, compiled by the lab of Martin Kirk at the University of New Mexico, for structure B yield a very large a_{iso} for ^{13}C of 54 MHz, however, much larger than observed experimentally. The calculated copper hyperfine also is highly rhombic, $\mathbf{A}(^{63,65}Cu)$ = [19,-94,105] MHz, in sharp disagreement with the observed isotropic coupling seen here with CO dehydrogenase. These observations argue against Structure B being responsible for the signal seen with CO dehydrogenase.

It is noteworthy that a recent X-ray crystallography study of the glycol- and glycerol-inhibited Mo centers of AOR claims a third structure variant, a direct Mo-C bond (structure F) for this species.[66] However, if for illustrative purposes we assume that the dipolar interaction arises solely from a through-space interaction of the ^{13}C with a point electron spin on Mo(V), the measured value T = 0.73 MHz

corresponds to a Mo-C distance of ~ 2.4 Å. Subtraction of a ^{13}C local contribution to the observed T_{obs} = 0.73 MHz, would further increase the resultant Mo-C distance[60], thus ruling out a direct Mo-C bond in CO dehydrogenase. A similar analysis[60] has helped rule out a direct Mo-C bond in the "very rapid" Mo(V) signal of xanthine oxidase prepared with 2-hydroxy-6-methylpurine (^{13}C-8).

Overall, a comparison of the ^{13}C coupling seen here (Table 5.1) with previously reported ^{13}C hyperfine tensors for a ligand to the paramagnetic Mo(V) enzyme species indicates that Structures A and B, as well as any structure with a Mo-CO bond, are unlikely to represent the structure of the binuclear center of CO dehydrogenase. Instead we propose that Structure C of Figure 5.2, with CO coordinated to the copper of the Mo(V)-Cu(I) binuclear center best represents the structure seen in the enzyme.

A structure having a Cu(I)-coordinated CO is consistent with both of the computational studies of the reaction of CO dehydrogenase that identify CO coordinated to the copper of a fully oxidized binuclear center as the starting point for catalysis.[41,62] In the case of the partially reduced complex examined in the present study, with the molybdenum in the EPR-active Mo(V) valence state, the enzyme cannot progress through the catalytic sequence, thus accounting for the accumulation of the signal in the course of our sample preparation. Our Mo(V)/Cu(I)•CO species in fact represents a paramagnetic analog to the *bona fide* Michaelis complex for the reaction, and is thus analogous to the species

giving rise to the well-characterized “Rapid” Mo(V) EPR signals in the related molybdenum-containing enzyme xanthine oxidase (albeit with a substantively different structure). [86]

Our ENDOR results provide direct experimental support for CO coordination to Cu(I) of the binuclear center of CO dehydrogenase. Upon binding of CO, the reaction progresses as shown in Figure 5.10 by nucleophillic attack of the equatorial Mo=O oxygen on the Cu-bound CO, with substrate likely activated to at least some degree by back bonding from the copper which leads to population of the CO π^* orbital. The DFT calculations of Hofmann and coworkers[13] indicate that this chemistry leads to a set of three species having the structures shown in a red box in Figure 5.10. Although presented as discrete intermediates in the computational work, we consider it likely that these species are readily interconverted. We further observe that they involve bonding of the carbon of substrate to each of the three atoms of the Mo-μ(S)-Cu core, and that subsequent work has shown each of the three core atoms to contribute significantly to the redox-active orbital.[79] We therefore present these species in Figure 5.10 as an ensemble of states from which the reaction proceeds further. Completion of the catalytic sequence involves formal reduction of the binuclear cluster and formation of CO_2 from this ensemble, with hydroxide from solvent necessarily being introduced into the molybdenum coordination sphere to regenerate the equatorial ligand of the molybdenum and complete the catalytic cycle.

In summary, the ENDOR and computational study presented here provides direct experimental evidence that the EPR signal seen in the course of substrate reduction of CO dehydrogenase arises from a partially reduced, Mo(V)/Cu(I), binuclear center with CO bound at the copper. This conclusion provides strong support for a reaction mechanism that begins with a fully oxidized binuclear cluster, with CO coordinated to copper and thereby activated for nucleophillic attack by the equatorial Mo=O ligand.

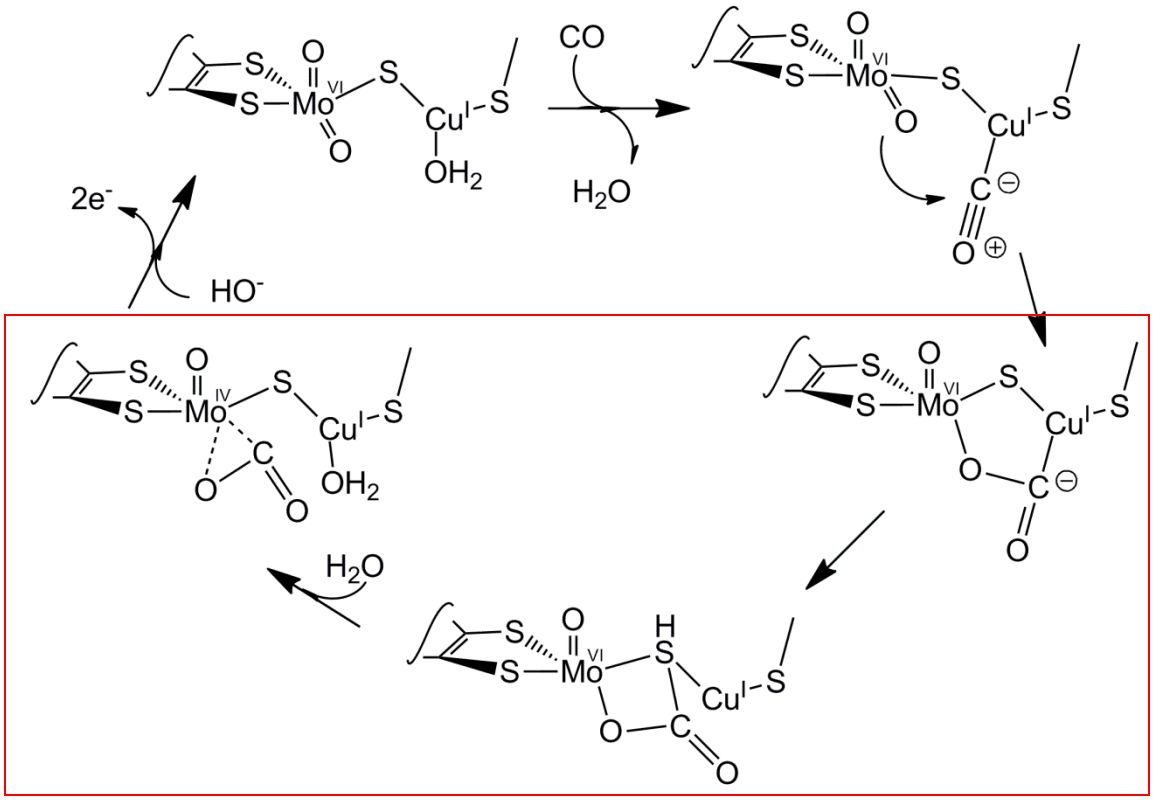

Figure 5.10. Reaction Mechanism of CO dehydrogenase

Upon binding of CO, the reaction progresses by nucleophillic attack of the equatorial Mo=O oxygen on the Cu-bound CO, with substrate likely activated to at least some degree by back-bonding from the copper which leads to population of the CO π* orbital.

Chapter 6

Kinetic and spectroscopic characterization of Hydrogenase activity present in CO dehydrogenase

6.1. Introduction

The molybdenum- and copper- containing CO dehydrogenase is not only unique in the active site it contains but also the reactions it will catalyze. The undisputed physiological role is CO oxidation for growth and energy. An additional function first described by Santiago *et. al.* is H_2 oxidation and formation, Equation 6.1.[87]

Eq 6.1: $H_2 \longleftrightarrow 2H^+ + 2e^-$

It was proposed in this work that H_2 formation may serve to protect the enzyme in the case of reductive stress build up. The reductive stress was established by Gourlay et. al. in computational and spectroscopic studies on an active site model to the enzyme that the singly occupied molecular orbital for the active site is anti-bonding with respect to the Cu^I-μS bond.[39] H_2 formation at the active site may serve to oxidize the site and prevent bond breakage and enzyme inactivation. The H_2 oxidation activity is likely not physiological as the organism contains a Ni-Fe hydrogenase expressed in the presence of H_2 but must do so under anaerobic conditions as with other Ni-Fe hydrogenases.[88-91] In the present work we have characterized the reduction of the Mo(VI)-Cu(I) CO

dehydrogenase by H_2, and find that the enzyme is indeed rapidly reduced by H_2 over a broad range of pH with no effect of molecular oxygen present in the reaction. In the course of the reaction, a new EPR signal attributable to the binuclear center is observed that provides important mechanistic clues as to the manner in which H_2 is oxidized.

6.3. Results

6.3.1. Steady-State Kinetics.

Steady state kinetics were carried out anaerobically as described in Materials and Methods, examining the dependence of catalytic velocity on [H_2] at 25 ^{0}C, pH 7.2, from 20 μM to 780 μM, using 1-4 benzoquinone[12] as the oxidizing substrate. The observed rates were plotted against H_2 concentration, as shown in Figure 6.1 (*left*), and the data fit to a hyperbolic function using the Michaelis-Menten kinetics equation, yielding a k_{cat} of 5.1 s^{-1} and a K_m of 283 μM.

6.3.2. Rapid Reaction Kinetics.

To further examine the reaction of CO dehydrogenase with H_2, rapid reaction kinetic experiments were performed, monitoring the bleaching of enzyme at 450 nm (due to bleaching of the iron-sulfur and FAD sites) upon reduction by H_2 under anaerobic conditions in 50 mM HEPES, pH 7.2, 25 ^{0}C. Kinetic transients at 450 nm were well-behaved and fit to single exponentials to

obtain k_{obs} for each H_2 concentration examined. Figure 6.1 (*right*) shows a plot of k_{obs} *vs.* [H_2], which exhibits the expected hyperbolic shape. When fitted with a hyperbolic equation, a limiting rate constant for reduction at infinite [H_2], k_{red}, and dissociation constant for H_2, K_d^{H2}, was determined to be 5.3 s^{-1} and 525 μM, respectively. The observed k_{red} is in good agreement with the steady-state k_{cat} of 5.1 s^{-1}, indicating that the rate-limiting step in overall catalysis resides in the reductive half reaction, as seen with CO as substrate.[34] Rate constants obtained at 550 nm, monitoring reduction of the Fe-S clusters alone, were in good agreement with those obtained at 450 nm, with no evidence of the accumulation of long wavelength-absorbing intermediates. The reductive half-reaction was examined over the pH range 6 to 10 (50mM phosphate (pH 6.0), 50mM HEPES (pH 7.2), 50mM Tris-HCl (pH 8.0), 50mM Tris-HCl (pH 9.0), and 50mM CAPS (pH 10.0), and in each case hyperbolic plots of k_{obs} *vs.* [H_2] were observed (Figure 6.1, *right*). The kinetic parameters thus obtained are summarized in Table 6.1; k_{red}, K_d^{H2} and k_{red}/K_d^{H2} are found to vary only modestly (by no more than a factor of three) over the pH range. We conclude that no reversible substrate- or enzyme-based ionizations are involved in the rate-limiting chemistry of H_2 oxidation.

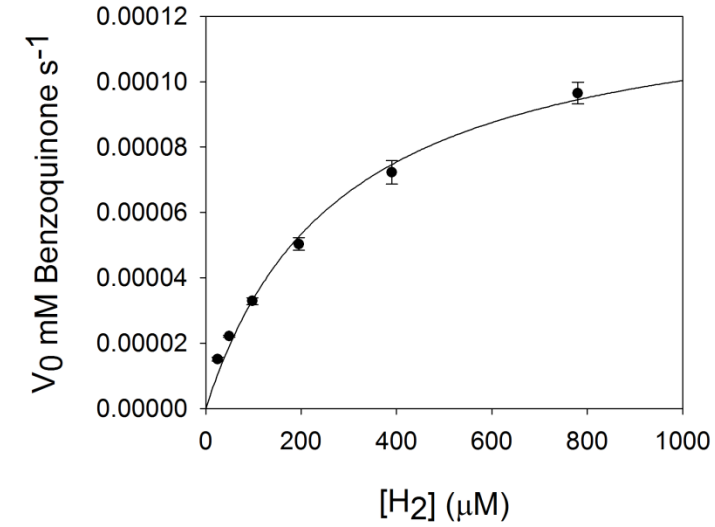
0.00012
0.00010
0.00008
0.00006
0.00004
0.00002
0.00000
V0 mM Benzoquinone s-1
0
200
400
600
800
1000
[H2] (μM)

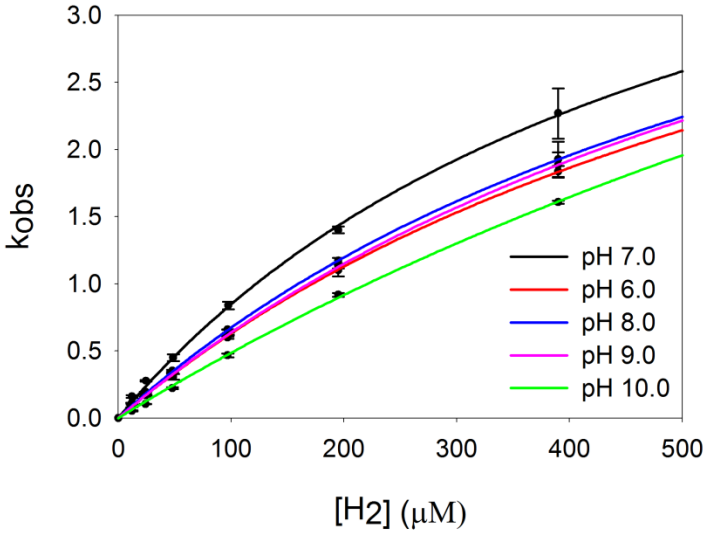
3.0
2.5
2.0
1.5
1.0
0.5
0.0
kobs
0
100
200
300
400
500
[H2] (μM)
pH 7.0
pH 6.0
pH 8.0
pH 9.0
pH 10.0

Figure 6.1. Steady-state and rapid reaction kinetics of CO dehydrogenase with H_2 as substrate.

Top: Steady state H_2 concentration dependence of CO dehydrogenase using 50 µM 1-4 Benzoquinone as the electron acceptor in 50 mM HEPES, pH 7.2 at 25 ^{0}C. Plots of the initial rates, following 1-4 benzoquinone reduction at 247 nm after mixing a final concentration of 25 nM CO dehydrogenase with H_2 dissolved in 1-4 benzoquinone, versus [H_2] were fit with the Michaelis–Menten equation using Sigma Plot (R^2 = 0.995) to give a k_{cat}^{H2} of 5.1 s^{-1} and K_m^{H2} of 283 µM.

Bottom: Rapid reaction kinetic plots of the rate k_{obs}^{H2} following the reduction of 5µM CO dehydrogenase at 450 nm versus [H_2], from 12 µM to 390 µM, at (50 mM Phosphate pH 6.0, 50 mM HEPES pH 7.2, 50 mM TRIS-HCl pH 8.0 and pH 9.0, and 50 mM CAPS pH 10.0.), 25 ^{0}C. Plots were fit using equation 2 to yield a rate of reduction and substrate dissociation constant, k_{red}^{H2} and K_d^{H2}. The optimum pH, 7.2, gave k_{red}^{H2} of 5.3 s^{-1} and K_d^{H2} of 525 µM (R^2= .999).

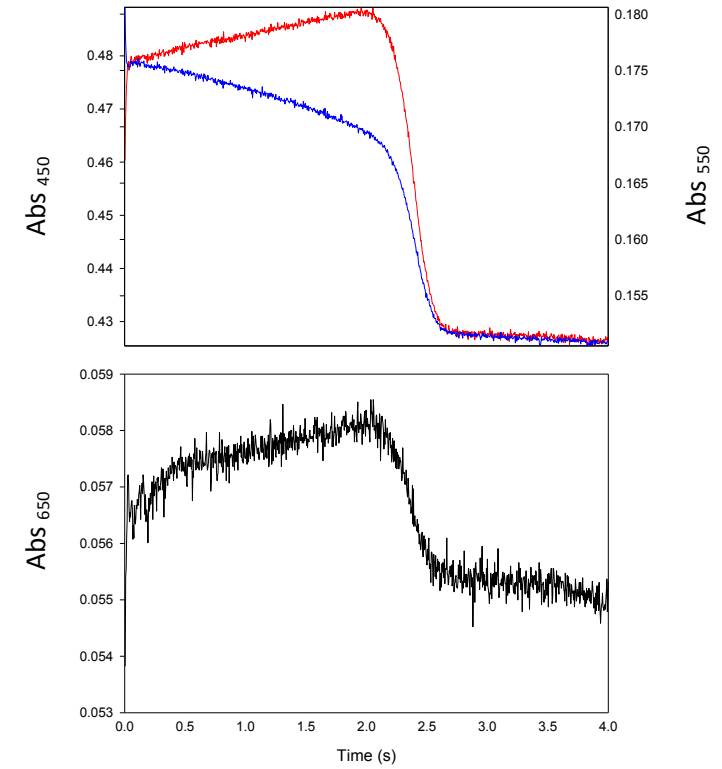
Abs 450
Abs 550
Abs 650
Time (s)

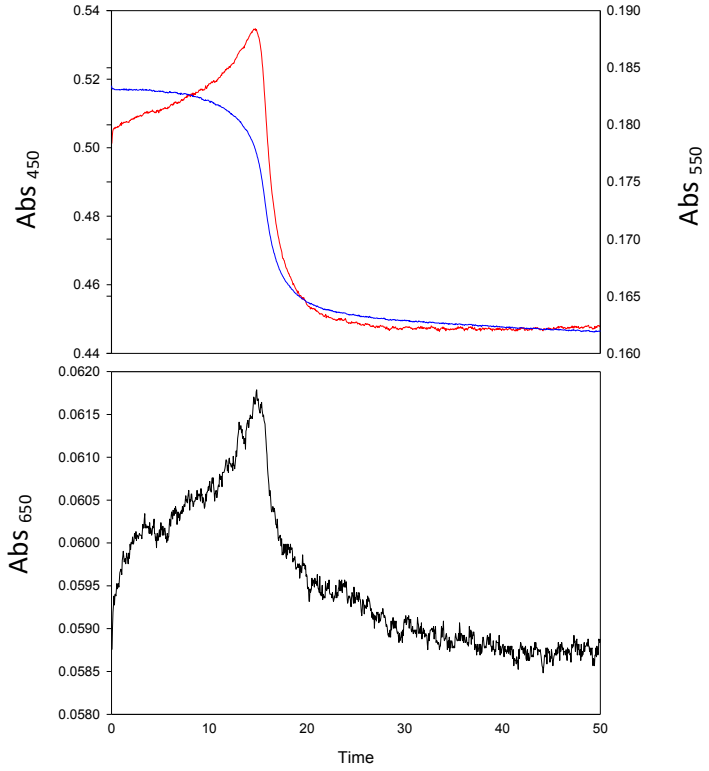
Abs 450
Abs 550
Abs 650
Time

Figure 6.2. Enzyme-monitored turnover of CO dehydrogenase in the presence of CO or H_2 and 1-4 benzoquinone.

UV- visible monitoring of CO dehydrogenase spectral change of 450 (blue), 550 (red) and 650 nm (black) following 10 μM of the enzyme mixed with ~30 μM 1-4 benzoquinone and 500 μM CO (*top*) or 390 μM H_2 (*bottom*). During the time course in the presence of excess CO or H_2, the enzyme remains oxidized until 1-4 benzoquinone is fully reduced followed by the enzyme reduction. Increases in absorbance observed between 500 and 700 nm indicate the accumulation and disappearance of a reaction intermediate likely a flavin semi-quinone or molybdenum to copper charge transfer complex.

Table 6.1. Kinetic parameters of CO dehydrogenase oxidation of H_2

	$k_{red}^{H_2}$ (s^{-1})	$K_d^{H_2}$ (μM)	$k_{red}/K_d^{H_2}$	k_{cat} (s^{-1})	K_m (μM)
pH 6.0	**5.4**	**750**	**7.2×10^3**		
pH 7.2	**5.3**	**525**	**1.0×10^4**	**5.1**	**283**
pH 8.0	**5.4**	**700**	**7.7×10^3**		
pH 9.0	**5.8**	**812**	**7.1×10^3**		
pH 10.0	**8**	**1562**	**5.1×10^3**		
pD 7.2	**5.0**	**633**	**7.8×10^3**		
pH 7.2 with D_2	**2.8**	**809**	**3.5×10^3**		

Enzyme-monitored turnover experiments confirmed the reductive half reaction was rate limiting, evident by the enzyme remaining >90% oxidized during turnover and only becoming reduced after loss of oxidized 1-4 benzoquinone. In the course of turnover there is an increase in the wavelengths between 500 and 700 nm, Figure 6.2, indicating the accumulation of a flavin semi-quinone or presence of a charge transfer complex between the molybdenum and copper which is also observed when CO or H_2 is used as a substrate.

As discussed in Chapter 4, the copper of the binuclear center can be replaced with silver, with retention of the CO oxidizing activity (albeit at a reduced rate compared to native enzyme).[58] Kinetic studies with the silver-substituted enzyme with H_2 were also attempted but, as reflected in the failure to observe any enzyme bleaching under an atmosphere of H_2, this form of the enzyme was not reduced by H_2 under any reaction conditions examined.

Solvent and primary kinetic isotope experiments were next carried out in 50mM HEPES, pD 7.2 or pH 7.2 respectively over the concentration range 12 μM to 390 μM at 25^0C. Hyperbolic curves were again obtained. In the case of the solvent isotope experiment with H_2 in D_2O, fits (Table 6.1) yielded a k_{red} of 5.0 s^{-1} and $K_d{}^{H_2}$ of 633 μM, with a resulting kinetic isotope effect (KIE = $^{H}k_{red}/^{D}k_{red}$) of 1.07 (*i.e.*, unity within the limits of error). The absence of a solvent kinetic isotope effect is consistent with the lack of pH dependence of the reductive half-

reaction. By contrast, similar treatment of the data obtained in the primary isotope effect experiment (D_2 in H_2O buffer) yielded a k_{red} of 2.8 s^{-1} and K_d of 809.9 μM, indicating a modest primary KIE of 1.89 (Table 6.1).

Finally, in order to obtain the activation parameters for the reaction, the temperature dependence of the rate constant for enzyme reduction over the range 5 ^{0}C to 30 ^{0}C was determined in 50 mM HEPES, pH 7.2, using 780 μM H_2 (before mixing). Rate constants obtained from exponential fits to the kinetic transients were averaged and an Arrhenius plot (Figure 6.3, *left*) of log(k_{obs}) vs. 1/T, to obtain an effective activation energy (E_a) of 30.6 kJ/mole; an Eyring plot (Figure 6.3, *right*) of the same data yielded an enthalpy and entropy of activation ($\Delta H^{\ddagger}$ and $\Delta S^{\ddagger}$) of the transition state yielded values of 28.2 kJ/mol and -146 J/K•mol, respectively. The value for $\Delta H^{\ddagger}$ is in excellent agreement with the value for E_a of 30.6 kJ/mol, given that RT = 1.7 kJ/mol at room temperature). The calculated Gibbs free energy of activation ($\Delta G^{\ddagger}$) of 71.6 kJ/mole, compares to a theoretical activation barrier of 15.7 kJ/mole for the Ni-Fe hydrogenase and a value of 63.4 kJ/mole and 68.4 kJ/mole for the carbon monoxide oxidation reaction with native and silver-substituted CO dehydrogenase respectively.[34,92] The activation parameters are summarized in Table 6.2.

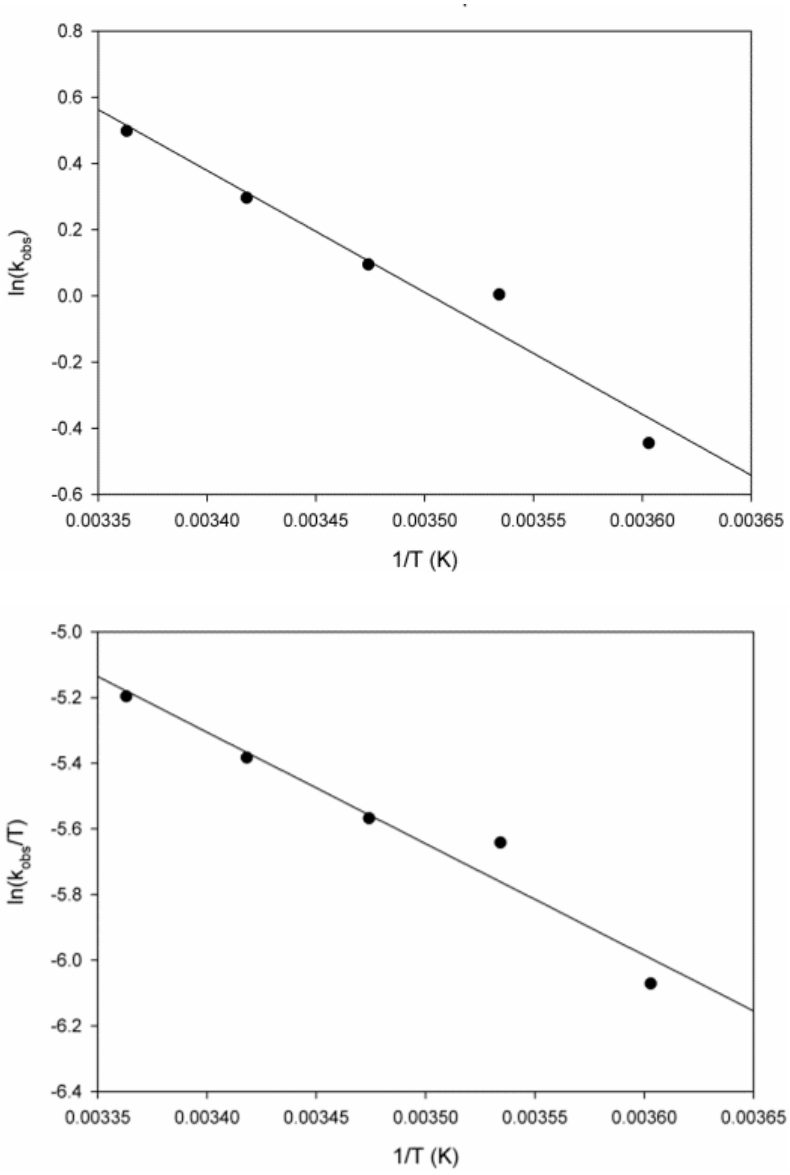

Figure 6.3. The temperature dependence of CO dehydrogenase reduction by H_2. Rates were obtained from 5 – 30 ^{0}C using 5 μM CO dehydrogenase reduced with 390 μM H_2. Observed rates were plotted in Arrhenius (*top*) and Erying (*bottom*) plots for the determination of activation energy of CO dehydrogenase reduction.

Table 6.2. Activation energy parameters of CO dehydrogenase

	Cu-CO dehydrogenase (pH 7.2)- CO*	Ag-CO dehydrogenase (pH 7.2)- CO	Cu-CO dehydrogenase (pH 7.2)- H_2	Ni-Fe Hydrogenase**
E_a	47.8	42.65	30.6	
$\Delta H^{\ddagger}$, kJ/mole	45.4	40.23	28.2	
$\Delta S^{\ddagger}$, J/ K•mole	-60.4	-94.4	-145.7	
$\Delta G^{\ddagger}$, kJ/mole	63.4	68.4	71.6	15.7

*** Zhang et. al[34]**
****Siegbahn et. al [92]**

6.3.3. Electron Paramagnetic Resonance Spectroscopy.

The previously described EPR spectrum of the binuclear center of CO dehydrogenase that has been partially reduced by CO, was found to have rhombic g tensor of $\mathbf{g}_{1,2,3}$ = [2.0010, 1.9604, 1.9549], with extremely large hyperfine coupling to the ^{63,65}Cu nucleus (I = 3/2) of $|\mathbf{A}_{1,2,3}(^{63,65}\text{Cu})|$ = 117, 164, 132 MHz but no coupling to protons;[34] this spectrum is reproduced in Figure 6.4A. The oxidized enzyme has Mo(VI) and Cu(I), and with Cu(I) being a closed shell d^{10} system. The one-electron reduced, EPR-active state of the binuclear center is formally Mo(V) and Cu(I), although a recent investigation of a model compound with a bridging Mo(V)-μS-Cu(I) core exhibiting ^{63,65}Cu hyperfine coupling comparable to that seen with the enzyme has demonstrated that the redox-active orbital is extensively delocalized over the three core atoms, with some 44% Mo d_{xy}, 25% S *p* and 21% Cu $d_{xz,z}{}^2$ (as well as some undefined amount of Cu *s*) character.[79] It is the highly delocalized nature of the redox-active orbital, singly occupied in the EPR-active state, which accounts for the extremely large copper hyperfine observed in the signal. Enzyme that has been partially reduced with H_2 exhibits a new EPR spectrum that is quite distinct from that seen with the CO-reduced enzyme, as shown in Figure 6.3B. In an attempt to simplify this complex spectrum, the sample was prepared in buffer containing D_2O. As shown in Figure 6.4C (black line), the observed spectrum was indeed considerably simplified, with fits (Figure 6.4C red line) yielding $\mathbf{g}_{1,2,3}$ = [2.0127, 1.9676, 1.9594], with approximately isotropic hyperfine coupling $|\mathbf{A}_{1,2,3}(^{63,65}\text{Cu})|$ = [169, 200, 170]

MHz. The quality of the fit (Figure 6.4C) clearly indicates that the signal arises from a single species. These values are quite different from those exhibited by the CO-reduced enzyme, with substantially larger $\mathbf{g}_{av}$ and greater hyperfine coupling to the copper. With the **g**-tensor and ^{63,65}Cu |**A**| tensor thus defined, the signal seen with H_2-reduced spectrum in H_2O could be adequately fit with only proton hyperfine coupling constants as variables. The parameters that yielded the best fits reflected coupling to two approximately equivalent solvent-exchangeable protons with $|\mathbf{A}_{1,2,3}(^{1}H)|$ = [80, 20, 130] MHz, in addition to coupling for the copper of $|\mathbf{A}_{1,2,3}(^{63,65}Cu)|$ = [170, 200, 170] MHz (and $\mathbf{g}_{1,2,3}$ = [2.0127, 1.9676, 1.9594]), as shown in Figure 6.4B (red line). Although the quality of the fit is considered acceptable, particularly given the number of variables that are involved, we cannot exclude the possibility that additional, more weakly coupled protons are present. When the enzyme is reduced with D_2, the spectrum identical to the spectrum of the H_2 reduced enzyme in H_2O, indicating that if the coupled protons originate from substrate, they exchange very rapidly with solvent under turnover conditions. As with the CO-reduced enzyme previously reported, the H_2-reduced enzyme was not stable, as evidenced by the accumulation of Cu^{II} in the sample; the inactivation of the enzyme was in fact much faster with H_2 than with CO.[25,34]

The EPR signal of H_2-reduced CO dehydrogenase resembles, but is distinct from, that seen when enzyme is partially reduced non-catalytically using sodium dithionite,[43] as reproduced in Figure 6.4D. Given the presence of the

protons in the spectrum an attempt was made to record the dithionite-reduced enzyme at high pH, pH 9.0 and 10.0, but no difference in the spectrum was observed, indicating that the pK_a's for the site(s) were greater than 11. Furthermore, several attempts were made to produce a dithionite reduced spectrum in D_2O. These included extended incubation with the oxidized enzyme in D_2O (>36 hr) prior to reduction and enzyme reduced by dithionite and incubated in D_2O under anaerobic conditions (>30 min). The resulting EPR signal was always a mixture of the protonated and deuterated spectra, as shown in Figure 6.4E. When an appropriately weighted fraction of the protonated spectrum (Figure 6.4D) is subtracted out from that in Figure 6.4E, the resulting spectrum (Figure 6.4F) resembles that seen with H_2-reduced enzyme in the presence of D_2O (Figure 6.4C), but with distinct **g** and |**A**| tensors (Table 6.3). The EPR spectrum of silver-substituted enzyme reduced by dithionite was obtained (Figure 6.5C), but in this case the observed spectrum is essentially identical to that of the CO-reduced silver-substituted enzyme in either H_2O or D_2O (Figure 6.5A and 6.5B) and exhibits no proton hyperfine coupling. This strongly suggests that in the former case CO is not bound to silver in the signal-giving species. The lack of proton coupling in the silver-substituted enzyme makes it unlikely that the molybdenum subnucleus is the site of protonation.

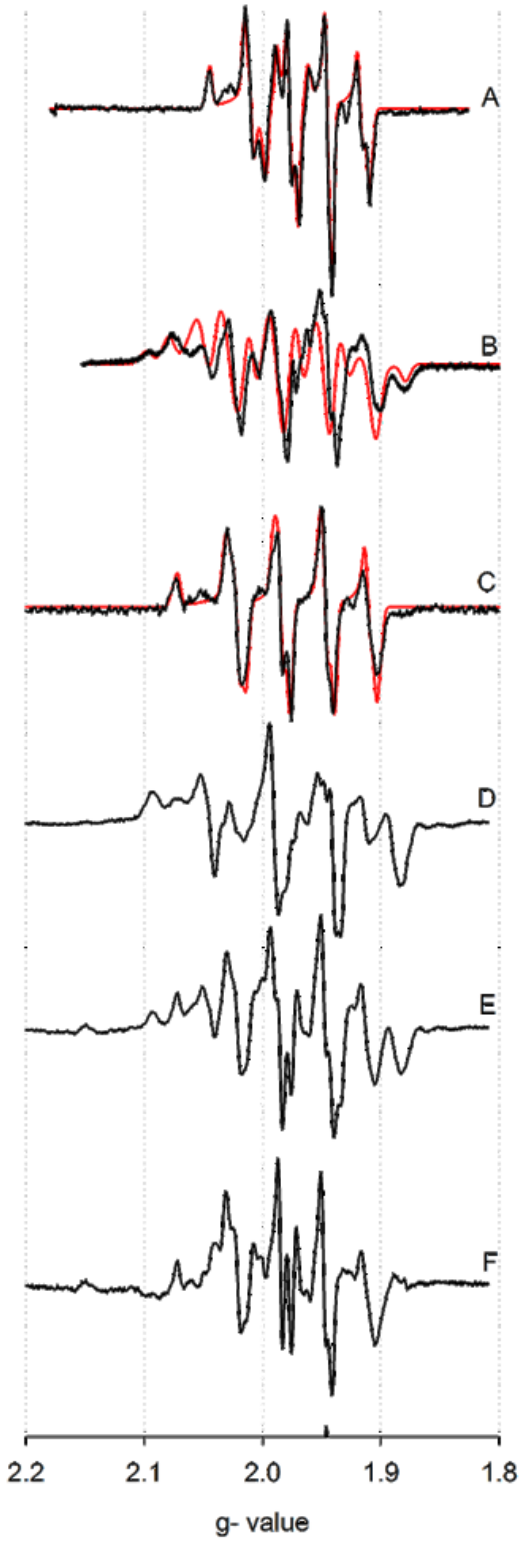
A
B
C
D
E
F
2.2
2.1
2.0
1.9
1.8
g- value

Figure 6.4. EPR spectra manifested by CO dehydrogenase under various conditions of CO dehydrogenase partially reduced by CO, H_2, or dithionite.

A. CO-reduced CO dehydrogenase in 50 mM HEPES, pH 7.2, with simulation in red; *B*. H_2-reduced CO dehydrogenase in 50mM HEPES, pH 7.2, with simulation in red; *C*. H_2-reduced CO dehydrogenase in 50 mM HEPES, pD 7.2, with simulation in red; D. Dithionite-reduced CO dehydrogenase in 50 mM HEPES, pH 7.2; *E*. Dithionite-reduced CO dehydrogenase in 50 mM HEPES, pD 7.2; *F.* Spectrum E minus Spectrum D.

The EPR instrument settings were: 9.45 GHz microwave frequency; 4 milliwatt microwave power; 5 Gauss modulation amplitude; 150 K.

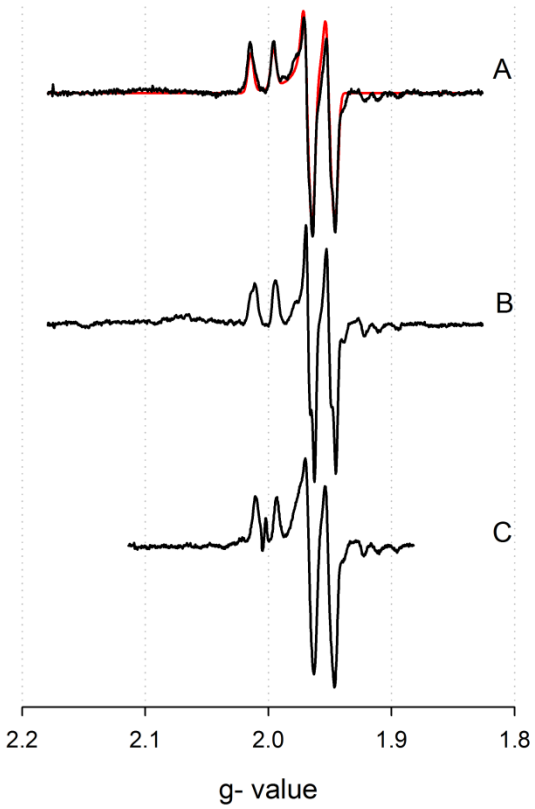

Figure 6.5. EPR spectra manifested by the silver substituted CO dehydrogenase under various conditions

A. CO-reduced silver-substituted CO dehydrogenase in 50mM HEPES, pH 7.2, with simulation in red; *B*. CO reduced silver-substituted CO dehydrogenase in 50 mM HEPES, pD 7.2; *C*. Dithionite-reduced silver-substituted CO dehydrogenase in 50mM HEPES, pH 7.2.

The EPR instrument settings were: 9.45 GHz microwave frequency; 4 milliwatt microwave power; 5 Gauss modulation amplitude; 150 K.

Table 6.3 EPR simulation parameters

	*Cu-CO dehydrogenase CO/H_2O	Ag-CO dehydrogenase CO/H_2O	Cu-CO dehydrogenase H_2/H_2O	Cu-CO dehydrogenase H_2/D_2O
$\mathbf{g}_1$	2.0010	2.0043	2.0127	2.0127
$\mathbf{g}_2$	1.9604	1.9595	1.9676	1.9676
$\mathbf{g}_3$	1.9549	1.9540	1.9594	1.9594
$\mathbf{g}_{avg}$	1.9721	1.9726	1.9799	1.9799
$\lvert\mathbf{A}_1\rvert$(MHz)	117	81.98	169.13	169.13
$\lvert\mathbf{A}_2\rvert$ (MHz)	164	78.85	200.28	200.28
$\lvert\mathbf{A}_3\rvert$ (MHz)	132	81.89	170.23	170.23
$\lvert\mathbf{A}_1\rvert$ (MHz) H_a (H_b)			80 (80)	
$\lvert\mathbf{A}_2\rvert$ (MHz) H_a (H_b)			20 (20)	
$\lvert\mathbf{A}_3\rvert$ (MHz) H_a (H_b)			130 (120)	
Euler Angle – α (radians)	-		-0.55	-0.55
Euler Angle – β (radians)	0.54		-1.95	-1.95
Euler Angle – γ (radians)	0.54		1.93	1.93
Line width (Gauss)		0.51	.8	0.71

*Zhang et. al.[34]

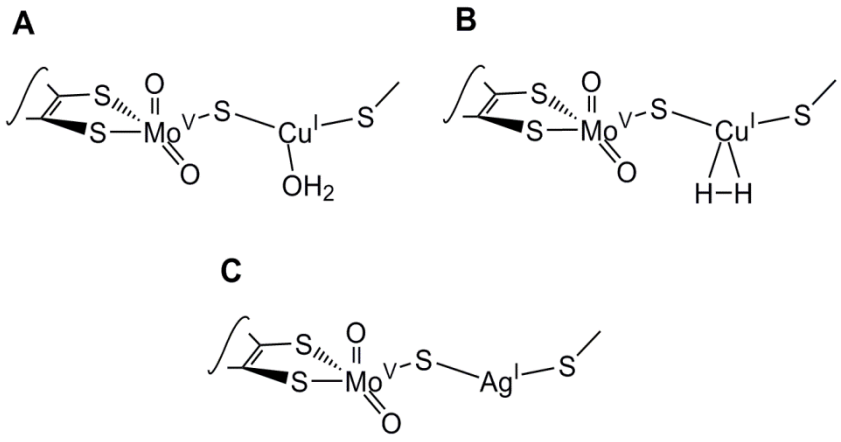

Figure 6.6. Possible structures for the EPR-active species seen with CO dehydrogenase.

A and B represent possible native CO dehydrogenase structures reduced by dithionite or H_2 respectively. C represents a possible silver substituted CO dehydrogenase structure reduced by dithionite.

6.3. Discussion

We find that the molybdenum- and copper- containing CO dehydrogenase from *O. carboxidovorans* is readily reduced by H_2, with a k_{red}, 5.3 s^{-1} and a $K_d^{H_2}$ of 525 μM. k_{red} from the rapid reaction study is in very good agreement with the steady-state derived k_{cat}, 5.1, indicating the rate limiting step in turnover is in the reductive half-reaction (as is the case with CO as substrate)[34]. The lack of a significant pH dependence to the reductive half-reaction over the pH range 6-10 (Table 6.1) indicates that no substrate- or enzyme- based ionizations in the experimentally accessible pH range are involved in the rate-limiting step of the reaction. We note that the Ni-Fe hydrogenase of A*llochromatium vinosum* also exhibits no pH dependence in its hydrogenase activity.[93]

Partial reduction of enzyme with H_2 yields an EPR signal distinctly different from that seen with CO as reductant, with more anisotropic g-values and larger coupling to the ^{63,65}Cu nucleus ($\mathbf{g}_{1,2,3}$ = [2.0127, 1.9676, 1.9594] and $|\mathbf{A}_{1,2,3}(^{63,65}Cu)|$ = [169, 200, 170] MHz, Table 6.3) and, significantly, strong coupling to two protons that is lost on preparation of the EPR sample in D_2O. The spectra exhibited by H_2-reduced CO dehydrogenase in both H_2O and D_2O are similar in form to, but with distinct **g** and **A** parameters from, those produced when the enzyme is simply partially reduced by sodium dithionite under similar conditions. By contrast, the EPR signal seen with dithionite-reduced silver-

substituted enzyme exhibits no proton coupling (bearing in mind that H_2 does not reduce the silver-substituted enzyme).

Considering first the structure giving rise to the signal seen with dithionite-reduced enzyme, the likeliest source of the two strongly coupled protons is the HO-/H_2O known crystallographically to be bound to the Cu at a distance of 2.4 Å.[20,23] Indeed, given the Cu-O distance and the fact that the oxygen is stacked on top of the π cloud of Phe_{290}, it is most likely that the ligand is a water molecule (with two protons) rather than a negatively charged hydroxide. Presumably for steric reasons (given the restricted access to the active site), the water is not readily solvent-exchangeable. This interpretation is consistent with the absence of coupled protons with the dithionite-reduced silver-substituted enzyme, which lacks the coordinated water at the silver. The signal-giving species with native and silver-substituted enzyme can thus be formulated as Mo(V)/Cu(I)•H_2O and Mo(V)/Ag(I), respectively, as shown in Figure 6.6.

Finally, with the H_2-reduced native enzyme, given the effectiveness with which the native CO dehydrogenase oxidizes H_2, and not silver substituted, we propose that H_2 first binds at the copper of the binuclear center similarly to CO,[41,62] displacing the H_2O coordinated to the copper prior to catalysis. We believe that the observed EPR signal (as with CO as substrate described in Chapter 5) arises from enzyme that has already become partially reduced by reaction with prior turnover under the reaction conditions, such that H_2 is bound

to a partially reduced Mo(V)/Cu(I) binuclear center, resulting in a complex that cannot progress through the catalytic cycle until the center has become fully oxidized (via intramolecular electron transfer to the other redox-active sites of the enzyme). The signal-giving species, in fact, reflects a paramagnetic analog of the Michaelis complex. The situation is directly analogous to the long-studied "Rapid" signals seen with the closely related molybdenum-containing enzyme xanthine oxidase,[94] that have been shown to arise from substrate similarly bound to partially reduced enzyme, as well as the complex described in Chapter 5 where CO there is evidence for a copper carbonyl complex that gives rise to the observed EPR signal when the enzyme is reduced with excess CO.[95]

Binding of H_2 to metals, and specifically Cu(I), such as is proposed has chemical precedent,[96-98] and is known to involve side-on η^2 binding that polarizes substrate, facilitating its ionization to a metal hydride, for which precedent also exists.[96-99] This accounts for the rapid exchange with solvent, but the pH-independence of the observed reaction with H_2 and the observation of two strongly coupled protons in the EPR signal of H_2-reduced enzyme requires that the pK_a for this ionization be greater than ~12. An EPR sample of the enzyme in H_2O but reduced with D_2 and quickly frozen (within 10 sec) showed the same strong coupling to protons seen in the H_2-reduced sample, indicating that this exchange is relatively rapid, likely facilitated by the highly conserved glutamate residue in the active site (Glu_{763}). The rapid protonation/deprotonation of bound H_2 is in fact catalytically productive, as the Cu(I)-hydride species formed

transiently can itself deprotonate, with (when beginning with the fully oxidized Mo(VI)/Cu(I) binuclear center) the two reducing equivalents simply entering the highly delocalized redox-active orbital of the binuclear center. Catalysis with H_2 as substrate is thus proposed to proceed as shown in Figure 6.7, with H_2 first binding at the copper of the binuclear center, displacing the bound water, and becoming polarized. Successive ionizations, first of bound H_2 and then the resulting hydride, lead to full deprotonation and two-electron reduction of the binuclear center, formally to the Mo(IV)/Cu(I) state. Given the experimentally observed rapid exchange of solvent protons into the bound hydride, at least the first of these prototropic equilibria must be rapid compared to catalysis. Furthermore, given the pH-independence of the reaction the pK_a for this step must be high, meaning that the equilibrium favors the H_2 complex over the hydride. This accounts for the observation of two protons rather than one in the EPR signal, and also rationalizes the modest reactivity of enzyme toward H_2 as compared to CO. The failure to observe any reversible reaction suggests that deprotonation of the copper hydride intermediate is strongly downhill thermodynamically, and functionally irreversible.

In conclusion, the oxidation of H_2 by the molybdenum- and copper- CO dehydrogenase requires a fully constituted active site with bound copper, not silver, and occurs with a pH-independent k_{red} of 5.3 s^{-1}. The observed EPR signal seen upon reduction of enzyme with H_2 is distinct from that seen with CO as substrate or with dithionite as non-catalytic reductant. The proton coupling

observed in the dithionite-reduced enzyme is lost in the presence of bicarbonate, and is proposed to arise from the crystallogrpahically observed water molecule coordinated to the copper of the binuclear center. On the basis of these observations, a reaction mechanism can be proposed in which catalysis is initiated by side-on binding of H_2 to the copper of the binuclear center, which predisposes its ionization through a copper hydride intermediate; chemical precedent exists for both such species.[97-101] Subsequent ionization of the copper hydride leads to formal reduction of the binuclear center to a Mo(IV)/Cu(I) state, taking advantage of the center's extremely delocalized redox-active orbital. Glutamate 763 is well-positioned in the active site to facilitate these deprotonation events.

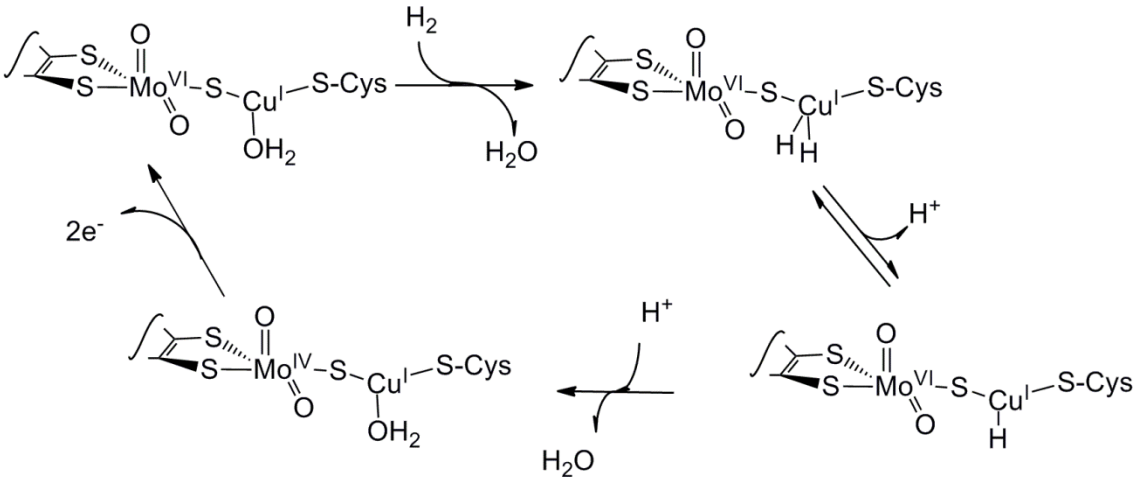

Figure 6.7. The proposed reaction mechanism of CO dehydrogenase with H_2.

Catalysis proceeds by displacement of H_2O from the copper of the binuclear center by H_2, followed by successive deprotonations as shown to introduce a pair of reducing equivalents into the highly delocalized redox-active orbital of the binuclear center.

Chapter 7

Inhibitors of CO dehydrogenase

7.1. Introduction

Little has been established with regard to what kinds of compounds inhibit the molybdenum- and copper- containing CO dehydrogenase. Cyanide is known to inhibit a variety of xanthine oxidase family enzymes by removing the equatorial sulfur that is required for catalysis to form the inhibited molybdenum tri-oxo species, Figure 7.1, that is non-functional in most cases.[38] Cyanide has a similar effect to CO dehydrogenase removing the bridging μ-S as well as the copper from the active site.[43] This inhibition irreversibly disassembles the active site leaving the protein in the tri-oxo state until a reconstitution protocol is preformed, as described in Chapter 2. In addition to cyanide, *n*-butylisonitrile also inhibits the enzyme to yield the inhibitory complex described by crystallographic data where the carbon of the nitrile is bound to the equatorial sulfur and oxygen of the molybdenum to form a four-member ring and the nitrogen is bound to copper (Figure 7.1).[23] This structure is the basis for a catalytic mechanism based on this structure but there have been no further studies performed on this complex to examine the reversibility of the process or if the enzyme could oxidize the substrate. Here we investigate the ability for *n*-butylsionitrile to reduce CO dehydrogenase complex and the EPR of the inhibited species.

In addition to the inhibition by cyanide we have investigated inhibition of CO dehydrogenase by bicarbonate. Unlike the nickel- and iron- containing CO dehydrogenase, the molybdenum- and copper- containing CO dehydrogenase does not appear to catalyze carbon dioxide reduction, the reverse of the physiological reaction. This reversal of the physiological catalytic activity may be due to product inhibition by carbon dioxide (or the hydrated form bicarbonate) on the enzyme, preventing it from reversing the reaction and forming carbon monoxide. In order to access the type and degree of inhibition by bicarbonate we have characterized the steady state kinetics as well as the EPR of the bicarbonate bound structure reduced by dithionite. We find that bicarbonate acts as an uncompetitive inhibitor, binding to the reduced form of the enzyme, likely bridging the molybdenum and copper in the active site to form a six-member ring structure.

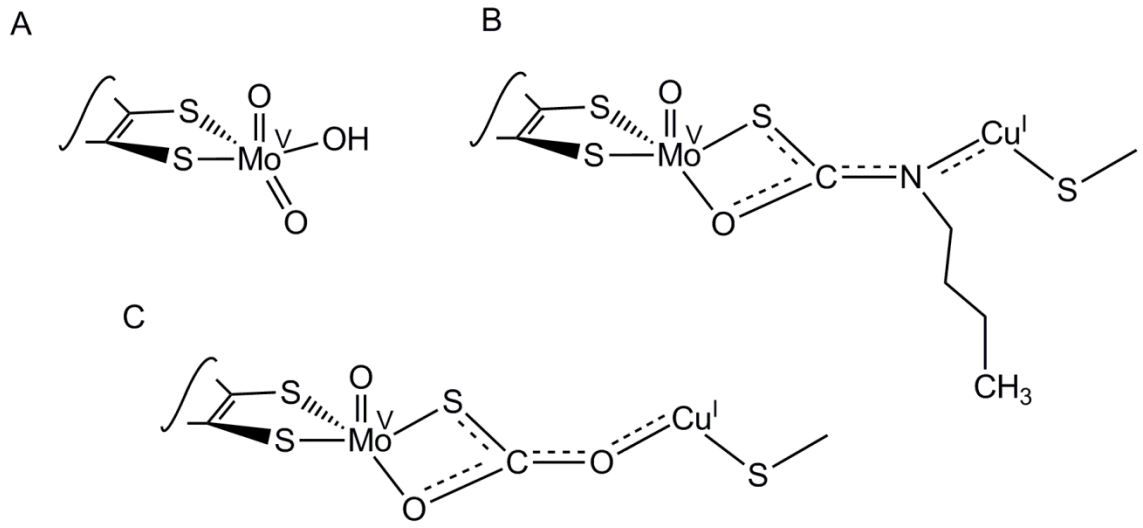

Figure 7.1. Structures of various inactive states of CO dehydrogenase

A. The tri-oxo inactive CO dehydrogenase; B. *n*-butylisonitrile bound state of CO dehydrogenase; C. Non-productive carbon monoxide coordination into the active site of CO dehydrogenase.

7.2. Results

7.2.1. Reaction of n-butylisonitrile with CO dehydrogenase

We first examined the ability of *n*-butylisonitrile to reduce the enzyme by UV-vis spectroscopy monitoring the bleaching of the enzyme at 450 nm and 550 nm, indicating the reduction of the flavin and iron-sulfur clusters respectively. After addition of the inhibitor to anaerobic CO dehydrogenase in a sealed cuvette there is bleaching at 450 nm, Figure 7.2, and an increase between 500 and 600 nm, most likely due to accumulation of flavin semiquinone over 18 hours. The decrease in the spectrum at 450 nm only accounts for one third of the total absorbance decrease when the functional enzyme is taken into account, indicating only one turnover of the enzyme has occurred.

We then examined this inhibition by EPR, Figure 7.3, and find the presence of a flavin radical, as well as one of the EPR signals that represent the inactive form of the enzyme, with a loss of the coupling from I = 3/2 copper nucleus. Notably, there is no indication of free copper in solution so it is likely still coordinated into the active site of the enzyme.

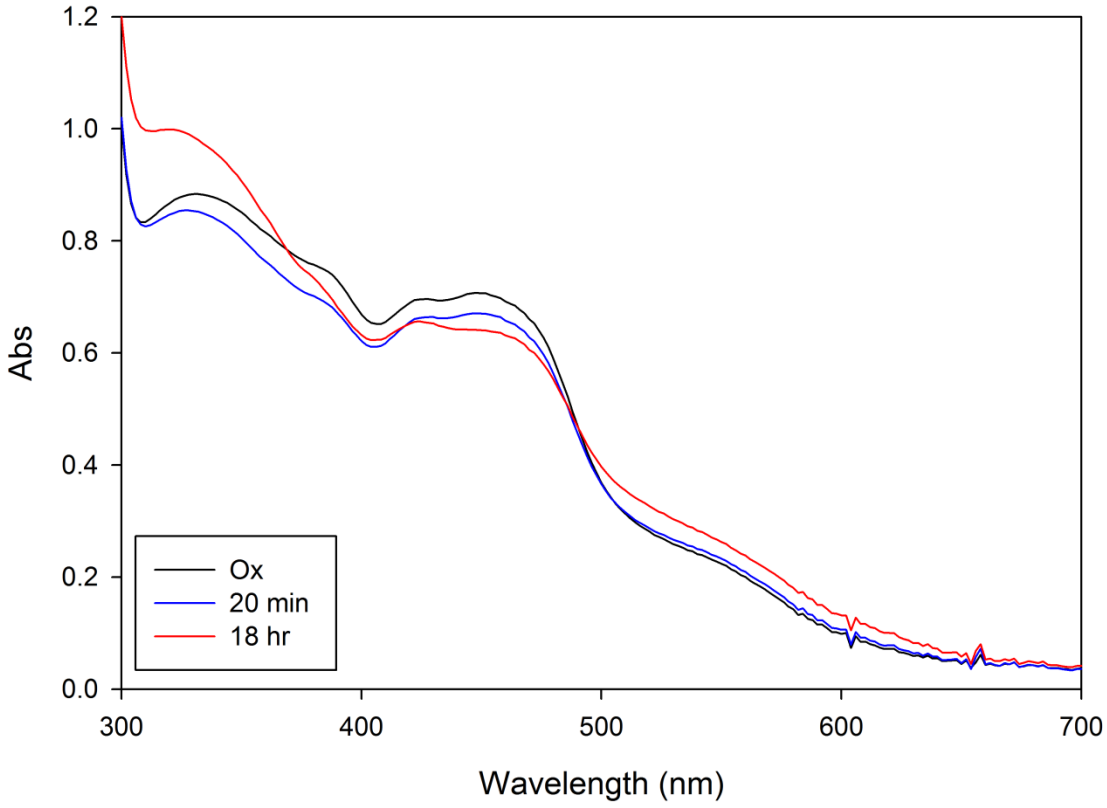

Figure 7.2. UV-vis spectra of CO dehydrogenase reacted with *n*-butylisonitrile.

UV-vis spectra of 20μM Anaerobic CO dehydrogenase oxidized (black) then reacted with 100μM *n*-butylisonitrile and monitored over 18 hours.

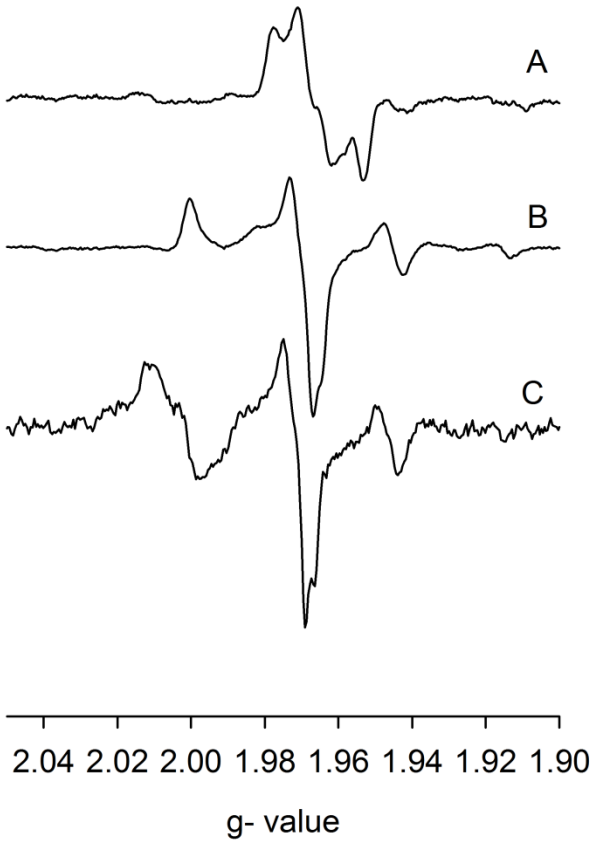

Figure 7.3. EPR spectra of the inactive forms of CO dehydrogenase

A. Inactive CO dehydrogenase reduced by dithionite in 50mM HEPES, pH 7.2; *B*. As purified inactive resting state of CO dehydrogenase in 50mM HEPES, pH 7.2; *C*. CO dehydrogenase reduced by *n*-butylisonitrile in 50mM HEPES, pH 7.2.

The EPR instrument settings were: 9.45 GHz microwave frequency; 4 milliwatt microwave power; 5 Gauss modulation amplitude; 150 K.

7.2.2. Inhibition of CO dehydrogenase by bicarbonate

Finally, the inhibition of CO dehydrogenase by bicarbonate (the hydrated form of product CO_2 of carbon monoxide oxidation) was examined by steady state kinetics, Figure 7.4, following the reduction of 25μM methylene blue at 615 nm at of various concentrations of bicarbonate and carbon monoxide and initiated by the addition of 25 nm CO dehydrogenase. Plots of the averaged observed rate, k_{obs}, at each concentration of carbon monoxide were plotted against carbon monoxide concentration (4-250 μM CO) and were fit with a hyperbolic curve in Sigma plot (Systat software) to yield an apparent maximum turnover rate, $k_{cat,app}$ and apparent Michaelis constant, $K_{m,app}$. We find that there is a decrease in k_{cat} and decrease in K_m with increasing concentrations of bicarbonate. At 200 mM bicarbonate the $k_{cat,app}$ is 16.1 s^{-1}, this is a decrease of ~32% compared to the uninhibited functionality. In addition to a decrease in apparent k_{cat} there is also a change in the apparent $K_{m,app}$ of 430 nM, compared to 15μM for the uninhibited enzyme, this is a 30 fold increase in apparent binding affinity of carbon monoxide (this is only an estimate due to the limitations of the experiment and ability to go to concentrations of carbon monoxide below ~5 μM).[34] At 100 mM bicarbonate the $k_{cat,app}$ is 20.6 s^{-1} and an estimated $K_{m,app}$ of 1.8 μM and at 10 mM bicarbonate the $k_{cat,app}$ is 28.6 s^{-1} and an estimated $K_{m,app}$ of 800 μM. The effects of inhibition by bicarbonate were investigated by rapid reaction kinetics monitoring the reduction of the enzyme, but no effect was observed.

To better understand how bicarbonate is interacting with the active site of CO dehydrogenase, we investigated whether bicarbonate is bound to the partially reduced enzyme by EPR. We find it binds to the active site of the reduced enzyme resulting in an EPR spectrum (Figure 7.5) that gives a unique line shape that is distinct from all previously observed EPR spectra for CO dehydrogenase. The bicarbonate inhibited spectrum did not exhibit any coupling to protons in H_2O, and in fact resembles, but is distinct from the H_2-reduced enzyme in D_2O described in Chapter 6, Figure 7.5. Simulations of the bicarbonate spectrum yield a single signal-giving species with $\mathbf{g}_{1,2,3}$ = [2.0020, 1.9618, 1.9548] and $|\mathbf{A}_{1,2,3}(^{63,65}Cu)|$ = [193, 191, 221] MHz. The g- values are similar to that of the CO bound EPR spectrum described in Chapter 5, but with larger coupling to the copper nucleus. To verify that the EPR signal generated in the presence of bicarbonate is bicarbonate coordinated to the active site of the enzyme we have used ^{13}C labeled bicarbonate and observe line broadening, Figure 7.6, indicating the I=1/2 ^{13}C nucleus is coupled to the unpaired electron in the signal giving species. In particular we observe slightly greater coupling than observed when CO dehydrogenase is reduced by ^{13}CO as discussed in Chapter 5, although the coupling is still unresolved by EPR and will require ENDOR for a better understanding of the coordination.

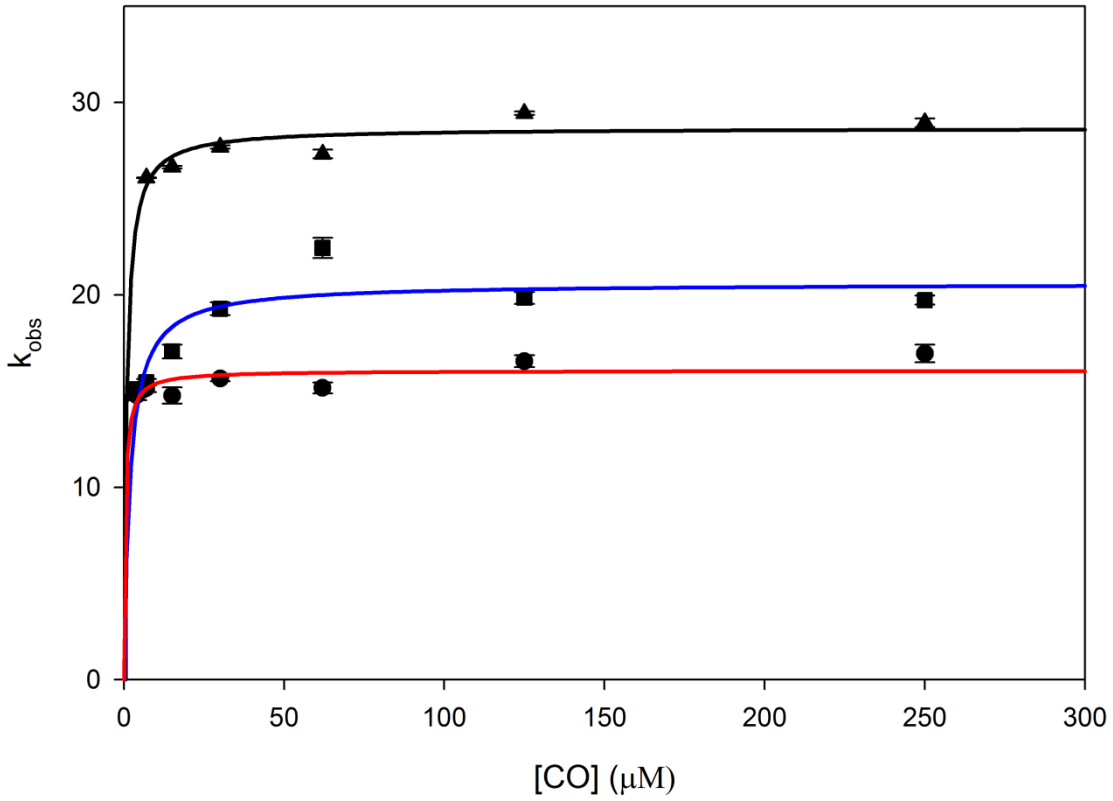

Figure 7.4. Steady state kinetic plots of CO dehydrogenase reduction by CO in the presence of bicarbonate.

Plots of k_{obs} *versus* [CO] for the steady state reaction following the reduction of methylene blue at 615 nm in presence of various concentrations of bicarbonate, reactions were initiated by the addition of 25 nM CO dehydrogenase. 10mM bicarbonate (▲,black fit line), 100mM bicarbonate(■, blue fit line), and 200mM bicarbonate (●, red fit line) in 50 mM HEPES, pH 7.2, 25° C. Solid Line, fit with a hyperbolic equation using SigmaPlot (Systat Software, Inc.).

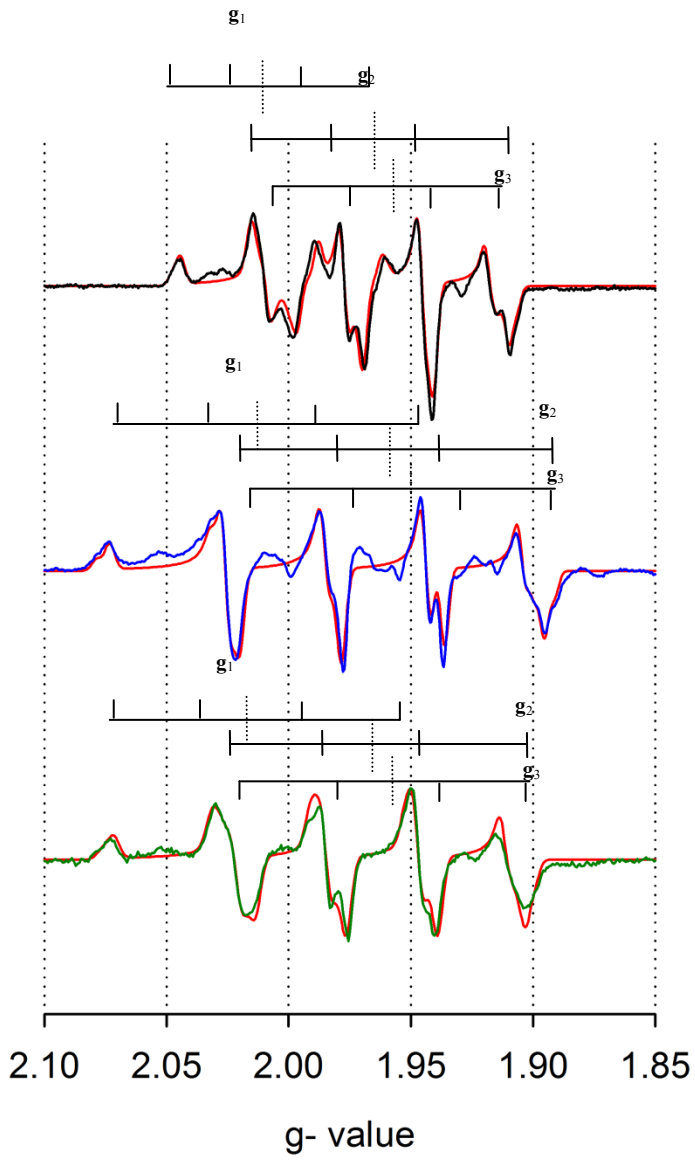

Figure 7.5. EPR spectra of CO dehydrogenase under various conditions

Top: CO dehydrogenase reduced by CO in 50mM HEPES, pH 7.2 (black), with simulation in red; *Middle*: CO dehydrogenase reduced by dithionite in 400mM bicarbonate (blue), 50mM HEPES, pH 7.2, with simulation in red; *Bottom*: CO dehydrogenase reduced by H_2 in 50mM HEPES, pD 7.2 (green), with simulation in red

The EPR instrument settings were: 9.45 GHz microwave frequency; 4 milliwatt microwave power; 5 Gauss modulation amplitude; 150 K.

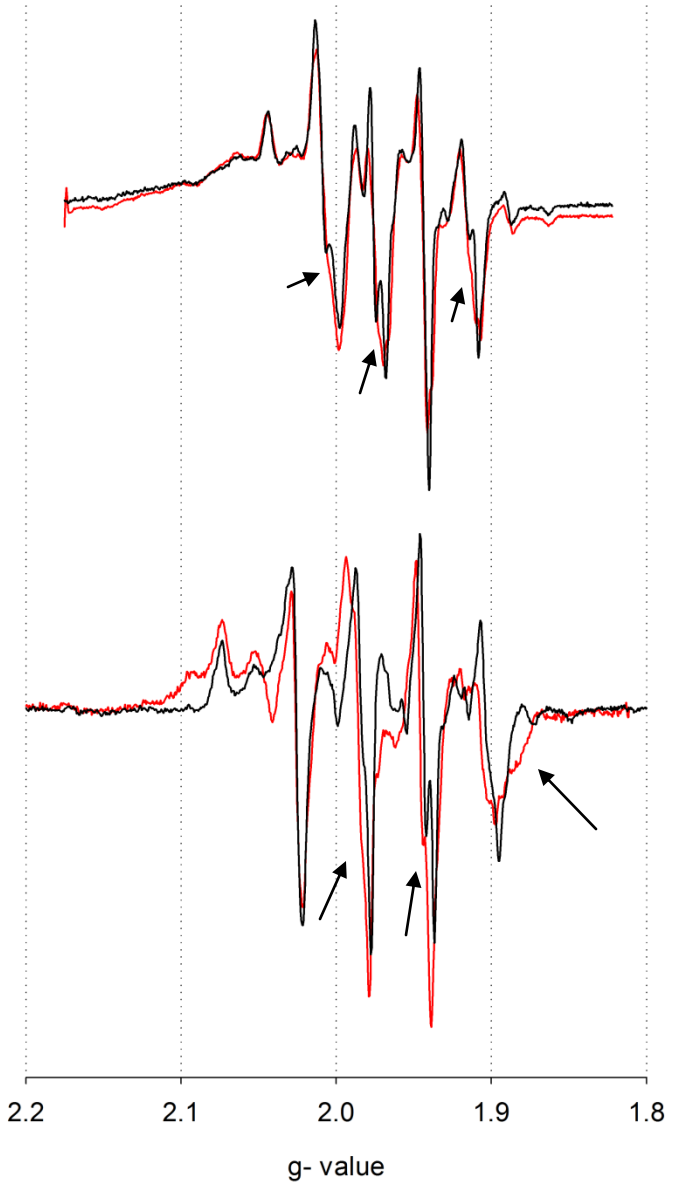

Figure 7.6. EPR spectra of the CO dehydrogenase coupled to a ^{13}C nucleus from CO or bicarbonate

Top: CO dehydrogenase reduced by ^{12}CO (black) or ^{13}CO(red) in 50mM HEPES, pH 7.2; *Bottom*: CO dehydrogenase reduced by dithionite in 400mM bicarbonate (^{12}C- black or ^{13}C-red), 50mM HEPES, pH 7.2. Arrows indicate areas of unresolved coupling to the ^{13}C nucleus.

The EPR instrument settings were: 9.45 GHz microwave frequency; 4 milliwatt microwave power; 5 Gauss modulation amplitude; 150 K.

7.3. Discussion

Here we have investigated the inhibitory effects of *n*-butylisonitrile and bicarbonate on CO dehydrogenase. We find that, as suggested by the crystal structure and computational studies, *n*-butylisonitrile reacts with the enzyme, reducing it by two electrons and forming a stable inhibition complex with the inhibitor coordinated between the molybdenum and copper of the enzyme. This complex abolishes the observed copper coupling to the Mo(V) species observed by EPR. The EPR signal of the cyanide inhibited enzyme appears rhombic and identical to the resting EPR signal of the enzyme. This resting signal may in fact be a dead end product of the enzyme reacted with carbon monoxide. This complex was suggested as a possible reaction intermediate by computational studies but was suggested as a non-productive intermediate.[40,41] This signal can be abolished upon reactivation of the enzyme using the protocol outlined in Chapter 2.

While *n*-butylisonitrile is a functionally irreversible inhibitor, bicarbonate is an uncompetitive inhibitor based on the steady state kinetics observed at various bicarbonate concentrations, reducing the k_{cat} and k_m as the bicarbonate concentration is increased. Uncompetitive inhibition is characterized by the inhibitor, bicarbonate, binding to a different form of the enzyme than the substrate, carbon monoxide. Complex formation is evident in the EPR of the bicarbonate bound sample having a distinctly different spectrum compared to the

carbon monoxide coordinated sample. The signal can be made using either dithionite or carbon monoxide as the reductant, although in the presence of excess carbon monoxide only the carbon monoxide bound signal is observed. This indicates that bicarbonate only coordinates to the reduced form of the enzyme, possibly involving the active site copper as this is the site of carbon monoxide coordination. Additionally, when ^{13}C labeled bicarbonate is used in the sample line broadening of the signal is observed to a greater degree to that seen with ^{13}CO due to a greater degree of coupling for the bicarbonate sample.

As discussed in Chapter 6, the dithionite-reduced enzyme gives an EPR spectrum with two coupled protons, attributable to the water coordinated to the copper of the binuclear center; the EPR signal seen with dithionite-reduced enzyme in the presence of bicarbonate has no observable coupled protons, the absence of proton coupling suggests strongly that bicarbonate has displaced the bound water from the copper. Three structures can be considered, as shown in Figure 7.7. The first of these has bicarbonate coordinated in a monodentate fashion to the copper and with the equatorial Mo=O unprotonated (or, alternatively, protonated but in a configuration that leads to very weak coupling). The second possibility has bicarbonate bridging between the Mo and Cu of the binuclear center in a bidentate fashion, displacing both the copper-coordinated water and the equatorial Mo=O. A third possible structure has bicarbonate bound to the molybdenum in place of the equatorial oxygen, the absence of proton coupling would then be due to steric interference by bicarbonate. Our

present preference based on the observed kinetics, $^{12,13}C$ EPR and on entropic grounds is the second structure, but a definitive answer must await crystallographic or ENDOR analysis of the bicarbonate complex.

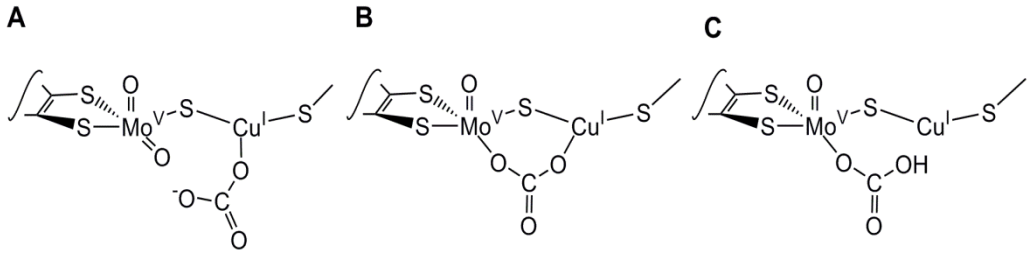

Figure 7.7. Possible structures of bicarbonate bound to the active site of CO dehydrogenase.

Chapter 8

Conclusions

8.1. Summary

8.1.1 CO dehydrogenase donates reducing equivalents directly to the quinone pool.

The molybdenum- and copper- containing CO dehydrogenase from *Oligotropha carboxidovorans* catalyzes the oxidation of carbon monoxide to carbon dioxide, utilizing the reducing equivalents from the reaction as an energy source and the carbon dioxide formed as a carbon source.[15,16,102] In Chapter 3, we have identified components of the quinone pool, most likely ubiquinone and not cytochrome b_{561}, as the likely physiological electron acceptor for the enzyme. CO dehydrogenase rapidly reduces a variety of quinones with a preference for 1-4 benzoquinone, with a k_{ox} of 125 s^{-1}. Ubiquinone-1 also proved to be an effective oxidizer of CO dehydrogenase with a k_{ox}/K_d, 2.88 x 10^5 $M^{-1}s^{-1}$ and k_{cat}/K_m, 2.9 x 10^4 $M^{-1}s^{-1}$. 1-4 benzoquinone and ubiquinone-1 are both analogs of the physiological ubiquinone-10.

The site of electron transfer was verified to be the FAD, using a protocol developed by Chakraborty et. al. where the flavin is covalently modified by diphenyliodonium cloride to keep the flavin in the reduced state.[45] This modification severely inhibits electron transfer to the quinones.

The direct utilization of the quinone pool establishes a new category of physiological electron acceptors for the xanthine oxidase family of molybdenum enzymes, with NAD+ and O_2 already known to be electron acceptors for other family members.

8.1.2. Silver may be substituted for copper in the binuclear center and retain significant activity

In Chapter 2 we have described a technique for removing the copper of the binuclear active site of CO dehydrogenase and reconstituting the active site with silver. The silver-substituted form was characterized in Chapter 4 and compared to the native enzyme where it was established by Zhang et. al. that CO oxidation is rate-limiting in catalysis, taking place at $51 s^{-1}$.[34] This rate is independent of pH and CO concentration (due to experimental limitations concentrations were limited to greater than 5 μM).[34]

Reconstitution of CO dehydrogenase with silver is easily determined by EPR were we saw splitting of the ^{107,109}Ag I=1/2 nucleus (100% natural abundance) in place of the ^{63,65}Cu I=3/2 nucleus (100% natural abundance) with similar coupling to the unpaired electron as seen in the Cu-TPP (5,10,15,20-Tetraphenyl-21H,23H-porphine) and Ag-TPP complexes. By using carbon monoxide to produce the EPR spectrum we ensured that only the functional active sites of CO dehydrogenase are observed. The silver substituted enzyme remained active toward CO oxidation, with a rate of reduction of 8 s^{-1}. Like the

native copper containing enzyme no pH dependence or CO concentration dependence was observed (limitations of pH and CO concentration dependence were limited to a pH range of 6-10 and a substrate concentration of 5μM to 1mM).

Looking further into the coordination of carbon monoxide to copper or silver reveals a likely explanation as to why the rates are reduced for the sliver substituted protein. Carbon monoxide, when coordinating to a metal, binds through sigma donation to the metal *d* orbitals and the metals back donate electron density to the anti-bonding pi orbital of carbon monoxide. This donation/back donation interaction lengthens and polarizes the carbon oxygen bond of carbon monoxide, the back donation has been observed to be greater for copper than silver in many metal carbonyl compounds.[55,56] The result is that carbon monoxide is less activated when coordinated to silver rather than copper. The coordination and activation toward nucleophillic attack by oxygen (originating from hydroxide or the equatorial molybdenum-oxo group) establishes a role for copper in the unique bi-nuclear active site of the enzyme.

8.1.3. The EPR signal giving species of CO dehydrogenase partially reduced by CO gives evidence for a CO binding to copper, providing insight into the mechanism of CO oxidation

In previous studies by Zhang et. al.[34] it was reported that when CO dehydrogenase is reduced with ^{13}CO there is unresolved coupling from the ^{13}C nucleus present in the EPR spectrum. In order to resolve this coupling we have collaborated with Brian Hoffman at Northwestern to employ electron nuclear double resonance (ENDOR) spectroscopy in Chapter 5. This technique utilizes the EPR spectrum of the enzyme to monitor NMR transitions of NMR active nuclei coupled to the unpaired electron.

The most remarkable EPR/ENDOR feature of this species is the large and positive *isotropic* hyperfine coupling to copper, with $a_{iso}(^{63,65}Cu)$ = +148 MHz, with negligible anisotropic hyperfine coupling to the I = 3/2 nuclear spin. The Cu hyperfine coupling in CO dehydrogenase is consistent with a d^{10} Cu(I) ion whose closed-shell electronic configuration acquires a large *positive* a_{iso} from delocalization of the electron spin in the 'Mo(V) SOMO' over the entire [Mo(V)-(μ-S)-Cu(I)] unit, into the 4*s* orbital of Cu. The assignment of Cu(I) in the active site is also consistent with x-ray absorption spectroscopy and computational studies of CO dehydrogenase, as well as computational and spectroscopic studies of a model compound for the active site.[39-41]

The hyperfine coupling to ^{13}C in the ENDOR signal manifested by ^{13}CO-reduced CO dehydrogenase also is distinctive in being highly isotropic. The isotropic coupling, $a_{iso}(^{13}C)$ = +17.4 MHz, and the anisotropic component seen, **T** = 0.73 MHz, indicate that it is unlikely to arise from a species with a Mo-C bond and indicate that the distance between the ^{13}C and Mo is at least 2.4Å.

A structure having a Cu(I)-coordinated CO is consistent with both of the computational studies of the reaction of CO dehydrogenase that identify CO coordinated to the copper of a fully oxidized binuclear center as the starting point for catalysis.[41,62] In the case of the partially reduced complex examined in the present study, with the molybdenum in the EPR-active Mo(V) valence state, the enzyme cannot progress through the catalytic sequence, thus accounting for the accumulation of the signal in the course of our sample preparation. Our Mo(V)/Cu(I)•CO species in fact represents a paramagnetic analog to the *bona fide* Michaelis complex for the reaction, and is thus analogous to the species giving rise to the well-characterized “Rapid” Mo(V) EPR signals in the related molybdenum-containing enzyme xanthine oxidase.[86]

Our ENDOR results presented in Chapter 5 provide direct experimental support for CO coordination to Cu(I) of the binuclear center of CO dehydrogenase. Upon binding of CO, the reaction progresses by nucleophillic attack of the equatorial Mo=O oxygen on the Cu-bound CO, with substrate likely activated to at least some degree by back-bonding from the copper which leads

to population of the CO π^* orbital. Completion of the catalytic sequence involves formal reduction of the binuclear cluster and formation of CO_2 from this ensemble, with hydroxide from solvent necessarily being introduced into the molybdenum coordination sphere to regenerate the equatorial ligand of the molybdenum and complete the catalytic cycle.

8.1.4. Hydrogen can effectively reduce the enzyme

In addition to being able to oxidize carbon monoxide, hydrogenase activity has been reported for the CO dehydrogenase where the specific activity for H_2 oxidation is 10-16% when compared to the CO oxidizing specific activity.[87] In Chapter 6 we have furthered this investigation by characterizing the kinetics and EPR spectrum of the enzyme reacted with H_2. The enzyme is readily reduced by H_2, with a k_{red}, 5.3 s^{-1} and a $K_d^{H_2}$ of 525 μM. k_{red} from the rapid reaction study is in very good agreement with the steady-state derived k_{cat}, 5.1, indicating that the rate-limiting step in turnover is in the reductive half-reaction (as is the case with CO as substrate).[34] The lack of a significant pH dependence to the reductive half-reaction over the pH range 6-10 indicates that no substrate- or enzyme-based ionizations in the experimentally accessible pH range are involved in the rate-limiting step of the reaction.

Partial reduction of enzyme with H_2 yields an EPR signal distinctly different from that seen with CO as reductant, with more anisotropic g-values and larger coupling to the ^{63,65}Cu nucleus ($\mathbf{g}_{1,2,3}$ = [2.0127, 1.9676, 1.9594] and $|\mathbf{A}_{1,2,3}(^{63,65}\text{Cu})|$ = [169, 200, 170] MHz) and, significantly, strong coupling to two protons that is lost on preparation of the EPR sample in D_2O.

Finally, with the H_2-reduced native enzyme, given the effectiveness with which the native CO dehydrogenase, but not silver-substituted enzyme, oxidizes H_2, we propose that H_2 first binds at the copper of the binuclear center similarly to CO,[41,62] displacing the H_2O coordinated to the copper prior to catalysis. We believe that the observed EPR signal (as with CO as substrate described in Chapter 5) arises from enzyme that has already become partially reduced by reaction with prior turnover under the reaction conditions, such that H_2 is bound to a partially reduced Mo(V)/Cu(I) binuclear center, resulting in a complex that cannot progress through the catalytic cycle until the center has become fully oxidized (via intramolecular electron transfer to the other redox-active sites of the enzyme). The signal-giving species, again, reflects a paramagnetic analog of the Michaelis complex.

Binding of H_2 to metals, and specifically Cu(I), such as is proposed has chemical precedent,[96-98] and is known to involve side-on η^2 binding that polarizes substrate, facilitating its ionization to a metal hydride, for which precedent also exists.[96-99] This accounts for the rapid exchange with solvent, but the pH-

independence of the observed reaction with H_2 and the observation of two strongly coupled protons in the EPR signal of H_2-reduced enzyme requires that the pK_a for this ionization be greater than ~12. The rapid protonation/deprotonation of bound H_2 is catalytically productive, as the Cu(I)-hydride species formed transiently can itself deprotonate, with (when beginning with the fully oxidized Mo(VI)/Cu(I) binuclear center) the two reducing equivalents simply entering the highly delocalized redox-active orbital of the binuclear center. Furthermore, given the pH-independence of the reaction the pK_a for this step must be high, meaning that the equilibrium favors the H_2 complex over the hydride. This accounts for the observation of two protons rather than one in the EPR signal, and also rationalizes the modest reactivity of enzyme toward H_2 as compared to CO. The failure to observe any reversible reaction suggests that deprotonation of the copper hydride intermediate is strongly downhill thermodynamically, and functionally irreversible.

8.1.5. Inhibition of CO dehydrogenase

Finally, in Chapter 7 we have investigated the effects of two inhibitors, *n*-butylisonitrile and bicarbonate, on CO dehydrogenase. The first inhibitor investigated, *n*-butylisonitrile, was previously characterized by crystallography and proposed to be analogous to a structure proposed for a reaction intermediate for CO oxidation.[23] We find, as suggested by the crystal structure and computational studies, that *n*-butylisonitrile reacts with the enzyme, reducing it by

two electrons, forming a stable inhibition complex in the process, with inhibitor coordinated between the molybdenum and copper of the enzyme.

The second inhibitor investigated, bicarbonate, is an uncompetitive inhibitor based on the steady state kinetics observed at various bicarbonate concentrations, reducing the k_{cat} and k_m as the bicarbonate concentration is increased. As discussed in Chapter 6, the dithionite-reduced enzyme gives an EPR spectrum with two coupled protons while the EPR signal seen with dithionite-reduced enzyme in the presence of bicarbonate does not have these coupled protons. This suggests strongly that bicarbonate has displaced the bound water from the copper of the binuclear center. On the basis of the observed kinetics we find it likely that the bicarbonate is coordinated to both the copper and molybdenum, forming a six-member ring.

8.2 Future Directions

In comparison to the much better understood xanthine oxidase detailed insight into the mechanism of CO dehydrogenase is yet to be forthcoming. Although we have made great strides in understanding the mechanism of CO dehydrogenase and the roles of the active site metals in catalysis, there are several areas that require further investigation.

Following the ENDOR work with labeled carbon monoxide, investigations into the coordination of bicarbonate are needed to confirm the binding location of bicarbonate to the active site. These studies may reveal possible reasons as to why the reverse reaction (carbon dioxide reduction) is not observed.

It is also not known where the oxygen used to oxidize carbon monoxide originates. There are two possibilities; the first, and more likely, is the equatorial oxygen on molybdenum. The second, proposed by Gourlay et. al., is hydroxide from solvent.[39] To investigate this further ENDOR and ^{17}O labeled water can be used to monitor whether or not the equatorial oxygen is exchanged in the course of turnover as was done with xanthine oxidase. If there is no evidence for exchange ^{17}O or ^{18}O water in addition to ^{13}CO can be used to monitor the incorporation of label from water by NMR or mass spectrometry.

The investigations on the model compound for the active site of CO dehydrogenase have suggested that there is substantial orbital overlap of the Mo-μS-Cu active site of the enzyme. This is evident in CO dehydrogenase by the amount of coupling observed by the copper nucleus to the unpaired electron,

however these studies do not include the bridging sulfur as the natural abundant $^{32,34}S$ (99% abundance) is silent in the EPR and ENDOR investigations to date. By substituting the ^{33}S (I=3/2) nucleus into the bridging position by cyanide treatment followed by ^{33}S incorporation we can investigate the sulfur coupling to the EPR signal of the enzyme.

We have also examined the ability of the enzyme to oxidize H_2 and learned that this unique active site is capable of acting on substrates other than the physiological CO. There are other possible substrates for the enzyme that include ethylene and acetylene, as well as small aldehydes. A close examination of the active site residues reveals that there are many similarities between the aldehyde oxidizing members of the xanthine oxidase family and CO dehydrogenase. Understanding these possible reactions may give a more complete understanding of the enzyme and roles of the active site amino acids and metals.

Finally, in addition to investigations into the active site and mechanism of the protein, little is known about the maturation of the enzyme and assembly of its binuclear center. We have begun a collaboration with Silke Leimküehler at the University of Potsdam, who has begun the necessary steps to begin an investigation, to better understand how the cofactor is assembled and inserted into the active site of the enzyme. This will aid in the development of an expression system for CO dehydrogenase with the goal of mutation studies of conserved active site residues as well as residues near the flavin binding pocket

of the medium subunit that may influence the redox-partner of the enzyme as well as the redox-potential of the flavin.

Portions of this dissertation are adapted from the following publications:

Wilcoxen, J., Zhang, B., and Hille, R. (2011) Reaction of the Molybdenum- and Copper-Containing Carbon Monoxide Dehydrogenase from *Oligotropha Carboxydovorans* with Quinones. Biochemistry 50, 1910-1916. Copyright (2011) American Chemical Society.

Wilcoxen, J., Snider, S., and Hille, R. (2011) Substitution of Silver for Copper in the Binuclear Mo/Cu Center of Carbon Monoxide Dehydrogenase from Oligotropha Carboxidovorans. Journal of the American Chemical Society 133, 12934-12936. Copyright (2011) American Chemical Society.

Muralidharan Shanmugam, Jarett Wilcoxen, Diana Habel-Rodriguez, George E Cutsail III, Martin L. Kirk, Brian M. Hoffman, and Russ Hille (2013) ^{13}C and $^{63,65}Cu$ ENDOR studies of CO dehydrogenase from *Oligotropha carboxidovorans*. Experimental evidence in support of a copper-carbonyl intermediate. Journal of the American Chemical Society. Copyright (2013) American Chemical Society.

Wilcoxen, J and Hille, R. (2013) The Hydrogenase Activity of the Mo/Cu Containing Carbon Monoxide Dehydrogenase of *Oligotropha carboxidovorans*. The Journal of Biological Chemistry. 2013; © the American Society for Biochemistry and Molecular Biology.

References:

1. Schwarz, G., Hagedoorn, P.-L., and Fischer, K. (2007) Molybdate and Tungstate: Uptake, Homeostasis, Cofactors, and Enzymes. in *Molecular Microbiology of Heavy Metals* (Nies, D., and Silver, S. eds.), Springer Berlin Heidelberg. pp 421-451
2. Hille, R. (2002) Molybdenum and Tungsten in Biology. *Trends Biochem Sci* **27**, 360-367
3. Brondino, C. D., Passeggi, M. C. G., Caldeira, J., Almendra, M. J., Feio, M. J., Moura, J. J. G., and Moura, I. (2004) Incorporation of Either Molybdenum or Tungsten into Formate Dehydrogenase from Desulfovibrio Alaskensis Ncimb 13491; Epr Assignment of the Proximal Iron-Sulfur Cluster to the Pterin Cofactor in Formate Dehydrogenases from Sulfate-Reducing Bacteria. *Journal of Biological Inorganic Chemistry* **9**, 145-151
4. Sevcenco, A. M., Bevers, L. E., Pinkse, M. W. H., Krijger, G. C., Wolterbeek, H. T., Verhaert, P., Hagen, W. R., and Hagedoorn, P. L. (2010) Molybdenum Incorporation in Tungsten Aldehyde Oxidoreductase Enzymes from Pyrococcus Furiosus. *Journal of bacteriology* **192**, 4143-4152
5. Dean, J. A. (1992) *Lange's Handbook of Chemistry*, 14th ed., McGraw-Hill, New York. NY
6. Hidai, M. (1999) Chemical Nitrogen Fixation by Molybdenum and Tungsten Complexes. *Coordination Chemistry Reviews* **185-6**, 99-108
7. Hille, R. (1996) The Mononuclear Molybdenum Enzymes. *Chem Rev* **96**, 2757-2816
8. Hu, Y. L., and Ribbe, M. W. (2013) Biosynthesis of the Iron-Molybdenum Cofactor of Nitrogenase. *Journal of Biological Chemistry* **288**, 13173-13177
9. Hille, R. (2013) The Molybdenum Oxotransferases and Related Enzymes. *Dalton Transactions* **42**, 3029-3042
10. Hover, B. M., Loksztejn, A., Ribeiro, A. A., and Yokoyama, K. (2013) Identification of a Cyclic Nucleotide as a Cryptic Intermediate in Molybdenum Cofactor Biosynthesis. *J Am Chem Soc* **135**, 7019-7032
11. Neumann, M., and Leimkuhler, S. (2011) The Role of System-Specific Molecular Chaperones in the Maturation of Molybdoenzymes in Bacteria. *Biochemistry research international* **2011**, 850924
12. Wilcoxen, J., Zhang, B., and Hille, R. (2011) Reaction of the Molybdenum- and Copper-Containing Carbon Monoxide Dehydrogenase from *Oligotropha Carboxydovorans* with Quinones. *Biochemistry* **50**, 1910-1916
13. Ragsdale, S. W., and Pierce, E. (2008) Acetogenesis and the Wood-Ljungdahl Pathway of Co2 Fixation. *Bba-Proteins Proteom* **1784**, 1873-1898
14. Kang, B. S., and Kim, Y. M. (1999) Cloning and Molecular Characterization of the Genes for Carbon Monoxide Dehydrogenase and Localization of Molybdopterin, Flavin Adenine Dinucleotide, and Iron-Sulfur Centers in the Enzyme of Hydrogenophaga Pseudoflava. *Journal of bacteriology* **181**, 5581-5590
15. Meyer, O., and Schlegel, H. G. (1978) Oxidation of Carbon Monoxide in Cell Extracts of *Pseudomonas Carboxydovorans*. *Arch. Microbiol.* **118**, 35-43
16. Meyer, O., and Schlegel, H. G. (1978) Reisolation of the Carbon Monoxide Utilizing Hydrogen Bacterium Pseudomonas Carboxydovorans (Kistner) Comb. Nov. *Archives of microbiology* **118**, 35-43
17. Ferry, J. G. (1995) Co Dehydrogenase. in *Annual Review of Microbiology* (Ornston, L. N. ed.). pp 305-333

18. King, G. M., and Weber, C. F. (2007) Distribution, Diversity and Ecology of Aerobic Co-Oxidizing Bacteria. *Nature Reviews Microbiology* **5**, 107-118
19. Meyer, O., and Schlegel, H. G. (1980) Carbon Monoxide:Methylene Blue Oxidoreductase from *Pseudomonas Carboxydovorans*. *J. Bacteriol.* **141**, 78-80
20. Dobbek, H., Gremer, L., Meyer, O., and Huber, R. (1999) Crystal Structure and Mechanism of Co Dehydrogenase, a Molybdo Iron-Sulfur Flavoprotein Containing S-Selanylcysteine. *Proc Natl Acad Sci U S A* **96**, 8884-8889
21. Gremer, L., Kellner, S., Dobbek, H., Huber, R., and Meyer, O. (2000) Binding of Flavin Adenine Dinucleotide to Molybdenum-Containing Carbon Monoxide Dehydrogenase from Oligotropha Carboxidovorans. Structural and Functional Analysis of a Carbon Monoxide Dehydrogenase Species in Which the Native Flavoprotein Has Been Replaced by Its Recombinant Counterpart Produced in Escherichia Coli. *The Journal of biological chemistry* **275**, 1864-1872
22. Hanzelmann, P., Dobbek, H., Gremer, L., Huber, R., and Meyer, O. (2000) The Effect of Intracellular Molybdenum in Hydrogenophaga Pseudoflava on the Crystallographic Structure of the Seleno-Molybdo-Iron-Sulfur Flavoenzyme Carbon Monoxide Dehydrogenase. *Journal of molecular biology* **301**, 1221-1235
23. Dobbek, H., Gremer, L., Kiefersauer, R., Huber, R., and Meyer, O. (2002) Catalysis at a Dinuclear [Cusmo(==O)Oh] Cluster in a Co Dehydrogenase Resolved at 1.1-a Resolution. *Proc Natl Acad Sci U S A* **99**, 15971-15976
24. Cypionka, H., and Meyer, O. (1983) Carbon Monoxide-Insensitive Respiratory Chain of Pseudomonas Carboxydovorans. *Journal of bacteriology* **156**, 1178-1187
25. Meyer, O., Gremer, L., Ferner, R., Ferner, M., Dobbek, H., Gnida, M., Meyer-Klaucke, W., and Huber, R. (2000) The Role of Se, Mo and Fe in the Structure and Function of Carbon Monoxide Dehydrogenase. *Biological chemistry* **381**, 865-876
26. Moersdorf, G., Frunzke, K., Gadkari, D., and Meyer, O. . (1992) Microbial Growth on Carbon Monoxide. *Biodegredation* **3**, 61-82
27. Dobbek, H., Gremer, L., Meyer, O., and Huber, R. (1999) Crystal Structure and Mechanism of Co Dehydrogenase, a Molybdo Iron-Sulfur Flavoprotein Containing S-Selanylcysteine. *Proceedings of the National Academy of Sciences of the United States of America* **96**, 8884-8889
28. Dobbek, H., Gremer, L., Kiefersauer, R., Huber, R., and Meyer, O. (2002) Catalysis at a Dinuclear Cusmo(==O)Oh Cluster in a Co Dehydrogenase Resolved at 1.1-Angstrom Resolution. *Proceedings of the National Academy of Sciences of the United States of America* **99**, 15971-15976
29. Schubel, U., Kraut, M., Morsdorf, G., and Meyer, O. (1995) Molecular Characterization of the Gene Cluster Coxmsl Encoding the Molybdenum-Containing Carbon Monoxide Dehydrogenase of Oligotropha Carboxidovorans. *Journal of bacteriology* **177**, 2197-2203
30. Santiago, B., Schubel, U., Egelseer, C., and Meyer, O. (1999) Sequence Analysis, Characterization and Co-Specific Transcription of the Cox Gene Cluster on the Megaplasmid Phcg3 of Oligotropha Carboxidovorans. *Gene* **236**, 115-124
31. Gnida, M., Ferner, R., Gremer, L., Meyer, O., and Meyer-Klaucke, W. (2003) A Novel Binuclear [Cusmo] Cluster at the Active Site of Carbon Monoxide Dehydrogenase: Characterization by X-Ray Absorption Spectroscopy. *Biochemistry* **42**, 222-230

32. Ishikita, H., Eger, B. T., Okamoto, K., Nishino, T., and Pai, E. F. (2012) Protein Conformational Gating of Enzymatic Activity in Xanthine Oxidoreductase. *Journal of the American Chemical Society* **134**, 999-1009
33. Atkins, P., Overton, T., Rourke, J., Weller, M., Armstrong, F., Salvador, P., Hagerman, M., Spiro, T., and Stiefel, E. (2006) *Inorganic Chemistry*, 4th ed., W. H. Freeman and Company, New York
34. Zhang, B., Hemann, C. F., and Hille, R. (2010) Kinetic and Spectroscopic Studies of the Molybdenum-Copper Co Dehydrogenase from *Oligotropha Carboxidovorans*. *The Journal of biological chemistry* **285**, 12571-12578
35. Van Heuvelen, A. (1976) Electron Transport in Xanthine Oxidase. A Model for Other Biological Electron Transport Chains. *Biophys J* **16**, 939-951
36. Page, C. C., Moser, C. C., Chen, X., and Dutton, P. L. (1999) Natural Engineering Principles of Electron Tunnelling in Biological Oxidation-Reduction. *Nature* **402**, 47-52
37. Hille, R., and Anderson, R. F. (2001) Coupled Electron/Proton Transfer in Complex Flavoproteins: Solvent Kinetic Isotope Effect Studies of Electron Transfer in Xanthine Oxidase and Trimethylamine Dehydrogenase. *The Journal of biological chemistry* **276**, 31193-31201
38. Cammack, R., Barber, M. J., and Bray, R. C. (1976) Oxidation-Reduction Potentials of Molybdenum, Flavin and Iron-Sulphur Centres in Milk Xanthine Oxidase. *The Biochemical journal* **157**, 469-478
39. Gourlay, C., Nielsen, D. J., White, J. M., Knottenbelt, S. Z., Kirk, M. L., and Young, C. G. (2006) Paramagnetic Active Site Models for the Molybdenum-Copper Carbon Monoxide Dehydrogenase. *J Am Chem Soc* **128**, 2164-2165
40. Hofmann, M., Kassube, J. K., and Graf, T. (2005) The Mechanism of Mo-/Cu-Dependent Co Dehydrogenase. *Journal of biological inorganic chemistry : JBIC : a publication of the Society of Biological Inorganic Chemistry* **10**, 490-495
41. Siegbahn, P. E. M., and Shestakov, A. F. (2005) Quantum Chemical Modeling of Co Oxidation by the Active Site of Molybdenum Co Dehydrogenase. *Journal of Computational Chemistry* **26**, 888-898
42. Albarran, G., Schuler, R. H. . (2008) Determination of the Spectroscopic Properties and Chromatographic Sensitivities of Substituted Quinones by Hexachlorate(Iv) Oxidation of Hydroquinone. *Talanta* **74**, 884-850
43. Resch, M., Dobbek, H., and Meyer, O. (2005) Structural and Functional Reconstruction in Situ of the [Cusmoo2] Active Site of Carbon Monoxide Dehydrogenase from the Carbon Monoxide Oxidizing Eubacterium *Oligotropha Carboxidovorans*. *Journal of biological inorganic chemistry : JBIC : a publication of the Society of Biological Inorganic Chemistry* **10**, 518-528
44. Kita, K., Vibat, C. R., Meinhardt, S., Guest, J. R., and Gennis, R. B. (1989) One-Step Purification from Escherichia Coli of Complex Ii (Succinate: Ubiquinone Oxidoreductase) Associated with Succinate-Reducible Cytochrome B556. *The Journal of biological chemistry* **264**, 2672-2677
45. Chakraborty, S., and Massey, V. (2002) Reaction of Reduced Flavins and Flavoproteins with Diphenyliodonium Chloride. *The Journal of biological chemistry* **277**, 41507-41516

46. Davoust, C. E., Doan, P. E., and Hoffman, B. M. (1996) Q-Band Pulsed Electron Spin-Echo Spectrometer and Its Application to Endor and Eseem. *Journal of Magnetic Resonance Series A* **119**, 38-44
47. Doan, P. E., Telser, J., Barney, B. M., Igarashi, R. Y., Dean, D. R., Seefeldt, L. C., and Hoffman, B. M. (2011) Fe-57 Endor Spectroscopy and 'Electron Inventory' Analysis of the Nitrogenase E-4 Intermediate Suggest the Metal-Ion Core of Femo-Cofactor Cycles through Only One Redox Couple. *Journal of the American Chemical Society* **133**, 17329-17340
48. Rohde, M., Mayer, F., and Meyer, O. (1984) Immunocytochemical Localization of Carbon-Monoxide Oxidase in Pseudomonas-Carboxydovorans - the Enzyme Is Attached to the Inner Aspect of the Cytoplasmic Membrane. *Journal of Biological Chemistry* **259**, 4788-4792
49. Jacobitz, S., and Meyer, O. (1989) Removal of Co Dehydrogenase from Pseudomonas-Carboxydovorans Cytoplasmic Membranes, Rebinding of Co Dehydrogenase to Depleted Membranes, and Restoration of Respiratory Activities. *Journal of bacteriology* **171**, 6294-6299
50. Meyer, O., Frunzke, K., Gadkari, D., Jacobitz, S., Hugendieck, I., and Kraut, M. (1990) Utilization of Carbon-Monoxide by Aerobes - Recent Advances. *Fems Microbiology Reviews* **87**, 253-260
51. Kim, Y. M., and Hegeman, G. D. (1981) Electron Transport System of an Aerobic Carbon Monoxide-Oxidizing Bacterium. *Journal of bacteriology* **148**, 991-994
52. Gonzalez, C. F., Ackerley, D. F., Lynch, S. V., and Matin, A. (2005) Chrr, a Soluble Quinone Reductase of Pseudomonas Putida That Defends against H2o2. *Journal of Biological Chemistry* **280**, 22590-22595
53. Stoll, S., and Schweiger, A. (2006) Easyspin, a Comprehensive Software Package for Spectral Simulation and Analysis in Epr. *Journal of Magnetic Resonance* **178**, 42-55
54. Brown, T. G., and Hoffman, B. M. (1980) N-14, H-1, and Metal Endor of Single-Crystal Ag(Ii)(Tpp) and Cu(Ii)(Tpp). *Molecular Physics* **39**, 1073-1109
55. Hurlburt, P. K., Rack, J. J., Luck, J. S., Dec, S. F., Webb, J. D., Anderson, O. P., and Strauss, S. H. (1994) Nonclassical Metal-Carbonyls - Ag(Co) (+) and Ag(Co)(2) (+). *Journal of the American Chemical Society* **116**, 10003-10014
56. Xu, Q., and Jiang, L. (2006) Oxidation of Carbon Monoxide on Group 11 Metal Atoms: Matrix-Isolation Infrared Spectroscopic and Density Functional Theory Study. *Journal of Physical Chemistry A* **110**, 2655-2662
57. Zhang, B., Hemann, C. F., and Hille, R. (2010) Kinetic and Spectroscopic Studies of the Molybdenum-Copper Co Dehydrogenase from Oligotropha Carboxidovorans. *Journal of Biological Chemistry* **285**, 12571-12578
58. Wilcoxen, J., Snider, S., and Hille, R. (2011) Substitution of Silver for Copper in the Binuclear Mo/Cu Center of Carbon Monoxide Dehydrogenase from *Oligotropha Carboxidovorans*. *Journal of the American Chemical Society* **133**, 12934-12936
59. McWhirter, R. B., and Hille, R. (1991) The Reductive Half-Reaction of Xanthine-Oxidase - Identification of Spectral Intermediates in the Hydroxylation of 2-Hydroxy-6-Methylpurine. *Journal of Biological Chemistry* **266**, 23724-23731
60. Manikandan, P., Choi, E. Y., Hille, R., and Hoffman, B. M. (2001) 35 Ghz Endor Characterization of the "Very Rapid" Signal of Xanthine Oxidase Reacted with 2-

Hydroxy-6-Methylpurine ((13)C8): Evidence against Direct Mo-C8 Interaction. *Journal of the American Chemical Society* **123**, 2658-2663

61. Bray, R. C., and Vanngard, T. (1969) Rapidly Appearing Molybdenum Electron-Paramagnetic-Resonance Signals from Reduced Xanthine Oxidase. *Biochemical Journal* **114**, 725-&
62. Hofmann, M., Kassube, J. K., and Graf, T. (2005) The Mechanism of Mo-/Cu-Dependent Co Dehydrogenase. *Journal of Biological Inorganic Chemistry* **10**, 490-495
63. Solomon, E. I., Baldwin, M. J., and Lowery, M. D. (1992) Electronic-Structures of Active-Sites in Copper Proteins - Contributions to Reactivity. *Chemical Reviews* **92**, 521-542
64. Resch, M., Dobbek, H., and Meyer, O. (2005) Structural and Functional Reconstruction in Situ of the Cusmoo2 Active Site of Carbon Monoxide Dehydrogenase from the Carbon Monoxide Oxidizing Eubacterium Oligotropha Carboxidovorans. *Journal of Biological Inorganic Chemistry* **10**, 518-528
65. Romao, M. J., Archer, M., Moura, I., Moura, J. J. G., Legall, J., Engh, R., Schneider, M., Hof, P., and Huber, R. (1995) Crystal-Structure of the Xanthine Oxidase-Related Aldehyde Oxidoreductase from *D-Gigas*. *Science* **270**, 1170-1176
66. Santos-Silva, T., Ferroni, F., Thapper, A., Marangon, J., Gonzalez, P. J., Rizzi, A. C., Moura, I., Moura, J. J. G., Romao, M. J., and Brondino, C. D. (2009) Kinetic, Structural, and Epr Studies Reveal That Aldehyde Oxidoreductase from *Desulfovibrio Gigas* Does Not Need a Sulfido Ligand for Catalysis and Give Evidence for a Direct Mo-C Interaction in a Biological System. *Journal of the American Chemical Society* **131**, 7990-7998
67. Houseman, A. L. P., Oh, B. H., Kennedy, M. C., Fan, C. L., Werst, M. M., Beinert, H., Markley, J. L., and Hoffman, B. M. (1992) N-14, N-15, C-13, Fe-57 and H-1, H-2 Q-Band Endor Study of Fe-S Proteins with Clusters That Have Endogenous Sulfur Ligands. *Biochemistry* **31**, 2073-2080
68. Shanmugam, M., Zhang, B., McNaughton, R. L., Kinney, R. A., Hille, R., and Hoffman, B. M. (2010) The Structure of Formaldehyde-Inhibited Xanthine Oxidase Determined by 35 Ghz H-2 Endor Spectroscopy. *Journal of the American Chemical Society* **132**, 14015-14017
69. Hille, R. (2010) Epr Studies of Xanthine Oxidoreductase and Other Molybdenum-Containing Hydroxylases. in *Metals in Biology: Applications of High-Resolution Epr to Metalloenzymes* (Hanson, G., and Berliner, L. eds.). pp 91-120
70. Roberts, J. E., Brown, T. G., Hoffman, B. M., and Peisach, J. (1980) Electron Nuclear Double Resonance Spectra of Stellacyanin, a Blue Copper Protein. *J. Am. Chem. Soc.* **102**, 826-829
71. Hori, H., Ikeda-Saito, M., and Yonetani, T. (1981) Electromagnetic Properties of Hemoproteins. Vi. Single Crystal Epr of Myoglobin Nitroxide. Freezing-Induced Reversible Changes in the Molecular Orientation of the Ligand. *J. Biol. Chem.* **256**, 7849-7855
72. Doan, P. E. (2011) Combining Steady-State and Dynamic Methods for Determining Absolute Signs of Hyperfine Interactions: Pulsed Endor Saturation and Recovery (Pestre). *Journal of Magnetic Resonance* **208**, 76-86
73. Kinney, R. A., Hetterscheid, D. G. H., Hanna, B. S., Schrock, R. R., and Hoffman, B. M. (2010) Formation of { Hiptn3n Mo(Iii)H}(-) by Heterolytic Cleavage of H-2 as Established by Epr and Endor Spectroscopy. *Inorganic Chemistry* **49**, 704-713

74. Holm, R. H., Kennepohl, P., and Solomon, E. I. (1996) Structural and Functional Aspects of Metal Sites in Biology. *Chem. Rev.* **96**, 2239-2314
75. LaCroix, L. B., Shadle, S. E., Wang, Y. N., Averill, B. A., Hedman, B., Hodgson, K. O., and Solomon, E. I. (1996) Electronic Structure of the Perturbed Blue Copper Site in Nitrite Reductase: Spectroscopic Properties, Bonding, and Implications for the Entatic/Rack State. *Journal of the American Chemical Society* **118**, 7755-7768
76. Penfield, K. W., Gay, R. R., Himmelwright, R. S., Eickman, N. C., Norris, V. A., Freeman, H. C., and Solomon, E. I. (1981) Spectroscopic Studies on Plastocyanin Single-Crystals - a Detailed Electronic-Structure Determination of the Blue Copper Active-Site. *Journal of the American Chemical Society* **103**, 4382-4388
77. Roberts, J. E., Cline, J. F., Lum, V., Gray, H. B., Freeman, H., Peisach, J., Reinhammar, B., and Hoffman, B. M. (1984) Comparative Endor Study of Six Blue Copper Proteins. *J. Am. Chem. Soc* **106**, 5324
78. Chow, C., Chang, K., and Willett, R. D. (1973) Electron Spin Resonance Spectra and Covalent Bonding in the Square-Planar Cucl42− and Cubr42− Ions. *J. Chem. Phys.* **59**, 2629
79. Gourlay, C., Nielsen, D. J., White, J. M., Knottenbelt, S. Z., Kirk, M. L., and Young, C. G. (2006) Paramagnetic Active Site Models for the Molybdenum-Copper Carbon Monoxide Dehydrogenase. *Journal of the American Chemical Society* **128**, 2164-2165
80. Howes, B. D., Bennett, B., Bray, R. C., Richards, R. L., and Lowe, D. J. (1994) C-13-Endor Studies of the Inhibited Species of Xanthine-Oxidase - the First Direct Evidence for a Molybdenum-Carbon Bond in a Biological System. *Journal of the American Chemical Society* **116**, 11624-11625
81. Howes, B. D., Bray, R. C., Richards, R. L., Turner, N. A., Bennett, B., and Lowe, D. J. (1996) Evidence Favoring Molybdenum-Carbon Bond Formation in Xanthine Oxidase Action: O-17 and C-13-Endor and Kinetic Studies. *Biochemistry* **35**, 1432-1443
82. Howes, B. D., Bray, R. C., Richards, R. L., Turner, N. A., Bennett, B., and Lowe, D. J. (1996) Evidence Favoring Molybdenum-Carbon Bond Formation in Xanthine Oxidase Action: O-17- and C-13-Endor and Kinetic Studies (Vol 35, Pg 1432, 1996). *Biochemistry* **35**, 3874-3874
83. Manikandan, P., Choi, E. Y., Hille, R., and Hoffman, B. M. (2001) 35 Ghz Endor Characterization of the "Very Rapid" Signal of Xanthine Oxidase Reacted with 2-Hydroxy-6-Methylpurine (13c8): Evidence against Direct Mo−C8 Interaction. *J. Am. Chem. Soc* **123**, 2658-2663
84. Sempombe, J., Stein, B., and Kirk, M. L. (2011) Spectroscopic and Electronic Structure Studies Probing Covalency Contributions to C-H Bond Activation and Transition-State Stabilization in Xanthine Oxidase. *Inorganic Chemistry* **50**, 10919-10928
85. Pauff, J. M., Zhang, J. J., Bell, C. E., and Hille, R. (2008) Substrate Orientation in Xanthine Oxidase - Crystal Structure of Enzyme in Reaction with 2-Hydroxy-6-Methylpurine. *Journal of Biological Chemistry* **283**, 4818-4824
86. Hille, R., Kim, J. H., and Hemann, C. (1993) Reductive Half-Reaction of Xanthine-Oxidase - Mechanistic Role of the Species Giving Rise to the Rapid Type-1 Molybdenum(V) Electron-Paramagnetic Resonance Signal. *Biochemistry* **32**, 3973-3980

87. Santiago, B., and Meyer, O. (1996) Characterization of Hydrogenase Activities Associated with the Molybdenum Co Dehydrogenase from *Oligotropha Carboxydovorans*. *FEMS* **136**, 157-162
88. Bhatnagar, L., Krzycki, J. A., and Zeikus, J. G. (1987) Analysis of Hydrogen Metabolism in Methanosarcina Barkeri: Regulation of Hydrogenase and Role of Co-Dehydrogenase in H2 Production. *FEMS Microbiol. Lett.* **41**, 337-343
89. Menon, S., and Ragsdale, S. W. (1996) Unleashing Hydrogenase Activity in Carbon Monoxide Dehydrogenase/Acetyl-Coa Synthase and Pyruvate:Ferredoxin Oxidoreductase. *Biochemistry* **35**, 15814-15821
90. Santiago, B., and Meyer, O. (1997) Purification and Molecular Characterization of the H2 Uptake Membrane-Bound Nife-Hydrogenase from the Carboxidotrophic Bacterium *Oligotropha Carboxydovorans*. *J. Bacteriol* **179**, 6053
91. Fuhrmanna, S., Fernera, M., Jeffkeb, T., Henneb, A., Gottschalkb, G., and Meyer, O. (2003) Complete Nucleotide Sequence of the Circular Megaplasmid Phcg3 of Oligotropha Carboxidovorans: Function in the Chemolithoautotrophic Utilization of Co, H2 and Co2. *Gene* **322**, 67-75
92. Siegbahn, P. E., Tye, J. W., and Hall, M. B. (2007) Computational Studies of [Nife] and [Fefe] Hydrogenases. *Chem Rev* **107**, 4414-4435
93. Léger, C., Jones, A. K., Roseboom, W., Albracht, S. P. J., and Armstrong, F. A. (2002) Enzyme Electrokinetics: Hydrogen Evolution and Oxidation by Allochromatium Vinosum [Nife]-Hydrogenase. *Biochemistry* **41**, 15739-15746
94. Bray, R. C., and Vanngard, T. (1969) "Rapidly Appearing" Molybdenum Electron-Paramagnetic-Resonance Signals from Reduced Xanthine Oxidase. *The Biochemical journal* **114**, 725-734
95. Hille, R., Kim, J. H., and Hemann, C. (1993) Reductive Half-Reaction of Xanthine Oxidase: Mechanistic Role of the Species Giving Rise to the "Rapid Type 1" Molybdenum(V) Electron Paramagnetic Resonance Signal. *Biochemistry* **32**, 3973-3980
96. Wang, N., Wang, M., Chen, L., and Sun, L. (2013) Reactions of [Fefe]-Hydrogenase Models Involving the Formation of Hydrides Related to Proton Reduction and Hydrogen Oxidation. *Dalton Trans* **42**, 12059-12071
97. Frohman, D. J., Grubbs, G. S., 2nd, Yu, Z., and Novick, S. E. (2013) Probing the Chemical Nature of Dihydrogen Complexation to Transition Metals, a Gas Phase Case Study: H2-Cuf. *Inorg Chem* **52**, 816-822
98. Kemper, P. R., Weis, P., Bowers, M. T., and Maıtre, P. (1998) Origin of Bonding Interactions in Cu+(H2)N Clusters: An Experimental and Theoretical Investigation. *J. Am. Chem. Soc* **120**, 13494-13502
99. Hulley, E. B., Welch, K. D., Appel, A. M., Dubois, D. L., and Bullock, R. M. (2013) Rapid, Reversible Heterolytic Cleavage of Bound H2. *J Am Chem Soc* **135**, 11736-11739
100. Moser, R., Boskovic, Z. V., Crowe, C. S., and Lipshutz, B. H. (2010) Cuh-Catalyzed Enantioselective 1,2-Reductions of a,B-Unsaturated Ketones. *J. Am. Chem. Soc* **132**, 7852-7853
101. Mahoney, W. S., Brestensky, D. M., and Stryker, J. M. (1988) Selective Hydride-Mediated Conjugate Reduction of a,B Unsaturated Carbonyl Compounds Using [(Ph~P)Cuhlti. *J. Am. Chem. Soc* **110**, 291-293

102. Meyer, O., Lalucat, J., and Schlegel, H. G. (1980) *Pseudomonas-Carboxydohydrogena* (Sanjieva and Zavarzin) Comb Nov - Monotrichous, Nonbudding, Strictly Aerobic, Carbon Monoxide-Utilizing Hydrogen Bacterium Previously Assigned to Seliberia. *International Journal of Systematic Bacteriology* **30**, 189-195